MODELLING THE ROLE OF FOSSIL FUELS AND HUMAN ACTIVITIES IN CARBON (IV) OXIDE EMISSIONS AND GLOBAL WARMING USING COMPARTMENTAL AND CHEMICAL KINETICS MODELS

GICHERU JAMES GATHUNGU

A THESIS SUBMITTED TO THE KIRINYAGA UNIVERSITY IN PARTIAL FULFILLMENT OF THE REQUIREMENTS FOR THE AWARD OF THE DEGREE OF DOCTOR OF PHILOSOPHY IN APPLIED AND COMPUTATIONAL MATHEMATICS IN THE SCHOOL OF PURE AND APPLIED SCIENCES, KIRINYAGA UNIVERSITY.

AUGUST, 2026

DECLARATION

This thesis is my original work and has not been presented for a degree or any other award in any other Institution.

GICHERU JAMES GATHUNGU

PA300/S/15528/21

Signed..... Date.....

This thesis has been submitted for examination with our approval as University Supervisors.

Signed..... Date.....

DR. CYRUS GITONGA NGARI, Ph.D
Department of Pure and Applied Sciences,
Kirinyaga University.

Signed..... Date.....

DR. PETER NJORI WANJOHI,Ph.D
Department of Pure and Applied Sciences,
Kirinyaga University.

COPYRIGHT

© 2026 GICHERU JAMES GATHUNGU

All rights reserved.

No part of this thesis may be reproduced, stored in a retrieval system, or transmitted in any form or by any means, electronic, mechanical, photocopying, recording or otherwise, without the prior written permission of the author or Kirinyaga University.

DEDICATION

Dedicated to my wife Peninah,chidren Emmanuel,Abigael,Anabel and Othniel who allowed me time off to complete this study and my parents Stephen and Mary for encouragements and support.

ACKNOWLEDGEMENTS

I express my sincere gratitude to the Almighty God, for His guidance, wisdom and direction which has made this proposal a success. I am highly grateful to my supervisors Dr Ngari and Dr Wanjohi for their support, inspiration and patience throughout this work. My special thanks goes to all the lecturers who made valuable contribution in shaping this work in context, organization and structure at its various stages.

ABSTRACT

Atmospheric carbon dioxide (CO_2) emissions resulting from fossil fuel combustion and human activities remain the primary drivers of global warming and climate change, necessitating the development of robust mathematical models capable of describing their complex dynamics and supporting effective mitigation strategies. This thesis develops and analyses two complementary mathematical modelling frameworks for investigating atmospheric carbon dioxide emissions and natural carbon sequestration processes. The first framework formulates a global compartmental model incorporating human activities, fossil fuel consumption, vegetation dynamics and atmospheric carbon dioxide, while the second develops a nonlinear lumped chemical kinetics model describing the interactions among kerosene, liquefied petroleum gas (LPG), petrol, diesel, oxygen, carbon dioxide, water vapour, glucose and carbonic acid. The governing systems are formulated using ordinary differential equations based on the principles of mass conservation and the law of mass action, followed by rigorous analyses of positivity, boundedness, existence, uniqueness, equilibrium and local stability. Numerical simulations were performed in MATLAB using the Runge–Kutta and `ode15s` solvers, while global sensitivity analysis was conducted using Latin Hypercube Sampling (LHS) and Partial Rank Correlation Coefficients (PRCC). The compartmental model demonstrates that increasing fossil fuel consumption and intensified human activities significantly increase atmospheric carbon dioxide concentrations, whereas increasing vegetation enhances carbon sequestration and reduces atmospheric carbon dioxide accumulation. Model fitting predicts a potential global temperature increase ranging from approximately $0.59^{\circ}\mathrm{C}$ to $2.46^{\circ}\mathrm{C}$, with an upper estimate of $6.57^{\circ}\mathrm{C}$ under extreme conditions. The nonlinear chemical kinetics model admits a unique positive equilibrium $E^* = (9.3768,\ 0.0140,\ 0.2464,\ 20.1948,\ 6.6899,\ 11.3105,\ 8.9884,\ 38.7624,\ 19.9072)$, and the Jacobian evaluated at this equilibrium possesses strictly negative eigenvalues, confirming local asymptotic stability. Numerical simulations show smooth convergence of all state variables to their equilibrium values, while sensitivity analysis identifies the photosynthesis parameter as the most influential mechanism governing atmospheric carbon dioxide reduction. Furthermore, numerical bifurcation analysis demonstrates that the model remains structurally stable over the investigated parameter range. Overall, the proposed mathematical frameworks provide computationally efficient and analytically rigorous tools for understanding atmospheric carbon dioxide dynamics, evaluating greenhouse gas mitigation strategies and supporting evidence-based environmental policy towards achieving Sustainable Development Goal 13 (Climate Action).

TABLE OF CONTENTS

Declaration ii

COPYRIGHT iii

DEDICATION iv

ACKNOWLEDGEMENTS v

ABSTRACT vi

TABLE OF CONTENTS ix

ABBREVIATIONS AND ACRONYMS x

LIST OF TABLES xi

LIST OF FIGURES xii

1 INTRODUCTION 1

1.1 Background of the Study 1

1.1.1 Emissions 1

1.1.2 Fossil Fuels 3

1.1.3 Humans 3

1.1.4 Impacts of Carbon (iv) oxide (CO_2) emissions 4

1.1.5 Sustainable Development Goals, Kenya Vision 2030 and The Big four Agenda. 6

1.1.6 Mathematical models. 7

1.1.7 Compartmental models 9

1.1.8 Chemical kinetics 9

1.1.9 Research Gap 10

1.2 Statement of the problem 10

1.3 Research Objectives 12

1.3.1 Main objective 12

1.3.2 Specific objectives 12

1.4 Scope of the Study 12

1.5 Significance of the Study 13

1.6 Method of Study 14

2 Literature Review **16**
2.1 Introduction 16
2.2 Research Gap 23

3 MODEL FORMULATION AND ANALYSIS **26**
3.1 Introduction 26
3.2 Model Description 26
3.3 Model Formulation 28
3.3.1 Model variables and parameters. 28
3.3.2 Assumptions of the compartmental model 29
3.3.3 Model Framework 31
3.3.4 Model equations 32
3.3.5 Methods for Analysing the Compartmental Model 32
3.4 Chemical Kinetics Model 33
3.4.1 Assumptions of the Chemical Kinetics Model 34
3.4.2 Chemical Species and Their Representation 35
3.4.3 Application of the Law of Mass Action 36
3.4.4 Reaction Scheme 37
3.4.5 State Variables 37
3.4.6 Model Parameters 37
3.4.7 Governing Differential Equations 38
3.4.8 Initial Conditions 38
3.4.9 Vector Form 39
3.4.10 Nondimensionalization 39
3.4.11 Dimensionless Parameters 40
3.4.12 Dimensionless Model 41
3.4.13 Methods for Analysing the Chemical Kinetics Model 43

4 RESULTS AND DISCUSSIONS **46**
4.1 Results and Discussions for the Deterministic Compartmental Model 46
4.1.1 Positivity of the Deterministic Compartmental Model 47
4.1.2 Boundedness of the Deterministic Compartmental Model 52
4.1.3 Existence and Uniqueness of Solutions 56
4.1.4 Equilibrium Points 57
4.1.5 Jacobian Matrix 66
4.1.6 Local Stability Analysis 68
4.1.7 Global Stability Analysis 76
4.1.8 Bifurcation analysis 81
4.1.9 Model simulation and data fitting. 83
4.1.10 Effects of Selected Parameters on Carbon (IV) Oxide Emissions 85
4.1.11 Least Squares Parameter Estimation and Temperature Response 90
4.1.12 Phase Portrait and Interaction Dynamics 93
4.1.13 Interaction Between Drivers, Diesel Consumption and Carbon (IV) Oxide Emissions 95
4.2 CHEMICAL KINETICS MODEL 96
4.2.1 Positivity of Solutions 96

4.2.2 Boundedness of Solutions 97
4.2.3 Existence and Uniqueness of Solutions 98
4.2.4 Equilibrium Analysis 99
4.2.5 Numerical Evaluation of the Equilibrium Point 101
4.2.6 Jacobian Matrix 101
4.2.7 Characteristic Equation 103
4.2.8 Local Stability Analysis 103
4.2.9 Numerical Verification of Local Stability 104
4.3 Numerical Results and Discussion 105
4.3.1 Numerical Simulation Results 105
4.3.2 Atmospheric Dynamics 106
4.3.3 Carbon Sink Dynamics 107
4.3.4 Numerical Equilibrium Analysis 107
4.3.5 Jacobian Matrix and Local Stability Analysis 108
4.3.6 Global Sensitivity Analysis 110
4.3.7 Bifurcation Analysis 111

5 Conclusion and Recommendations 113
5.1 Conclusion 113
5.2 Recommendations 114
5.3 Recommendations for Further Research 115

A Supplementary Computational Materials 116
A.1 Characteristic Polynomial Coefficients 116
A.2 Equilibrium-specific substitutions 118
A.3 Routh–Hurwitz stability test 118
A.4 MATLAB Verification Output 119
A.5 Numerical Jacobian Matrix 120
A.6 MATLAB Computing Environment 120
A.7 MATLAB Project Structure 121
A.8 Supplementary Numerical Data 121
A.9 Software Availability 122
A.10 Research Publications Arising from the Thesis 122
A.11 Future Development of the Models 122

REFERENCES 130

RESEARCH LICENSE 131

PUBLICATION 132

PUBLICATION 133

ABBREVIATIONS AND ACRONYMS

CO_2	Carbon (IV) Oxide
GHG	Greenhouse Gas
GHGs	Greenhouse Gases
ODE	Ordinary Differential Equation
ODEs	Ordinary Differential Equations
LHS	Latin Hypercube Sampling
PRCC	Partial Rank Correlation Coefficient
GSA	Global Sensitivity Analysis
MATLAB	Matrix Laboratory
RK4	Fourth-Order Runge–Kutta Method
RK45	Runge–Kutta Method of Order Four–Five
SDG	Sustainable Development Goal
IPCC	Intergovernmental Panel on Climate Change
LPG	Liquefied Petroleum Gas
LSM	Least Squares Method
NLC	Newton's Law of Cooling
RH	Routh–Hurwitz

LIST OF TABLES

1.1 General types of chemical fuels 4

3.1 Definition of variables 28
3.2 Definition of parameters. 29
3.3 Chemical species considered in the chemical kinetics model 36
3.4 Baseline dimensionless parameter values used in the numerical simulations. 41
3.5 Dimensionless initial conditions used for numerical simulations. 42

4.1 Summary of the equilibrium cases of the deterministic compartmental model. 65
4.2 Model variables, descriptions and quantities 84
4.3 Model parameters and descriptions 84
4.4 Continuation of model parameters 85
4.5 Carbon (IV) Oxide emissions and annual warming data. 91
4.6 Least squares fitting results for Carbon (IV) Oxide emissions and annual warming. 91
4.7 Numerically computed positive equilibrium point. 101
4.8 Eigenvalues of the Jacobian matrix evaluated at the positive equilibrium point. 104
4.9 Numerically computed positive equilibrium point of the nonlinear chemical kinetics model. 108
4.10 Eigenvalues of the Jacobian matrix evaluated at the positive equilibrium point. 109

A.1 Computing environment used for numerical simulations. 121
A.2 MATLAB project files. 121

List of Figures

3.1 Model Framework 31

4.1 Backward bifurcation 83
4.2 Dynamics of Carbon (IV) Oxide emissions for varying values of ω_3, α_2 and ϕ_2. 86
4.3 Dynamics of Carbon (IV) Oxide emissions for varying values of θ_2, β_2 and ε_2. 87
4.4 Dynamics of Carbon (IV) Oxide emissions for varying values of γ_2, δ_2 and ρ_1. 88
4.5 Least squares fitting of the temperature-response model to the observed Carbon (IV) Oxide emissions and annual warming data using Excel Solver. 92
4.6 Predicted temperature response for the estimated minimum, average and maximum values of k_c. 92
4.7 Dynamics of the interaction between human population, plant cover and Carbon (IV) Oxide emissions. 94
4.8 Dynamics of Carbon (IV) Oxide emissions associated with the interaction between drivers and diesel consumption. 95
4.9 Temporal evolution of kerosene, LPG, petrol and diesel concentrations. 105
4.10 Temporal evolution of oxygen, carbon dioxide and water vapour. 106
4.11 Temporal evolution of glucose and carbonic acid concentrations. 107
4.12 Partial Rank Correlation Coefficients (PRCC) showing the relative influence of model parameters on carbon dioxide dynamics. 110
4.13 Variation of the equilibrium carbon dioxide concentration with the oxygen replenishment parameter β_O. 111

CHAPTER 1

INTRODUCTION

1.1 Background of the Study

1.1.1 Emissions

Emissions refer to the release or discharge of various substances, such as gases or particles, into the environment. These substances can come from natural processes, but the term is often used in the context of human activities that release pollutants or greenhouse gases into the air, water, or soil. Emissions can have significant environmental, health, and economic impacts, depending on the type and quantity of substances being released (Munsif et al., 2021).

Greenhouse Gas Emissions involve the release of gases that contribute to the greenhouse effect and global warming. Carbon dioxide (CO_2), methane (CH_4), nitrous oxide (N_2O), and fluorinated gases are common greenhouse gases emitted from activities such as burning fossil fuels, deforestation, and industrial processes.

A passenger vehicle mainly produces about 4.6 metric tons of carbon (iv) oxide per annum(Roa & Lima, 2023).This may vary due to a vehicle's fuel, number of miles covered per year and fuel usage. It is assumed that the average gasoline vehicle has a fuel economy of about 22.0 miles per gallon and moves about 11,500 miles per annum. Every gallon of gasoline burned emits about 8,887 grams of CO_2.

Automobiles also emit methane (CH_4) and nitrous oxide (N_2O) from the tailpipe and hydrofluorocarbon emissions from leaking air conditioners. The release of these gases are quite small in relation to CO_2. According to U.S. Environmental Protection Agency overview of U.S. Greenhouse Gas in 2020, combustion of fossil fuels such as petrol and diesel to ferry goods and people was the prime source of CO_2 emissions in 2020,

representing about 33% of total U.S. CO_2 emissions and 26% of total U.S. greenhouse gas emissions. .

In 2019, greenhouse gases (GHGs) produced directly from the transport sector were 8.7 GtCO_2-eq (increase from 5.0 GtCO_2-eq in 1990s) and this accounted 23% of global energy-related CO2 emissions. Direct transport emissions of 70% came from road vehicles, 1% from rail, 11% from shipping, and 12% came from aviation. In the developing regions of the world transport related emissions have risen more faster than in developed countries, a pattern which is likely to persist in coming decades(Kikstra et al., 2022)

Automobiles emissions have actually rose over the last two decades, and since 2010, the transport emissions have gone up faster than for any other end-use sector, averaging +1.8% annual growth. Global transport associated CO_2 emissions from road passenger and freight vehicles continues to reign and offer the largest mitigation potential.

In Kenya, Nairobi central business district private cars dominate above other vehicle types, releasing 73% of the total CO_2 emissions in the city. Private cars thus are greatest producers of CO_2 emissions with a total of 25.3 million grams of CO_2 equivalent (gCO_2e), between 2014 and 2019.Comparing with public service vehicles i.e matatus, emitted 6.89 million gCO_2e, light commercial vehicles 1.82 million gCO_2e, heavy goods vehicles 251,683 gCO2e and motorcycles 181,054 gCO_2e.(Sitati et al., 2022)

1.1.2 Fossil Fuels

A fossil fuel is a hydrocarbon-containing material such as coal, oil, and natural gas,McKie (2023) formed naturally in the Earth's crust from the remains of dead plants and animals that is extracted and burned as a fuel. Fossil fuels are a group of non-renewable energy resources that are formed from the remains of ancient plants and animals that lived millions of years ago. These remains have undergone a process of heat and pressure over geological time, transforming into substances rich in carbon and hydrocarbons.

Fossil fuels are the primary sources of energy that power much of modern civilization The first fuel was the combustion of firewood by Homo erectus nearly two million years ago(Schobert, 2013). Throughout history only fuels derived from plants or animal fat were used by humans. Charcoal, a wood derivative, has been used since at least 6,000 BCE for melting metals. Crude oil was distilled by Persian chemists, with clear descriptions given in Arabic handbooks such as those of Muhammad ibn Zakarīya Rāzi(Forbes, 1958).

He described the process of distilling crude oil/petroleum into kerosene, as well as other hydrocarbon compounds, in his Kitab al-Asrar (Book of Secrets). Kerosene was also produced during the same period from oil shale and bitumen by heating the rock to extract the oil, which was then distilled. Rāzi also gave the first description of a kerosene lamp using crude mineral oil, referring to it as the "naffatah"(Bilkadi, 1995).

Fossil fuels have been used for centuries, but their large-scale exploitation began during the Industrial Revolution in the 18th century. They have played a critical role in powering industries, transportation, electricity generation, and heating. However, the burning of fossil fuels releases carbon(iv)oxide (CO_2) and other greenhouse gases into the atmosphere, contributing to global warming and climate change. (IPCC, 2013).

Chemical fuels are grouped in two ways. First, by their physical properties, as a solid, liquid or gas. Secondly, on the basis of their occurrence: primary (natural fuel) and secondary (artificial fuel). Thus, a general classification of chemical fuels is(Schobert, 2013):

1.1.3 Humans

It took hundreds of thousands of years for the world population to rise to 1 billion – then in just another 200 years or so, it grew seven fold. In 2011, the global population reached the 7 billion mark, it stands at almost 7.9 billion in 2021, and it's expected to grow to around 8.5 billion in 2030, 9.7 billion in 2050, and 10.9 billion in 2100

Table 1.1: General types of chemical fuels

Type	**Primary (natural)**	**Secondary (artificial)**
Solid fuels	Wood, coal, peat, dung, etc.	Coke, charcoal
Liquid fuels	Petroleum	Diesel, gasoline, kerosene, LPG, coal tar, naphtha, ethanol
Gaseous fuels	Natural gas	Hydrogen, propane, methane, coal gas, water gas, blast furnace gas, coke oven gas

(Review, 2021).
Human activities contribute significantly to CO_2 emissions, which are a major driver of climate change and global warming. Some of the primary sources of CO_2 emissions from human activities include burning fossil fuels in transportation and for heating,deforestation,Waste and Wastewater Treatment among others.

The potential for human activities to increase the temperature of the Earth through greenhouse gas emissions has been described and calculated for over a century. Volumes of scientific research across multiple scientific disciplines agree that humans are warming the climate, and the 2013 IPCC Fourth Assessment Report states, "Human influence on the climate system is clear. This is evident from the increasing greenhouse gas concentrations in the atmosphere, positive radiative forcing, observed warming, and understanding of the climate system(Solomon et al., 2007)."

1.1.4 Impacts of Carbon (iv) oxide (CO_2) emissions

Carbon (IV) oxide, (CO_2), is a chemical compound composed of two oxygen atoms covalently bonded to a single carbon atom. It is a colorless, odorless gas at room temperature and is a vital component of Earth's atmosphere.
While CO_2 is vital for many biological processes and is a naturally occurring component of the atmosphere, its concentration has increased significantly due to human activities. This increase in CO_2 levels has contributed to the greenhouse effect and global warming.

CO_2 contributes the greater percentage to global warming because of its mass production. According to U.S. Environmental Protection Agency overview of U.S. Greenhouse Gas in 2020, CO_2 accounted for about 79% of all U.S. greenhouse gas

emissions from human activities. Carbon (iv) oxide is naturally present in the atmosphere as part of the Earth's carbon cycle which is the natural circulation of carbon among the atmosphere, oceans, soil, plants, and animals.

The carbon cycle is being altered due to increasing CO2 emissions to the atmosphere and by affecting the ability of natural sinks, like forests and soils, to absorb and store CO_2 from the atmosphere(Pingree et al., 2022).

From the Australian experience, the land sector must contribute significantly to mitigating anthropogenic greenhouse gas (GHG) emissions in coming decades, while concurrently expanding production of food and fibre (Moore et al., 2014). CO_2 emission affects not only climate change globally but also economic and political situations internationally(Meng et al., 2016). Therefore, lowering the emissions of CO_2, has been a prime issue not only in China but also in the entire world as it involves protection of the environmental ecology.

The global disaster of the 21st century is climate change. To a greater extent, these changes have been accelerated by the lifestyle of people. This has negatively impacted on the environment as greenhouse gas emissions continue to rise.Though Kazakhstan is considerably distanced from the World Ocean,it has a sharp and arid continental climate in most of its places. According to data for 1976-2017, Kazakhstan has a rapid growth rate of average annual air temperature than the global average. This increases the relevance of Sustainable Development Goals 13 to the country (Sultanova et al., 2020).

The present climate change has been characterized by an unexpected increase rate in the near-surface temperature and in the frequency and intensity of dangerous weather and climate events. To survive, society must be ready to come up with strategies and measures to offset the negative impacts of climate change. This necessiates at first to know how the climate will change in the future.

Global warming is negatively affecting the earth's climate system due to massive emissions of greenhouse gases (GHGs), Mandal et al. (2021) in his research on optimal mitigation of potential impact of climate change on coastal ecosystems.

CO_2 emissions acts as a blanket in the air, trapping heat in the atmosphere thus warming up the Earth(Klufallah et al., 2014). This layer limits the Earth from cooling causing global temperatures to rise.This would have an impact on food and water supplies, weather pattern, environmental conditions, and sea levels.Based on the National Oceanic and Atmospheric Administration (NOAA) Global Climate Summary, it stated that combined land and ocean temperature since 1880 has rose with an average rate of 0.07^0C per decade.

The temperature continues intensifying since 1981, with an average rate of 0.18^0C,

which is over twice as massive as previous times.This affects water supplies and brings changes on harvesting seasons. For example, climate change undermines coastal and marine regions with rising ocean levels, which raises demand for food crops. CO_2 also causes acid rain, which physically destroys trees Paoletti & Manes (2003) and the built environment(Cellura et al., 2018)(Kahl et al., 2006)

These effects of CO_2 emissions can be seen and felt now. They as well go beyond the rising global temperatures, which is harmfully affecting ecological systems and communities across the globe.

1.1.5 Sustainable Development Goals, Kenya Vision 2030 and The Big four Agenda.

The SDGs are set of global initiatives developed by UN which consists of 17 goals and 169 targets. Some SDGs are anchored on preceding Millennium Development Goals while others incorporate new ideas. Among the SDGs is Goal 13 on taking urgent action to combat climate change and its impacts(Hák et al., 2016).

In 2021, the global mean temperature recorded about 1.1^0C exceeding the pre-industrial level (from 1850 to 1900). As of 2015 to 2021 were the seven warmest years on record. The global annual mean temperature is projected to rise beyond 1.5^0C above pre-industrial levels in at least one of the next five years which is a worrying situation (Mitchell et al., 2017) (Slade, n.d.).

Climate finance gathered by developed countries amounted to $USD79.6billion$ in 2019, up from $USD78.3billion$ in 2018. It is approximated that $USD1.6trillion$ to $USD3.8$trillion will be needed each year through 2050 for the world to transition to a low-carbon future and avoid warming exceeding 1.5^0C (Mathur & Roy, 2021) .

About a third of global land areas will be affected by at least moderate drought by 2100. The sea level could rise by 30 to 60 centimetres by 2100, even with intense reduction in greenhouse gas emissions and global warming is limited to well below 2^0C.About 70 to 90 per cent of warm-water coral reefs will be vanished even with the achievement of 1.5^0C threshold; they would die off fully at the 2^0C level.3 billion to 3.6 billion people are vulnerable to climate change. By 2030, an estimated 700 million people will be at a danger of displacement by drought alone(of Economic & Affairs, 2022).

Kenya Vision 2030 is the country's development programme from 2008 to 2030. Its objective was to change Kenya into a middle-income country giving a high quality of life to all its citizens by 2030 in a clean and secure environment. Climate change has detrimental effects on Kenya's economic development and frustrates the actualization

of our Vision 2030 goals of forming a prosperous and competitive nation with a high quality of life.

Kenya's economy is greatly dependent on natural resources, meaning that recurring droughts, erratic rainfall patterns and floods will continue to contrary impact livelihoods and community assets. Kenya National Adaptation Plan illustrates Kenya's commitment to the Paris Agreement, to bring to life our vital responses to the impacts of climate change. Building climate tenacity in as low carbon as possible will ensure that Kenya contributes to the goals of the Paris Agreement and the Sustainable Development Goals(Kogo et al., 2021).

Projections of future climate patterns regarding temperature and precipitation indicate that Kenya's economy will remain vulnerable to their impacts.. Global Climate Modelling (GCM) data suggests that, in the 2030s, we can anticipate a rise in the average annual temperature ranging from 0.8^0C to 1.5^0C, with projections indicating a potential increase of 1.6^0C to 2.7^0C by the 2060s(Gebrechorkos et al., 2019).

Kenya Vision 2030 aimed for a series of five-year plans to achieve its goals. These included the First Medium Term Plan (MTP1) from 2008 to 2012, the Second Medium Term Plan (MTP2) spanning 2013 to 2017, and the Third Medium Term Plan (MTP3) covering 2018 to 2022. President Kenyatta recognized the need for a new approach to medium-term planning to expedite the realization of Vision 2030. To address this, he introduced the Big Four priorities, outlined in his Jamhuri Day Speech on December 12, 2017(Maobe, 2022).

These priorities, namely Food Security, Affordable Housing, Manufacturing, and Affordable Healthcare, were chosen to have a significant positive impact on the well-being of the Kenyan population. Importantly, each of these Big Four strategic areas aligns with at least one of the United Nations Sustainable Development Goals (SDG). Notably, the challenge of climate change directly affects food security by impacting agricultural production.(Munene, 2020).

1.1.6 Mathematical models.

The practice of employing mathematics to depict and address real-world challenges has its roots in ancient civilizations, notably the ancient Greeks. Figures such as Pythagoras, Euclid, and Archimedes played pivotal roles in advancing geometry and mathematical thought, thus establishing crucial underpinnings for subsequent developments in mathematical modeling (Cuomo, 2005).

The utilization of mathematical models to depict the release of CO_2 and its repercussions on the environment is a relatively recent advancement, primarily emerging during

the 20th century as concerns regarding climate change and global warming grew more pronounced. Identifying a sole originator or a precise inception date for this field is difficult, as it evolved organically and was shaped by numerous scientists, researchers, and institutions over the years (Yoro & Daramola, 2020).

A mathematical model is a tool that employs mathematical abstractions and a set of equations to depict real-world phenomena. To tackle the intricacies of reality, some simplifications and assumptions are often necessary when creating a model based on a real-life scenario. Essentially, a model serves as a means to examine the characteristics of a system and make predictions about its future behavior. In essence, a mathematical model offers an abstract representation of a tangible system using mathematical concepts and language, and this process of constructing such models is referred to as mathematical modeling (Develaki, 2020).

Models are built using different foundations depending on the question or problem they are designed to tackle. These models serve as representations of systems and facilitate the examination of system properties and, occasionally, the forecasting of future outcomes. Mathematical models can be classified into empirical, deterministic, stochastic, and mechanistic types. They are extensively employed in numerous scientific and technological fields, encompassing both the natural and social sciences. Their primary utility lies in modeling intricate systems, with a specific focus on living system (Kaiser et al., 2011).

Mathematical models offer a means to understand certain aspects of natural phenomena and forecast potential outcomes without the need for actual experiments. In contrast to the modeling of physical systems, scientists studying biological systems must account for the unique distinctions between living and non-living matter. Typically, systems involving non-living matter can be characterized using principles of conservation and invariance, with interactions between their components governed by the principles of quantum or classical mechanics (Develaki, 2020).

In contrast, the laws governing physical systems cannot be directly applied to living organisms due to their intricate internal complexity and the imperative of survival. Living entities exhibit complex behaviors such as respiration, consumption of food, self-defense against threats, and consequently, intricate processes involving the conversion of substances and energy occur within them. Throughout evolution,organisms have adapted and evolved new strategies for survival, including the ability to modify the functioning of their constituent elements and ultimately determining their reproduction or extinction based on prevailing conditions.

Mathematical modeling in chemistry is now a multidisciplinary field, requiring knowledge of both mathematics and chemistry. In chemistry, mathematical modeling helps

represent physical and chemical phenomena through mathematical equations, guiding the choice of model complexity. Chemical kinetic models link system properties (e.g., concentrations, pressure, temperature, electric potential) to the rates of species consumption or formation (Aris, 1999).
Mathematical modeling indeed plays a crucial role in climate research and is an effective tool for understanding and predicting the behavior of the climate system under various influences, including natural and anthropogenic perturbations. It remains a cornerstone of climate research and is essential for addressing the challenges posed by climate change. (Soldatenko et al., 2021).

1.1.7 Compartmental models

Compartmental model is a model that classifies individuals into different population groups or compartments based on certain characteristics, which are connected by the flow (migration or transformation) of individuals. This model is usually governed by nonlinear ordinary differential equations system that tracks the population as a function of time. Compartmental model is a framework where a system is looked as a set of compartments. It studies the flow of elements between these compartments and tries to understand the behavior. Each individual is one of the listed compartments in the model (Mandal et al., 2021).
The compartmental model provides a structural framework for viewing a system as a collection of distinct compartments. Its primary focus is to analyze the movement of elements between these compartments and gain insights into their behavior. Within this model, each individual is regarded as an integral part of the specified compartments (Mandal et al., 2021).

1.1.8 Chemical kinetics

Chemical kinetics, which is also referred to as reaction kinetics, is the field within physical chemistry that deals with the comprehension of how fast chemical reactions occur. The mathematical models we employ in this context are founded on a series of chemical reactions. Each reaction takes on a simple form that follows

$$A + B \xrightarrow{k} C + D \tag{1.1}$$

where A, B, C, and D are each chemical species in the reaction. Chemicals A and B are designated as the reactants as they engage in a reaction to produce C and D, known as the products, at a rate represented by 'k.' Since these kinetics involve the examination of rates of change, the reactions can be restructured and analyzed using a system of differential equations based on mass action principles.(Burkow et al., 2011).

1.1.9 Research Gap

Although numerous mathematical models have been developed to investigate Carbon (IV) Oxide emissions and climate change, most existing studies consider greenhouse gas emissions from a general perspective without explicitly modelling individual fossil fuels and their associated combustion mechanisms. Existing compartmental models largely describe the interactions between greenhouse gases and environmental factors without incorporating detailed chemical reaction kinetics. Similarly, many chemical kinetics studies investigate combustion reactions independently without integrating human activities and environmental dynamics into a unified mathematical framework.

Furthermore, relatively few studies simultaneously investigate qualitative analysis, bifurcation analysis, sensitivity analysis and optimal control within an integrated compartmental and chemical kinetics modelling framework. Consequently, there remains a need for a comprehensive mathematical model capable of describing the interactions among individual fossil fuels, human activities and Carbon (IV) Oxide emissions while providing analytical and numerical tools for evaluating effective emission mitigation strategies.

This study addresses these limitations by integrating compartmental modelling and nonlinear lumped chemical kinetics to investigate Carbon (IV) Oxide emission dynamics arising from individual fossil fuels and human activities.

1.2 Statement of the problem

Sustainable Development Goal (SDG) number 13, "Climate Action," specifically targets the reduction of greenhouse gas emissions, including carbon(iv) oxide. While the goal itself is focused on addressing emissions, there are still several gaps and challenges in achieving meaningful emissions reductions.Many countries' emission reduction targets are not aligned with the level of ambition required to limit global warming to well below 2 degrees Celsius above pre-industrial levels, as outlined in the Paris Agreement. These targets are often termed as inadequate to effectively mitigate climate change (Rogelj et al., 2016).

Achieving emissions reductions in certain sectors, such as heavy industry and transport industry, remains a significant challenge due to the limited availability of low-carbon technologies and the high cost of transitioning.Advancements in low-carbon and carbon capture technologies are essential for reducing emissions, but there are gaps in research, development, and deployment of these technologies, particularly in developing countries(Rogelj et al., 2016).

According to Mandal et al. (2021)diverse human activities involving sources of greenhouse gases and deforestation are major causes of the instability of nature. They estimated the approximate change in the atmospheric temperature and living beings near coastal areas because of frequent emissions of GHGs from different sources.A four compartmental model was formulated comprising G(t) and C(t) which represented the density of GHGs in the environment and the atmospheric temperature in degree celsius, respectively; whereas H(t) and E(t) was the number of human population and coverage areas of forest ecosystem near coastal areas, respectively, at time t.

They focused it generally and it is from this background that this study aims to formulate a deterministic model of emissions of CO_2 from individual fossil fuels and humans to understand the dynamics of the emissions of CO_2 .They considered coastal areas but we will approach it from global point of view.

According to Biswas et al. (2022)the effect of greenhouse gases (GHGs) is worldwide terrified anxiety to the public and scholars. Even this global problem is one of the great issues that continuously disturb the governments and environmentalists, but its solution findings are not out of the image at all. In this study, they proposed and analysed a mathematical model for the solvable management of GHGs by sowing the seeds of green building dynamic systems. Moreover, in the model, the human community is used to enhance the production power of individuals of green buildings by absorbing the GHGs.Although previous studies have contributed significantly to the understanding of greenhouse gas emissions and climate change, comparatively few have investigated Carbon (IV) Oxide emissions arising from individual fossil fuels together with human activities using an integrated compartmental and chemical kinetics modelling approach. Furthermore, limited attention has been devoted to combining qualitative analysis, numerical simulation, sensitivity analysis and optimal control within a single mathematical framework. These limitations motivate the development of the models presented in this study.

1.3 Research Objectives

1.3.1 Main objective

The main objective of this study was to model the emissions of Carbon(iv) Oxide from fossils and human activities using a compartmental model and chemical kinetics model.

1.3.2 Specific objectives

The specific objectives for the study are to;

1. To formulate a deterministic compartmental model describing the interactions among fossil fuels, human activities and Carbon (IV) Oxide emissions.
2. To investigate the qualitative properties of the compartmental model including positivity, boundedness, equilibrium points, local and global stability, bifurcation analysis and optimal control.
3. To formulate and analyse a nonlinear lumped chemical kinetics model describing Carbon (IV) Oxide production and removal dynamics.
4. To perform numerical simulations and sensitivity analysis in order to evaluate the influence of model parameters and identify effective Carbon (IV) Oxide emission mitigation strategies.

1.4 Scope of the Study

This study focuses on the mathematical modelling of Carbon (IV) Oxide emissions arising from fossil fuel combustion and human activities. The study develops deterministic compartmental and nonlinear lumped chemical kinetics models to describe the production, transformation and removal of Carbon (IV) Oxide. The analysis includes positivity, boundedness, equilibrium analysis, local and global stability, bifurcation analysis, sensitivity analysis and optimal control. Numerical simulations are performed using MATLAB to investigate the behaviour of the proposed models under different parameter values. Although climate change involves several greenhouse gases, this study is restricted to Carbon (IV) Oxide because of its dominant contribution to anthropogenic global warming.

1.5 Significance of the Study

The study of Carbon (IV) Oxide (CO_2) emissions from fossil fuels and human activities is critical to understanding the processes that contribute to global warming and climate change, and to identifying effective measures for mitigating their adverse effects. Mathematical models provide valuable insights into the complex interactions among human activities, fossil fuel consumption and Carbon (IV) Oxide emissions, thereby supporting the design of appropriate intervention strategies. Most existing mathematical models have investigated greenhouse gas emissions using generalized approaches (Mandal et al., 2021; Biswas et al., 2022; Burkow et al., 2011). In contrast, this study develops an integrated compartmental and nonlinear chemical kinetics modelling framework that explicitly considers individual fossil fuels and human activities in describing Carbon (IV) Oxide emission dynamics. The findings are therefore expected to contribute to both scientific knowledge and environmental policy formulation.

The significance of this study extends to several stakeholders, including government agencies, policy makers, environmental managers, researchers, industrial practitioners and future scholars.

1. **Government and Policy Makers**

   The proposed mathematical models provide quantitative tools that can assist government institutions and policy makers in evaluating the effectiveness of environmental policies aimed at reducing Carbon (IV) Oxide emissions. The findings may contribute to the formulation of sustainable policies on energy utilization, emission control, climate change mitigation and implementation of Sustainable Development Goal 13 (Climate Action).

2. **Environmental Protection Agencies**

   Environmental agencies responsible for monitoring greenhouse gas emissions may use the results of this study to improve their understanding of Carbon (IV) Oxide emission dynamics. The developed models can support environmental planning, emission forecasting and the evaluation of mitigation strategies such as afforestation, cleaner energy technologies and carbon capture initiatives.

3. **Researchers and the Scientific Community**

   This study contributes to the advancement of mathematical modelling by integrating deterministic compartmental modelling with nonlinear lumped chemical

kinetics. The developed framework provides a basis for future research in environmental modelling, climate science, combustion processes and applied mathematics. It also contributes to the growing body of knowledge on Carbon (IV) Oxide emission dynamics.

4. **Engineers and Industrial Practitioners**

   The results provide useful information on the contribution of individual fossil fuels to Carbon (IV) Oxide emissions and may assist engineers, industrial managers and energy planners in identifying cleaner production processes and improving combustion efficiency. The study also supports the development of technologies aimed at reducing industrial greenhouse gas emissions.

5. **Educational Institutions**

   The mathematical models, analytical techniques and numerical simulation procedures developed in this study provide useful teaching and research materials for universities and other institutions involved in mathematics, engineering, environmental science and climate change studies.

6. **Future Researchers**

   The modelling framework developed in this study provides a foundation for future investigations involving stochastic models, fractional-order differential equations, delay differential equations, spatially dependent models, machine learning approaches for parameter estimation and the inclusion of additional greenhouse gases. The study therefore opens several directions for further research in environmental mathematical modelling.

Overall, this study contributes to the understanding of Carbon (IV) Oxide emission dynamics by integrating compartmental modelling and nonlinear chemical kinetics within a unified mathematical framework. The analytical and numerical results are expected to support evidence-based decision making, enhance environmental management and contribute towards global efforts to mitigate climate change.

1.6 Method of Study

This study adopted a mathematical modelling approach to investigate the role of fossil fuels and human activities in Carbon (IV) Oxide (CO_2) emissions and global warming. Two complementary mathematical models were developed, namely a deterministic

compartmental model and a nonlinear lumped chemical kinetics model. The compartmental model was formulated using a system of nonlinear ordinary differential equations to describe the interactions among individual fossil fuels, human activities, Carbon (IV) Oxide emissions and atmospheric processes. The chemical kinetics model was formulated based on the law of mass action to investigate the production and removal dynamics of Carbon (IV) Oxide through combustion and atmospheric chemical reactions.

The qualitative properties of the compartmental model were investigated by establishing the positivity and boundedness of solutions, determining the equilibrium points, and analysing their local and global stability. The Jacobian matrix, eigenvalue analysis and Lyapunov stability theory were employed to determine the stability properties of the proposed model. Bifurcation analysis was also carried out to investigate the effects of parameter variation on the qualitative behaviour of the system.

The nonlinear lumped chemical kinetics model was analysed using the principles of chemical reaction kinetics and the law of mass action to describe the interaction among the selected fossil fuels, oxygen, Carbon (IV) Oxide, water vapour and carbonic acid. The resulting system of nonlinear ordinary differential equations was analysed theoretically and solved numerically to investigate the dynamics of Carbon (IV) Oxide production and removal.

Numerical simulations for both models were carried out using MATLAB to illustrate the analytical results and investigate the temporal behaviour of the state variables under different parameter values. Global sensitivity analysis was performed to determine the influence of the model parameters on Carbon (IV) Oxide emissions, while optimal control theory was employed to evaluate intervention strategies aimed at minimizing emissions arising from fossil fuel combustion and human activities.

The combined use of deterministic compartmental modelling, nonlinear chemical kinetics, qualitative analysis, numerical simulations, sensitivity analysis and optimal control provides a comprehensive framework for understanding Carbon (IV) Oxide emission dynamics and assessing effective climate change mitigation strategies.

CHAPTER 2

LITERATURE REVIEW

2.1 Introduction

This chapter reviews existing literature related to Carbon (IV) Oxide (CO_2) emissions, greenhouse gas dynamics, climate change, mathematical modelling, compartmental modelling and chemical kinetics. The review focuses on studies that have contributed to the development of mathematical models for understanding greenhouse gas emissions, global warming, carbon capture and climate mitigation strategies. Particular emphasis is placed on deterministic and nonlinear models, their analytical properties, numerical simulations and practical applications. The chapter also identifies the limitations of previous studies and establishes the research gap addressed by the present study.

Braddock et al. (1994) on the image greenhouse model as a mathematical system. In their paper, the authors introduced a mathematical representation of the Dutch IMAGE model, a widely recognized model of the enhanced greenhouse effect. This representation took the form of a dynamic system, where the main driving forces were human activities such as greenhouse gas emissions and land use changes. They showed that it was feasible to conduct a mathematical analysis of equilibrium and stability for this complex and nonlinear system. This analysis provided valuable insights into the environmental processes underlying the model.

Biswas et al. (2022) on Mathematical Model Applied to Green Building Concept for Sustainable Cities Under Climate Change.The study presented a mathematical model designed to manage and control greenhouse gases (GHGs) within green building systems. This model incorporated human involvement to enhance GHG absorption by occupants of green buildings. The authors extensively analyzed the model, assessing its stability at various equilibrium points, including trivial and global equilibriums, and provided evidence for the system's stability or instability. Furthermore, they used numerical simulations to illustrate how this model could impact the effectiveness of GHG reduction strategies.

Mandal et al. (2021) on a Mathematical Model to Investigate the Frequent Impact of Global Warming on Coastal Lives .The study introduced a mathematical model aimed at controlling greenhouse gases (GHGs) in green buildings, involving human participation to enhance GHG absorption. The researchers extensively analyzed the model,

evaluating its stability at various equilibrium points, including basic and overarching equilibriums, and provided evidence of its stability or instability. Furthermore, they used numerical simulations to illustrate how this model could affect the effectiveness of GHG reduction strategies.

Nkuturum et al. (2022) on mathematical modelling on the dynamics of climate change caused by carbon (iv) oxide emissions and their control measures.This study addressed the significance of carbon dioxide (CO_2) as a greenhouse gas in driving climate change. It developed a compartmental model using ordinary differential equations to explore how CO_2 emissions influence climate dynamics. The research also investigated the impact of control measures like awareness campaigns and environmental taxes. To analyze the model, the Differential Transformation Method (DTM) was used to approximate solutions for each component, and MATLAB R2007b was employed for numerical simulations. The results underscored the effectiveness of awareness campaigns and environmental taxes in reducing CO_2 emissions into the atmosphere.

Specht et al. (2016) on Mathematical model to calculate the sensitivity of anthropogenic CO_2 on global earth temperature, numerous climate models grapple with understanding the impact of human-induced CO_2 emissions on global temperatures due to their complexity. Simplified equations, akin to industrial furnace radiation exchange, assume a uniform Earth temperature and effectively model atmospheric temperature patterns. CO_2 acts as a heat-resistant barrier against outgoing long-wave radiation, requiring a 0.4 K temperature increase to compensate for doubled CO_2 levels. Human-generated CO_2 emissions have already elevated Earth's temperature by 0.2 K since 1860, with an additional 0.9 K attributed to CO_2-related effects. This suggests a future temperature increase surpassing 0.4 K, and the absence of CO_2 would render Earth 4 K colder.

Altamirano-Fernández et al. (2022) ,in their study aimed to understand the dynamics of carbon capture in fast-growing forest plantations, emphasizing their role in mitigating global warming. They developed a mathematical model, a tridimensional nonlinear system, incorporating variables such as living biomass, intrinsic biomass growth, and the impact of forestry fires on burned areas. Environmental humidity was treated as a parameter for simplicity. Using numerical approximations via the Runge-Kutta fourth-order method, they determined equilibria and their local stability, revealing that living biomass and stored carbon decline in each harvest cycle due to fire's adverse effects on soil. The model indicated that the maximum burned area occurs after reaching the peak biomass volume. Numerical simulations supported the model's validity, suggesting that preventing fires and soil fertilization are effective strategies to minimize biomass losses in subsequent regeneration cycles of fast-growing plantations.

Chang & Wang (2015) on Modelling and Computation in the Valuation of Carbon

Derivatives with Stochastic Convenience Yields, Anthropogenic greenhouse gas emissions have significantly increased in recent decades, contributing to climate change and global warming. To address this issue, carbon emission trading has emerged as a policy tool. While empirical research on carbon allowance and derivative prices exists, there is a shortage of theoretical results. In this paper, the authors develop a mathematical model for pricing CO_2 emission allowance derivatives with stochastic convenience yields, based on the absence of arbitrage opportunities. For American options, they transform the pricing problem into a linear parabolic variational inequality in two spatial dimensions and employ a power penalty method to solve it. They also create a fitted finite volume method to solve the resulting nonlinear partial differential equation, governing the valuation of futures, European, and American options. Numerical results demonstrate the method's efficiency and show that stochastic convenience yields impact the valuation of carbon emission derivatives. Sensitivity analyses are conducted to assess the effects of various parameters on valuation outcomes.

Cormos et al. (2010)on Techno-economical analysis of carbon dioxide absorption in mono-ethanolamine by mathematical modeling and simulation.This paper employs modeling and simulation to assess carbon dioxide absorption in MEA aqueous solutions within packed absorption columns, with the goal of implementing this technology in the power sector to mitigate greenhouse gas emissions. The mathematical model developed helps evaluate absorption rates and understand micro-level interactions in the column, encompassing mass and heat transfer processes and employing both ordinary and partial differential equations. MATLAB and ChemCAD software are used for modeling, shedding light on how absorption rates change as amine concentration decreases. The study also examines the evolution of process parameters like liquid and gas flows, composition, and temperatures. The paper emphasizes the analysis of techno-economic indicators, such as specific electricity, heat, and cooling consumption per kilogram of captured carbon dioxide, in advocating for the adoption of carbon dioxide absorption in MEA solutions to reduce greenhouse gas emissions, exemplified by an Integrated Gasification Combined Cycle (IGCC) case study.

Gaspar & Cormos (2012) on Dynamic modeling and absorption capacity assessment of CO_2 capture process .One of the most promising carbon dioxide capture technology is based on chemical gas–liquid absorption using alkanolamine solutions. In order to optimize the operating conditions of absorption–desorption cycle, the development of a detailed mathematical model was necessary. Several mass transfer and hydraulic correlation models were published in the literature, but study of predictive capacity for absorption process was required. The aims of this work were to check the mass transfer and hydraulic correlation models predictive capacity and to investigate the dynamic

behavior and absorption performance of four different type alkanolamine. The study showed that the implemented mathematical model reveals a good quality prediction of the absorption process for all alkanolamines. The analysis of simulation results highlighted that the mass transfer correlation model proposed by Wang et al. predicts well the effective mass transfer area and the mass transfer coefficient correlation. Model proposed by Billet and Schultes predicts well in case of MEA and DEA. And correlation model proposed by Rocha et al., predicts well in case of AMP and MDEA. The comparison of three hold up models show that the model proposed by Bravo et al. is capable to predict well this parameter in a wide column loading range.

Kong et al. (2019)on Second-generation stoichiometric mathematical model to predict methane emissions from oil sands tailings . Microbial metabolism of fugitive hydrocarbons produces greenhouse gas (GHG) emissions from oil sands tailings ponds (OSTP) and end pit lakes (EPL) that retain fluid tailings from surface mining of oil sands ores. Predicting GHG production, particularly methane (CH_4), would help oil sands operators mitigate tailings emissions and may assist regulators evaluating the trajectory of reclamation scenarios. Using empirical datasets from laboratory incubation of OSTP sediments with pertinent hydrocarbons, they developed a stoichiometric model for CH_4 generation by indigenous microbes. This model improved on previous first approximation models by considering long-term biodegradation kinetics for 18 relevant hydrocarbons from three different oil sands operations, lag times, nutrient limitations, and microbial growth and death rates. Laboratory measurements were used to estimate model parameter values and to validate the new model. Goodness of fit analysis showed that the stoichiometric model predicted CH_4 production well; normalized mean square error analysis revealed that it surpassed previous models. Comparison of model predictions with field measurements of CH_4 emissions further validated the new model.

Kumar et al. (2022) on Effects of greenhouse gases and hypoxia on the population of aquatic species: a fractional mathematical model Study of ecosystems has always been an interesting topic in the view of real-world dynamics. In their paper, they proposed a fractional-order nonlinear mathematical model to describe the prelude of deteriorating quality of water cause of greenhouse gases on the population of aquatic animals. In the proposed system, they recalled that greenhouse gases raise the temperature of water, and because of this reason, the dissolved oxygen level goes down, and also the rate of circulation of disintegrated oxygen by the aquatic animals rises, which causes a decrement in the density of aquatic species. they use a generalized form of the Caputo fractional derivative to describe the dynamics of the proposed problem. They also investigated equilibrium points of the given fractional-order model and discussed the asymptotic stability of the equilibria of the proposed autonomous model. They recalled

some important results to prove the existence of a unique solution of the model. For finding the numerical solution of the established fractional-order system, they applied a generalized predictor–corrector technique in the sense of proposed derivative and also justified the stability of the method. To express the novelty of the simulated results, they performed a number of graphs at various fractional-order cases. The given study was fully novel and useful for understanding the proposed real-world phenomena.

Bardos & Pironneau (2022) on Radiative transfer is at the heart of the mechanism to explain the greenhouse effect based on the partial infrared opacity of carbon dioxide, methane and other greenhouse gases in the atmosphere. In absence of thermal diffusion, the mathematical model consists of a first order integro-differential equation coupled with an integral equation for the light intensity and the temperature, in the atmosphere. They revisited this much studied system from a mathematical and numerical point of view. Existence and uniqueness and implicit solutions of the Milne problem for grey atmospheres are stated. Numerical simulations were given for grey and non-grey atmospheres and applied to calculate the effect of greenhouse gases. In the context of a transparent atmosphere for sunlight, it was found that by doubling the absorption coefficient in the infrared absorption range of CO_2 the temperature decreases by 2%. On the other hand, the same changes but in the low infrared range of the sunlight leads to an increase of temperature in the atmosphere. Several computer codes were written to cross-validate the results. The authors concluded that the radiative transfer model without thermal diffusion for an atmosphere transparent to the incident sunlight is not capable of explaining the greenhouse effect due to the greenhouse gases. A decreasing temperature due to an increasing proportion of CO_2 has been observed in the high atmosphere . In the lower atmosphere thermal diffusion and convection cannot be neglected and since the absorption coefficient are highly dependent on the temperature, a full ocean–atmosphere– biosphere climate model is required. Hence, driving conclusions from this study on climate change should be cautiously avoided and a review of the hypothesis of the radiative transfer argument commonly found in textbooks should be revisited.

Lv & Dang (2020) on Mathematical modeling of the reaction of metal oxides with methane. Methane reduction has attracted substantial interest in recent years because an abundant amount of natural gas has been found and methane possesses a strong reduction ability. However, due to the complexity of the reaction, the reductive-kinetics model has not been developed very well. This work reported a new mathematical model for methane reduction. The model was in a form of explicit functions incorporating many parameters to increase its precision. Particularly, it considered the comparison of methane cracking rate and reaction rate. Both the gas diffusion in the product layer and

chemical reaction. Controlled kinetics formulae were deduced by considering three kinds of shapes (spherical, cylindrical and lamellar) of particles. Also, by employing two parameters (shape coefficient Sc and equivalent diameter d0), the formulae for the same reduction mechanism could be unified to one formula, which was easier to use. The simulation of the model also considered both isothermal and non-isothermal processes of methane reduction. Furthermore, it could describe the reduction of oxides of varied-valence metals. The kinetics of reduction of metal oxides by methane agreed with the results obtained in the practical system.

Ogutu (2015) developed an energy balance mathematical model to study climate change through a reduced-complexity framework that integrates climate, economy, and biosphere interactions. The Coupled Climate-Economy-Biosphere (CoCEB) model adopts an integrated assessment approach, incorporating endogenous economic growth driven by physical and human capital accumulation. This enables the analysis of the sustainability of economic growth in the presence of increasing greenhouse gas emissions and their associated climate-induced economic damages. Unlike conventional integrated assessment models that treat mitigation costs as purely economic losses, this study considers mitigation efforts as productive investments that enhance energy efficiency and reduce carbon intensity. A key contribution of the study is the inclusion of land-use emissions and biotic carbon sinks, addressing a common limitation in many models that treat such emissions as exogenous. The findings indicate that investment in low-carbon technologies significantly reduces emissions and promotes long-term economic growth, while carbon capture and storage (CCS) shows diminishing returns at higher investment levels. Additionally, deforestation control contributes to emission reduction, though its economic impact is relatively modest. The study further highlights the sensitivity of results to cost parameter assumptions, emphasizing the importance of parameter selection in climate-economic modeling. Overall, the CoCEB model provides a simplified yet insightful framework for analyzing complex feedbacks between climate, economy, and biosphere systems.

Specht et al. (2016) proposed a simplified analytical model to evaluate the sensitivity of global temperature to anthropogenic CO_2 emissions. Recognizing the complexity of existing climate models, the study employs analytically tractable equations to describe the greenhouse effect by assuming a uniform Earth surface temperature. The model is based on radiation exchange principles analogous to those used in industrial furnace analysis, accounting for interactions between the Earth's surface, atmospheric gases, clouds, and space. The results demonstrated that atmospheric CO_2 acts as a radiative

barrier, increasing resistance to outgoing long-wave radiation and thereby raising surface temperature. Model validation using observed average Earth temperature shows that a doubling of atmospheric CO_2 concentration results in an approximate temperature increase of 0.4 K. Historical data indicate that anthropogenic CO_2 emissions have contributed about 0.2 K of warming since 1860, while the observed increase of approximately 0.9 K is attributed to additional feedback mechanisms. The study concludes that CO_2 plays a fundamental role in maintaining Earth's temperature, estimating that without it, global temperatures would be about 4 K lower.

Zenebe (2017) developed a mathematical model to investigate the effects of global climate change and decreasing forest cover on seasonal rainfall patterns. The study models global temperature and forest cover using logistic growth equations to capture long-term trends, while rainfall is represented as a periodic function through a second-order differential equation. This approach allows for the analysis of seasonal variability and extreme weather events such as droughts. The model incorporates predator-prey type interactions between forest cover, temperature, and rainfall, supported by correlation analysis. The findings highlight that rising global temperatures and declining forest cover significantly influence rainfall dynamics, emphasizing the interconnectedness of ecological and climatic systems.

Khasanov et al. (2020) presented a mathematical model describing the injection of carbon dioxide into a porous reservoir saturated with methane and its gas hydrate. The model incorporates both heat and mass transfer processes, as well as diffusion kinetics associated with the replacement of methane by CO_2 in gas hydrates. The study examines the effects of key parameters such as diffusion coefficient, reservoir permeability, and reservoir size on the dynamics of gas replacement. Results show that under conditions of high diffusion coefficients and low permeability, the replacement process occurs in a frontal regime dominated by filtration-driven mass transfer. Conversely, when diffusion is limited, the process is controlled primarily by gas diffusion within the hydrate structure. This work provides valuable insights into CO_2 sequestration technologies and their efficiency in mitigating atmospheric carbon emissions.

Collectively, these studies highlight the importance of mathematical modeling in understanding climate dynamics, carbon emissions, and mitigation strategies. They demonstrate the value of simplified and integrated models in capturing essential system interactions while addressing the limitations of highly complex models. Furthermore, they emphasize the critical role of parameter sensitivity, carbon sequestration mechanisms, and interdisciplinary approaches in developing effective climate change mitigation strategies.

Critical Analysis of Previous Studies

The reviewed studies demonstrate that mathematical modelling has become an indispensable tool for understanding greenhouse gas emissions, climate dynamics and mitigation strategies. Most of the models reviewed focus on a single aspect of the climate system, such as greenhouse gas transport, carbon capture, radiative transfer or combustion processes. Although these studies have significantly contributed to understanding individual processes, relatively few integrate fossil fuel combustion, human activities and atmospheric Carbon (IV) Oxide dynamics within a single mathematical framework.

Furthermore, many existing models emphasize either compartmental structures or chemical kinetics independently. Consequently, the combined influence of individual fossil fuels, combustion reactions and human activities on Carbon (IV) Oxide emissions has not been adequately investigated. These observations provide the motivation for the present study.

2.2 Research Gap

The reviewed literature demonstrates that considerable progress has been made in the application of mathematical modelling to greenhouse gas emissions, climate change, carbon capture, radiative transfer, and combustion processes. Existing studies have successfully employed deterministic, stochastic, fractional-order, and nonlinear mathematical models to investigate various aspects of greenhouse gas dynamics, environmental sustainability, and climate change mitigation (Braddock et al., 1994; Biswas et al., 2022; Mandal et al., 2021; Nkuturum et al., 2022; Specht et al., 2016).

Several studies have developed compartmental models to investigate the relationship between greenhouse gas emissions and climate dynamics. For instance, Mandal et al. (2021) formulated a compartmental model to investigate the impact of greenhouse gases on coastal ecosystems, while Biswas et al. (2022) proposed a mathematical model for green building systems aimed at reducing greenhouse gas concentrations. Similarly, Nkuturum et al. (2022) developed a deterministic compartmental model to investigate Carbon (IV) Oxide (CO_2) emissions and evaluate the effectiveness of awareness campaigns and environmental taxation as mitigation strategies. Although these studies provide important insights into greenhouse gas dynamics, they generally consider greenhouse gases collectively and do not explicitly model the contribution of individual fossil fuels to Carbon (IV) Oxide emissions. Furthermore, the combustion processes responsible for the generation of Carbon (IV) Oxide are not explicitly incorporated into

these compartmental modelling frameworks.

Considerable research has also been devoted to mathematical modelling of chemical reaction systems associated with carbon capture and combustion processes. Studies by Cormos et al. (2010), Gaspar & Cormos (2012), Kong et al. (2019), and Lv & Dang (2020) developed detailed chemical kinetics and reaction engineering models describing carbon capture, methane generation, and combustion processes. These studies significantly improved the understanding of reaction mechanisms, transport phenomena, and combustion dynamics. However, the developed models are primarily process-oriented and do not integrate combustion chemistry with human activities and environmental Carbon (IV) Oxide dynamics in a single mathematical framework. Consequently, their applicability in evaluating the combined effects of fossil fuel consumption, human activities and atmospheric Carbon (IV) Oxide emissions remains limited.

Other researchers have investigated Carbon (IV) Oxide emissions using climate models, radiative transfer models, carbon sequestration models and ecosystem models (Altamirano-Fernández et al., 2022; Bardos & Pironneau, 2022; Kumar et al., 2022; Ogutu, 2015; Zenebe, 2017; Khasanov et al., 2020). These studies demonstrate the usefulness of mathematical modelling in understanding climate dynamics and evaluating mitigation strategies. Nevertheless, many of these models focus on specific environmental processes such as biomass growth, forest fires, radiative transfer, methane replacement, or ecosystem interactions, without explicitly incorporating the production and removal dynamics of Carbon (IV) Oxide arising from individual fossil fuels and human activities.

A further limitation observed in the reviewed literature is that most studies concentrate on one modelling paradigm at a time. Models based on compartmental approaches rarely incorporate detailed combustion chemistry, while chemical kinetics models seldom include population dynamics, human activities, environmental interactions, or policy intervention mechanisms. Moreover, although several studies perform stability analysis and numerical simulations, comparatively few combine qualitative analysis, bifurcation analysis, global sensitivity analysis, and optimal control within an integrated modelling framework. This limits the ability of existing models to comprehensively investigate the combined influence of fossil fuel combustion and human activities on Carbon (IV) Oxide emission dynamics.

Therefore, despite the substantial contributions of previous studies, there remains a need for a comprehensive mathematical framework capable of integrating deterministic compartmental modelling with nonlinear lumped chemical kinetics in order to describe Carbon (IV) Oxide emissions arising from individual fossil fuels and human activities.

Such a framework should not only capture the combustion mechanisms responsible for Carbon (IV) Oxide production but also investigate the qualitative properties of the resulting models, including positivity, boundedness, equilibrium behaviour, local and global stability, bifurcation characteristics, sensitivity analysis and optimal control. Addressing these gaps provides a more comprehensive understanding of Carbon (IV) Oxide emission dynamics and offers quantitative tools for evaluating practical climate change mitigation strategies.

Accordingly, this study develops an integrated deterministic compartmental model together with a nonlinear lumped chemical kinetics model to investigate Carbon (IV) Oxide emission dynamics arising from individual fossil fuels and human activities. The study further performs qualitative mathematical analysis, numerical simulations, global sensitivity analysis and optimal control to provide scientific evidence that can support environmental planning, policy formulation and sustainable climate change mitigation.

Chapter Summary

This chapter has reviewed existing mathematical models related to greenhouse gas emissions, Carbon (IV) Oxide dynamics, climate change, carbon capture, compartmental modelling and chemical kinetics. The review has identified the strengths and limitations of previous studies and established the research gap addressed in this thesis. The next chapter presents the formulation of the proposed deterministic compartmental and nonlinear lumped chemical kinetics models together with the analytical methods employed in their investigation.

CHAPTER 3

MODEL FORMULATION AND ANALYSIS

3.1 Introduction

This chapter presents the formulation and mathematical analysis of the models developed to investigate the dynamics of Carbon (IV) Oxide (CO_2) emissions arising from fossil fuel combustion and human activities. Two complementary modelling approaches are considered. The first is a deterministic compartmental model that describes the interactions among human populations, fossil fuels, vegetation and atmospheric Carbon (IV) Oxide. The second is a nonlinear lumped chemical kinetics model describing the production and removal of Carbon (IV) Oxide through combustion and atmospheric chemical reactions.

The compartmental model is formulated using systems of nonlinear ordinary differential equations based on the principles of conservation of mass and population dynamics. The chemical kinetics model is derived using the law of mass action and effective reaction mechanisms. The qualitative properties of the proposed models are subsequently investigated through positivity, boundedness, equilibrium analysis, local and global stability, bifurcation analysis, sensitivity analysis and numerical simulations. These analyses provide a comprehensive framework for understanding Carbon (IV) Oxide emission dynamics and evaluating potential climate change mitigation strategies.

3.2 Model Description

The mathematical framework developed in this study consists of two complementary models for investigating Carbon (IV) Oxide (CO_2) emission dynamics. The first model is a deterministic compartmental model that describes the interactions among human activities, fossil fuel consumption, vegetation and atmospheric Carbon (IV) Oxide. The second model is a nonlinear lumped chemical kinetics model that describes the production and removal of Carbon (IV) Oxide through combustion, photosynthesis and carbonic acid formation.

The deterministic compartmental model is represented by eight state variables. The variable $H(t)$ represents the human population, while $R(t)$ represents the population of licensed drivers. The variable $F(t)$ represents vegetation or plant cover, which provides a natural mechanism for removing atmospheric Carbon (IV) Oxide through

photosynthesis. The variables $O(t)$, $L(t)$, $P(t)$ and $D(t)$ represent the quantities of kerosene, liquefied petroleum gas (LPG), petrol and diesel, respectively. Finally, $C(t)$ represents the concentration of atmospheric Carbon (IV) Oxide.

The model assumes that the human population is affected by recruitment, natural removal and movement into the licensed-driver compartment. Interactions between human activities and vegetation are represented by the terms involving H and F. Vegetation is replenished through its natural input and is enhanced by the presence of atmospheric Carbon (IV) Oxide through the term involving $\rho_2 FC$. At the same time, vegetation is reduced through interactions with human activities and through its natural removal rate.

The fossil fuel compartments represent the availability or consumption of the selected fuels within the model. The terms involving $\pi_3 M(1 - M/K_2)$ represent the supply of fossil fuels, with the parameters a_1, a_2 and a_3 determining the allocation of the supply among kerosene, LPG and petrol, respectively. The remaining fraction,

$$1 - a_1 - a_2 - a_3,$$

is allocated to diesel. Fossil fuel consumption by human activities and licensed drivers is represented by the corresponding interaction terms in the model.

Carbon (IV) Oxide is produced through the combustion and consumption of the different fossil fuels and through other anthropogenic activities. The production terms are represented by $\omega_3 HF$, $\alpha_2 HO$, $\phi_2 HL$, $\theta_2 RP$, $\beta_2 RD$, $\delta_2 HF$, $\varepsilon_2 RL$ and $\gamma_2 RO$. The removal of Carbon (IV) Oxide by vegetation through photosynthesis is represented by the term $\rho_1 FC$. Thus, the Carbon (IV) Oxide compartment provides an important link between human activities, fossil fuel consumption and natural environmental removal.

The interactions among these compartments result in a system of nonlinear ordinary differential equations. The nonlinearities arise primarily from the logistic terms describing population and fuel supply, together with the interaction terms involving products of state variables. The resulting system therefore provides a framework for investigating the temporal dynamics of Carbon (IV) Oxide emissions and for determining the conditions under which the system remains bounded and stable.

In addition to the compartmental model, a nonlinear lumped chemical kinetics model is developed to provide a more detailed description of the chemical processes responsible for Carbon (IV) Oxide production and removal. The chemical kinetics model incorporates the combustion of selected fossil fuels, photosynthesis and the formation of carbonic acid. The model is formulated using the law of mass action and the stoichiometric relationships of the reactions considered in the study.

The two modelling approaches are complementary. The compartmental model provides a macroscopic representation of the interactions among human activities, fossil fuels, vegetation and atmospheric Carbon (IV) Oxide, whereas the chemical kinetics model provides a mechanistic description of the underlying chemical processes. Their combined use enables the study to investigate Carbon (IV) Oxide emission dynamics from both environmental and chemical perspectives.

3.3 Model Formulation

This study develops two complementary mathematical models to describe the dynamics of Carbon (IV) Oxide emissions arising from fossil fuel combustion and human activities. The first model is a deterministic compartmental model that captures the interactions among the human population, fossil fuel consumption, vegetation and atmospheric Carbon (IV) Oxide. The second model is a nonlinear lumped chemical kinetics model that describes the production and removal of Carbon (IV) Oxide through combustion reactions and atmospheric processes.

The compartmental model consists of two interacting human populations, namely the general human population (H) and licensed drivers (R). Four fossil fuel compartments are incorporated to represent kerosene (O), liquefied petroleum gas (L), petrol (P) and diesel (D). The remaining compartments represent plants (F), which remove Carbon (IV) Oxide through photosynthesis, and atmospheric Carbon (IV) Oxide (C), which accumulates through combustion and other anthropogenic activities. The interactions among these compartments are represented using a system of nonlinear ordinary differential equations.

3.3.1 Model variables and parameters.

Table 3.1: Definition of variables

Variable	Description
H	Human population at time t
R	Drivers at time t
O	Others (use kerosene to represent them) at time t
L	Liquid petroleum gases at time t
P	Petrol
D	Diesel
F	Plants
C	Atmospheric carbon(iv) oxide

Table 3.2: Definition of parameters.

Parameter	Description
Ψ	Production rate of CO_2 through respiration ofhumans
Γ	Production rate of CO_2 through interaction of humans and kerosene
γ	Production rate of CO_2 through interaction of drivers and kerosene
ϕ	Production rate of CO_2 through interaction of humans and liquid petroleum gases
ε	Production rate of CO_2 through interaction of drivers and liquid petroleum gases
θ	Production rate of CO_2 through interaction of drivers and petrol
β	Production rate of CO_2 through interaction of drivers and diesel
π_F	Recruitment rate of plants
π_O	Recruitment rate of kerosene
π_L	Recruitment rate of liquid petroleum gases
π_P	Recruitment rate of petrol
π_D	Recruitment rate of diesel
ρ	Absorption rate of CO_2 by plants
ω	Consumption rate of plants by animals
δ	Production rate of CO_2 through interaction of humans and plants
η	Absorption rate of CO_2 in the rain
λ	Recruitment rate of drivers
μ	Natural death rate of humans,drivers and plants

3.3.2 Assumptions of the compartmental model

The following assumptions were made to formulate the compartmental model

1. Advection and diffusion of CO_2 in the atmosphere is insignificant.
2. Population recruitment is mainly dependent on plants as the primary source of food.
3. The only source of depletion of fuels is through combustion.
4. Plants recruitment is solely dependent on CO_2 without which they will be depleted because during photosynthesis, carbon dioxide is a crucial reactant that gives glucose molecules carbon and oxygen.
5. The recruitment of CO_2 from other sources and other means of its absorptions are negligible.
6. All humans are involved in CO_2 related activities.
7. Diesel and petrol are used only by drivers who are the people trained to use locomotives.

8. The concentration of carbon (iv) oxide will follow chemical kinetics equations.
9. The carbon (iv) oxide produced by animals is considered to be insignificant.
10. The carbon (iv) oxide produced by volcanic eruptions is insignificant.

3.3.3 Model Framework

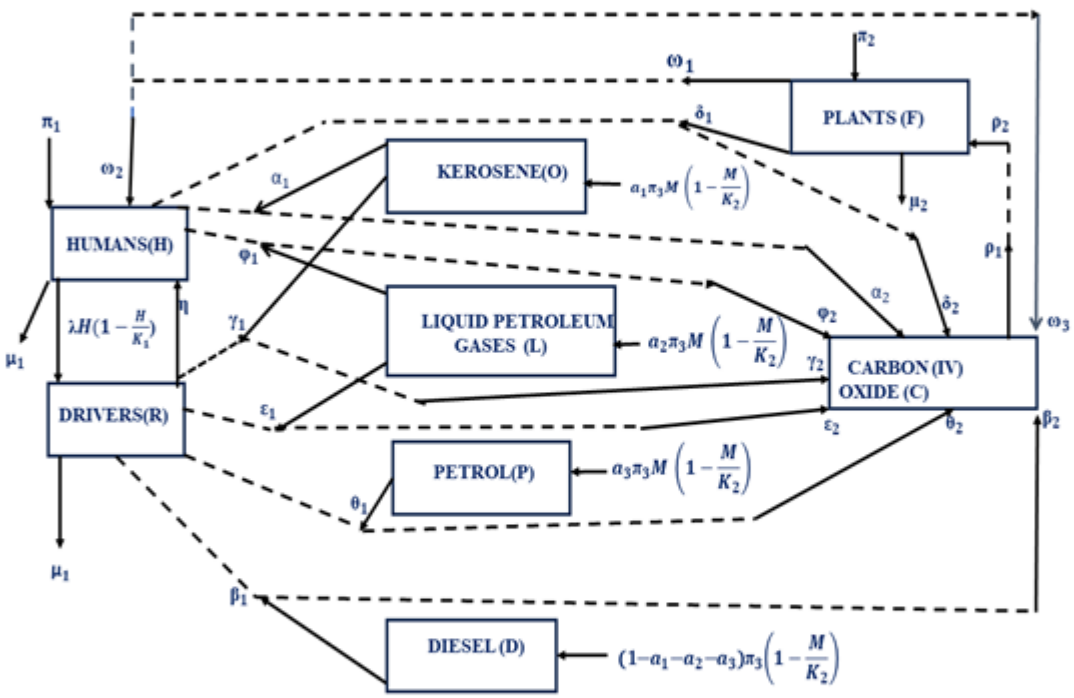

Figure 3.1: Model Framework

3.3.4 Model equations

The deterministic compartmental model is given by the following system of nonlinear ordinary differential equations:

$$\begin{cases} \dfrac{dH}{dt} = \pi_1 + \omega_2 HF + \eta R - \mu_1 H - \lambda H\left(1 - \dfrac{H}{K_1}\right), \\ \dfrac{dR}{dt} = \lambda H\left(1 - \dfrac{H}{K_1}\right) - \eta R - \mu_1 R, \\ \dfrac{dF}{dt} = \pi_2 + \rho_2 FC - \omega_1 HF - \delta_1 HF - \mu_2 F, \\ \dfrac{dO}{dt} = a_1\pi_3 M\left(1 - \dfrac{M}{K_2}\right) - \alpha_1 HO - \gamma_1 RO, \\ \dfrac{dL}{dt} = a_2\pi_3 M\left(1 - \dfrac{M}{K_2}\right) - \phi_1 HL - \varepsilon_1 RL, \\ \dfrac{dP}{dt} = a_3\pi_3 M\left(1 - \dfrac{M}{K_2}\right) - \theta_1 RP, \\ \dfrac{dD}{dt} = (1 - a_1 - a_2 - a_3)\pi_3 M\left(1 - \dfrac{M}{K_2}\right) - \beta_1 RD, \\ \dfrac{dC}{dt} = \omega_3 HF + \alpha_2 HO + \phi_2 HL + \theta_2 RP + \beta_2 RD + \delta_2 HF + \varepsilon_2 RL + \gamma_2 RO - \rho_1 FC. \end{cases} \tag{3.1}$$

The system in (3.1) describes the interactions among the human population, licensed drivers, vegetation, fossil fuels and atmospheric Carbon (IV) Oxide.

3.3.5 Methods for Analysing the Compartmental Model

The qualitative behaviour of the compartmental model was investigated using standard techniques in the theory of nonlinear ordinary differential equations. The positivity and boundedness of solutions were established to demonstrate that the model is mathematically and biologically meaningful. Equilibrium points were obtained by setting the right-hand side of the governing system equal to zero.

Local stability of the equilibrium points was investigated using the Jacobian matrix and eigenvalue analysis, while global stability was established using Lyapunov stability theory together with LaSalle's Invariance Principle where applicable. Bifurcation analysis was performed to investigate qualitative changes in the behaviour of the system arising from parameter variations.

Numerical simulations of the proposed model were carried out in MATLAB us-

ing the `ode45` solver to illustrate the analytical results and investigate the temporal behaviour of the state variables under different parameter values.

3.4 Chemical Kinetics Model

While the deterministic compartmental model provides a macroscopic description of the interactions among human activities, fossil fuel consumption and Carbon (IV) Oxide (CO_2) emissions, it does not explicitly describe the chemical processes responsible for the formation and removal of Carbon (IV) Oxide during combustion and atmospheric reactions. To complement the compartmental approach, this study develops a nonlinear lumped chemical kinetics model based on the fundamental principles of chemical reaction kinetics.

Chemical kinetics is concerned with the rates at which chemical reactions occur and the mechanisms through which reactants are converted into products. In combustion processes, different fossil fuels react with oxygen to produce Carbon (IV) Oxide, water vapour and thermal energy. The rate of production of these products depends on the nature of the fuel, reactant concentrations and the corresponding reaction-rate coefficients. Consequently, chemical kinetics provides an appropriate framework for quantifying Carbon (IV) Oxide production arising from the combustion of commonly used fossil fuels.

In this study, the chemical kinetics model considers four major fossil fuels, namely kerosene, liquefied petroleum gas (LPG), petrol and diesel, together with oxygen, Carbon (IV) Oxide, water vapour, glucose and carbonic acid. These species were selected because they represent the principal reactants and products involved in combustion, photosynthesis and atmospheric Carbon (IV) Oxide sequestration. The model also incorporates photosynthesis as a natural Carbon (IV) Oxide removal mechanism and carbonic acid formation as a physicochemical process through which Carbon (IV) Oxide is absorbed into rainwater.

The model is formulated using the principle of mass conservation and the law of mass action. Under this principle, the rate of each reaction is assumed to be proportional to the product of the concentrations of the reacting species raised to their respective stoichiometric coefficients. Since the study investigates the overall dynamics of Carbon (IV) Oxide emissions rather than detailed elementary reaction mechanisms, the combustion processes are represented using effective lumped reactions. This approach reduces mathematical complexity while preserving the dominant pathways governing Carbon (IV) Oxide production and removal.

The effective reaction network considered in this study is presented in the following subsection and forms the basis for deriving the nonlinear system of ordinary differential equations describing the chemical kinetics model.

3.4.1 Assumptions of the Chemical Kinetics Model

The formulation of the nonlinear lumped chemical kinetics model is based on the following assumptions:

1. The reaction system is assumed to be homogeneous, such that the reacting species are sufficiently well mixed and their concentrations are spatially uniform within the modelled system.

2. The selected fossil fuels, namely kerosene, liquefied petroleum gas (LPG), petrol and diesel, are represented by their respective representative hydrocarbon compounds. This provides a tractable representation of the combustion processes while retaining the dominant Carbon (IV) Oxide (CO_2) production pathways.

3. The combustion reactions are assumed to proceed according to the stoichiometric relationships specified in the reaction scheme. The stoichiometric coefficients are therefore used to determine the corresponding rates of consumption of reactants and production of products.

4. The rates of the chemical reactions are governed by the law of mass action. Consequently, the rate of each reaction is expressed as a function of the concentrations of the reacting species and the corresponding reaction-rate constant.

5. The reaction-rate constants are assumed to remain constant during a particular simulation. Effects of temperature variation on the reaction-rate constants are therefore not explicitly modelled unless otherwise stated.

6. Oxygen is assumed to be available as a reactant for the combustion processes. Its consumption is represented through the stoichiometric coefficients of the corresponding combustion reactions.

7. The combustion of the selected fossil fuels produces Carbon (IV) Oxide and water as the principal products considered in the model. Other minor combustion products and intermediate reaction species are not explicitly represented.

8. The detailed elementary reaction mechanisms of fossil-fuel combustion are lumped into effective overall reactions. This assumption reduces the complexity

of the model while retaining the principal pathways responsible for Carbon (IV) Oxide production.

9. Photosynthesis is represented as a Carbon (IV) Oxide removal mechanism. The conversion of Carbon (IV) Oxide and water into glucose and oxygen is represented by the corresponding overall photosynthetic reaction.

10. The formation of carbonic acid is represented by the reversible reaction between Carbon (IV) Oxide and water. This provides a simplified representation of the dissolution and chemical transformation of Carbon (IV) Oxide in atmospheric water.

11. The concentrations of all chemical species are assumed to remain non-negative throughout the evolution of the system. Consequently, the model is formulated in the non-negative region of the state space.

12. The system is assumed to be closed with respect to the chemical species explicitly included in the model, except for the specified input and removal processes. Unmodelled external sources and sinks are not explicitly represented.

13. The effects of spatial variation, atmospheric circulation, diffusion and transport are not explicitly considered. The model therefore focuses on the temporal dynamics of the selected chemical species.

14. Temperature, pressure and other environmental conditions are assumed to remain sufficiently constant over the period considered so that the effective reaction-rate parameters can be treated as constant.

15. The chemical kinetics model is intended to describe the dominant Carbon (IV) Oxide production and removal pathways rather than the complete atmospheric chemistry of Carbon (IV) Oxide.

3.4.2 Chemical Species and Their Representation

The chemical kinetics model considers the principal chemical species involved in the combustion, photosynthesis and Carbon (IV) Oxide sequestration processes. Table 3.3 presents the symbols used to represent the chemical species considered in the model and their corresponding names.

Table 3.3: Chemical species considered in the chemical kinetics model

Symbol	Meaning
C_3H_8	Propane
C_8H_{18}	Octane
$C_{10}H_{22}$	Decane
$C_{12}H_{26}$	Dodecane
O_2	Oxygen
CO_2	Carbon (IV) Oxide
H_2O	Water
H_2CO_3	Carbonic acid
$C_6H_{12}O_6$	Glucose

3.4.3 Application of the Law of Mass Action

The rates of the chemical reactions considered in this study are determined using the law of mass action. According to this principle, the rate of an elementary reaction is proportional to the product of the concentrations of the reacting species, with each concentration raised to a power corresponding to its stoichiometric coefficient. Thus, for a general reaction of the form

$$aA + bB \longrightarrow cC + dD, \tag{3.2}$$

the corresponding reaction rate can be written as

$$r = k[A]^a[B]^b, \tag{3.3}$$

where r is the reaction rate, k is the reaction-rate constant, and $[A]$ and $[B]$ denote the concentrations of the reactants A and B, respectively.

For example, for the combustion reaction

$$2C_{10}H_{22} + 31O_2 \longrightarrow 20CO_2 + 22H_2O, \tag{3.4}$$

the corresponding rate expression under the mass-action formulation is

$$r_1 = k_1[C_{10}H_{22}]^2[O_2]^{31}. \tag{3.5}$$

The stoichiometric coefficients determine the corresponding rates of consumption and production of the chemical species. Consequently, the rate of change of each species is obtained by multiplying the reaction rate by its stoichiometric coefficient, with a

negative sign for reactants and a positive sign for products. Applying this procedure to each reaction in the reaction scheme gives the nonlinear system of ordinary differential equations governing the chemical kinetics model.

3.4.4 Reaction Scheme

The effective reaction network considered in this study is

$$\begin{aligned} 2C_{10}H_{22} + 31O_2 &\longrightarrow 20CO_2 + 22H_2O, \\ C_3H_8 + 5O_2 &\longrightarrow 3CO_2 + 4H_2O, \\ 2C_8H_{18} + 25O_2 &\longrightarrow 16CO_2 + 18H_2O, \\ 2C_{12}H_{26} + 37O_2 &\longrightarrow 24CO_2 + 26H_2O, \\ C_6H_{12}O_6 + 6O_2 &\longrightarrow 6CO_2 + 6H_2O, \\ 6CO_2 + 6H_2O &\longrightarrow C_6H_{12}O_6 + 6O_2, \\ CO_2 + H_2O &\rightleftharpoons H_2CO_3. \end{aligned} \tag{3.6}$$

The reaction scheme in (3.6) describes the principal combustion, photosynthesis and carbonic acid formation processes considered in the chemical kinetics model. These reactions are interpreted as effective lumped pathways rather than elementary molecular reactions.

3.4.5 State Variables

The model consists of nine interacting state variables

$$K(t),\ O(t),\ C(t),\ W(t),\ L(t),\ P(t),\ D(t),\ G(t),\ H(t),$$

representing kerosene, oxygen, carbon dioxide, water vapour, liquefied petroleum gas (LPG), petrol, diesel, glucose and carbonic acid, respectively.

3.4.6 Model Parameters

Two classes of parameters are considered.

The first class consists of effective reaction-rate coefficients

$$k_1, k_2, \ldots, k_7,$$

which characterize the principal combustion and natural carbon-removal processes.

The second class consists of continuous input parameters

$$\Lambda_K,\ \Lambda_O,\ \Lambda_L,\ \Lambda_P,\ \Lambda_D,$$

together with natural loss coefficients

$$\mu_K,\ \mu_O,\ \mu_C,\ \mu_W,\ \mu_L,\ \mu_P,\ \mu_D,\ \mu_G,\ \mu_H.$$

3.4.7 Governing Differential Equations

Applying the principle of mass conservation together with the effective reaction-rate laws yields the following system of nonlinear ordinary differential equations:

$$\begin{cases} \dfrac{dK}{dt} = \Lambda_K - k_1 KO - \mu_K K, \\ \dfrac{dO}{dt} = \Lambda_O - 31k_1 KO - 5k_2 LO - 25k_3 PO - 37k_4 DO - 6k_5 GO + 6k_6 CW - \mu_O O, \\ \dfrac{dC}{dt} = 20k_1 KO + 3k_2 LO + 16k_3 PO + 24k_4 DO + 6k_5 GO - 6k_6 CW - k_7 CW - \mu_C C, \\ \dfrac{dW}{dt} = 22k_1 KO + 4k_2 LO + 18k_3 PO + 26k_4 DO + 6k_5 GO - 6k_6 CW - k_7 CW - \mu_W W, \\ \dfrac{dL}{dt} = \Lambda_L - k_2 LO - \mu_L L, \\ \dfrac{dP}{dt} = \Lambda_P - k_3 PO - \mu_P P, \\ \dfrac{dD}{dt} = \Lambda_D - k_4 DO - \mu_D D, \\ \dfrac{dG}{dt} = k_6 CW - k_5 GO - \mu_G G, \\ \dfrac{dH}{dt} = k_7 CW - \mu_H H. \end{cases} \tag{3.7}$$

3.4.8 Initial Conditions

The system is supplemented with non-negative initial conditions

$$
\begin{aligned}
K(0) &= K_0 > 0, \\
O(0) &= O_0 > 0, \\
C(0) &= C_0 > 0, \\
W(0) &= W_0 > 0, \\
L(0) &= L_0 > 0, \\
P(0) &= P_0 > 0, \\
D(0) &= D_0 > 0, \\
G(0) &= G_0 > 0, \\
H(0) &= H_0 \geq 0.
\end{aligned}
\tag{3.8}
$$

3.4.9 Vector Form

Define the state vector

$$\mathbf{X}(t) = (K, O, C, W, L, P, D, G, H)^T.$$

The governing system can be written compactly as

$$\boxed{\frac{d\mathbf{X}}{dt} = \mathbf{F}(\mathbf{X}),}$$

where

$$\mathbf{F} : \mathbb{R}^9_+ \to \mathbb{R}^9$$

is continuously differentiable.

The proposed model forms the basis for the theoretical analysis presented in the subsequent section. The inclusion of continuous input and natural loss processes guarantees the existence of a biologically and chemically meaningful positive equilibrium, thereby facilitating rigorous positivity, boundedness, stability and sensitivity analyses.

3.4.10 Nondimensionalization

To facilitate mathematical analysis and improve numerical stability, the governing system is transformed into dimensionless form. The transformation reduces the number of independent parameters and highlights the relative importance of the dominant physical and chemical processes.

Let

$$K_0,\ O_0,\ C_0,\ W_0,\ L_0,\ P_0,\ D_0,\ G_0,\ H_0$$

be characteristic reference concentrations of the corresponding chemical species. Furthermore, let

$$t_c = \frac{1}{k_1 O_0}$$

denote the characteristic time associated with kerosene combustion.

The dimensionless variables are defined as

$$\begin{aligned} x_1 &= \frac{K}{K_0}, \quad x_2 = \frac{O}{O_0}, \quad x_3 = \frac{C}{C_0}, \\ x_4 &= \frac{W}{W_0}, \quad x_5 = \frac{L}{L_0}, \quad x_6 = \frac{P}{P_0}, \\ x_7 &= \frac{D}{D_0}, \quad x_8 = \frac{G}{G_0}, \quad x_9 = \frac{H}{H_0}. \end{aligned} \tag{3.9}$$

The dimensionless time variable is

$$\tau = \frac{t}{t_c}.$$

Applying the chain rule,

$$\frac{d}{dt} = \frac{1}{t_c}\frac{d}{d\tau}.$$

Substituting these transformations into Equations (**??**)–(**??**) and dividing each equation by its corresponding reference concentration yields the normalized system.

3.4.11 Dimensionless Parameters

For convenience, the following dimensionless parameter groups are introduced:

$$\begin{aligned} \alpha_2 &= \frac{k_2 L_0}{k_1 K_0}, \quad \alpha_3 = \frac{k_3 P_0}{k_1 K_0}, \qquad \alpha_4 = \frac{k_4 D_0}{k_1 K_0}, \\ \alpha_5 &= \frac{k_5 G_0}{k_1 K_0}, \quad \alpha_6 = \frac{k_6 C_0 W_0}{k_1 K_0 O_0}, \quad \alpha_7 = \frac{k_7 C_0 W_0}{k_1 K_0 O_0}, \end{aligned} \tag{3.10}$$

together with the normalized inflow parameters

$$\begin{aligned} \beta_K &= \frac{\Lambda_K}{k_1 K_0 O_0}, \quad \beta_O = \frac{\Lambda_O}{k_1 K_0 O_0}, \\ \beta_L &= \frac{\Lambda_L}{k_1 K_0 O_0}, \quad \beta_P = \frac{\Lambda_P}{k_1 K_0 O_0}, \quad \beta_D = \frac{\Lambda_D}{k_1 K_0 O_0}, \end{aligned} \tag{3.11}$$

and the dimensionless natural loss coefficients

$$\begin{aligned} \delta_K &= \frac{\mu_K}{k_1 O_0}, \quad \delta_O = \frac{\mu_O}{k_1 O_0}, \quad \delta_C = \frac{\mu_C}{k_1 O_0}, \\ \delta_W &= \frac{\mu_W}{k_1 O_0}, \quad \delta_L = \frac{\mu_L}{k_1 O_0}, \quad \delta_P = \frac{\mu_P}{k_1 O_0}, \\ \delta_D &= \frac{\mu_D}{k_1 O_0}, \quad \delta_G = \frac{\mu_G}{k_1 O_0}, \quad \delta_H = \frac{\mu_H}{k_1 O_0}. \end{aligned} \tag{3.12}$$

Table 3.4: Baseline dimensionless parameter values used in the numerical simulations.

Parameter	Value	Description
α_2	0.70	LPG combustion coefficient
α_3	0.85	Petrol combustion coefficient
α_4	0.80	Diesel combustion coefficient
α_5	0.15	Biological oxidation coefficient
α_6	0.25	Photosynthesis coefficient
α_7	0.08	Carbonic acid formation coefficient
β_K	0.60	Kerosene inflow
β_O	4.50	Oxygen replenishment
β_L	0.40	LPG inflow
β_P	0.70	Petrol inflow
β_D	0.55	Diesel inflow
δ_K	0.05	Natural loss of kerosene
δ_O	0.03	Natural loss of oxygen
δ_C	0.04	Natural loss of carbon dioxide
δ_W	0.04	Natural loss of water vapour
δ_L	0.05	Natural loss of LPG
δ_P	0.05	Natural loss of petrol
δ_D	0.05	Natural loss of diesel
δ_G	0.03	Natural loss of glucose
δ_H	0.02	Natural loss of carbonic acid

3.4.12 Dimensionless Model

The normalized nonlinear lumped chemical kinetics model is therefore given by the following system of nonlinear ordinary differential equations:

$$
\begin{cases}
\dfrac{dx_1}{d\tau} = \beta_K - x_1x_2 - \delta_K x_1, \\
\dfrac{dx_2}{d\tau} = \beta_O - 31x_1x_2 - 5\alpha_2x_5x_2 - 25\alpha_3x_6x_2 - 37\alpha_4x_7x_2 - 6\alpha_5x_8x_2 + 6\alpha_6x_3x_4 - \delta_O x_2, \\
\dfrac{dx_3}{d\tau} = 20x_1x_2 + 3\alpha_2x_5x_2 + 16\alpha_3x_6x_2 + 24\alpha_4x_7x_2 + 6\alpha_5x_8x_2 - 6\alpha_6x_3x_4 - \alpha_7x_3x_4 - \delta_C x_3, \\
\dfrac{dx_4}{d\tau} = 22x_1x_2 + 4\alpha_2x_5x_2 + 18\alpha_3x_6x_2 + 26\alpha_4x_7x_2 + 6\alpha_5x_8x_2 - 6\alpha_6x_3x_4 - \alpha_7x_3x_4 - \delta_W x_4, \\
\dfrac{dx_5}{d\tau} = \beta_L - \alpha_2x_5x_2 - \delta_L x_5, \\
\dfrac{dx_6}{d\tau} = \beta_P - \alpha_3x_6x_2 - \delta_P x_6, \\
\dfrac{dx_7}{d\tau} = \beta_D - \alpha_4x_7x_2 - \delta_D x_7, \\
\dfrac{dx_8}{d\tau} = \alpha_6x_3x_4 - \alpha_5x_8x_2 - \delta_G x_8, \\
\dfrac{dx_9}{d\tau} = \alpha_7x_3x_4 - \delta_H x_9.
\end{cases}
\tag{3.13}
$$

The dimensionless system in (3.13) forms the basis for all subsequent theoretical and numerical investigations. The inclusion of normalized inflow and natural loss terms guarantees the existence of a non-trivial positive equilibrium under suitable parameter conditions, thereby enabling rigorous analyses of positivity, boundedness, equilibrium, local stability and global sensitivity.

Table 3.5: Dimensionless initial conditions used for numerical simulations.

Variable	Initial value
$x_1(0)$	0.80
$x_2(0)$	1.00
$x_3(0)$	0.50
$x_4(0)$	0.50
$x_5(0)$	0.60
$x_6(0)$	0.70
$x_7(0)$	0.55
$x_8(0)$	0.20
$x_9(0)$	0.10

3.4.13 Methods for Analysing the Chemical Kinetics Model

The nonlinear lumped chemical kinetics model is analysed using a combination of analytical and numerical techniques. The analysis is undertaken to establish the mathematical well-posedness of the model, determine the qualitative behaviour of its solutions, and identify the parameters that have the greatest influence on Carbon (IV) Oxide (CO_2) dynamics. In particular, the analysis comprises positivity, existence and uniqueness of solutions, boundedness, equilibrium analysis, local stability and global sensitivity analysis.

Positivity of Solutions

The positivity analysis is carried out to establish that the concentrations of all chemical species represented by the model remain non-negative whenever the initial concentrations are non-negative. This property is essential because negative concentrations have no physical meaning. The boundary behaviour of the vector field is examined to show that the non-negative orthant is positively invariant.

Existence and Uniqueness of Solutions

The existence and uniqueness analysis is performed to establish that the chemical kinetics model admits a unique solution for prescribed non-negative initial conditions. This is investigated by considering the continuity and local Lipschitz properties of the right-hand side of the system. Since the model is formulated as a system of nonlinear ordinary differential equations, these properties provide the conditions required for the existence of a unique local solution. Boundedness and the appropriate invariant region are then used to support the extension of the solution over the relevant time interval.

Boundedness of Solutions

Boundedness analysis is used to establish that the concentrations of the chemical species remain finite for all times under consideration. Suitable estimates are derived from the governing equations to identify a positively invariant and bounded region containing the solutions. This property ensures that the model does not predict unbounded concentrations and provides a mathematically meaningful framework for the subsequent equilibrium and stability analyses.

Equilibrium Analysis

The equilibrium points of the chemical kinetics model are obtained by setting all time derivatives in the system (3.7) equal to zero. Thus, the equilibrium state is determined by solving the resulting system of nonlinear algebraic equations. The biologically and chemically meaningful equilibrium is restricted to the non-negative region of the state space. The equilibrium analysis provides the basis for investigating the long-term behaviour of the chemical species and the stability of the resulting steady states.

Local Stability Analysis

The local stability of the equilibrium point is investigated by linearizing the nonlinear chemical kinetics system about the equilibrium. The Jacobian matrix of the system is evaluated at the equilibrium point, and the eigenvalues of the resulting matrix are examined. The equilibrium is locally asymptotically stable when all eigenvalues of the Jacobian matrix have negative real parts. This analysis determines the behaviour of small perturbations around the equilibrium and provides information on the local dynamics of Carbon (IV) Oxide and the other chemical species.

Global Sensitivity Analysis

Global sensitivity analysis is performed to determine the relative importance of the model parameters in explaining variations in the selected model outputs. Unlike local sensitivity analysis, which examines the effect of varying one parameter around a nominal value, global sensitivity analysis considers simultaneous variation of multiple parameters over their prescribed ranges.

Latin Hypercube Sampling (LHS) is used to generate an efficient sample of the parameter space. The sampled parameter sets are subsequently used to solve the chemical kinetics system numerically, and the resulting model outputs are used to calculate Partial Rank Correlation Coefficients (PRCCs). The PRCC method quantifies the monotonic relationship between individual model parameters and the selected output while accounting for the influence of the remaining parameters.

The magnitude of a PRCC indicates the strength of the association between a parameter and the model output, while its sign indicates the direction of the association. A positive PRCC indicates that an increase in the parameter is associated with an increase in the selected output, whereas a negative PRCC indicates an inverse relationship. Parameters with large absolute PRCC values are therefore considered influential in determining the dynamics of Carbon (IV) Oxide emissions.

The results of the sensitivity analysis are used to identify the parameters that have the greatest influence on Carbon (IV) Oxide production and removal. These results provide additional insight into the mechanisms governing the chemical kinetics model and help identify parameters that may be relevant when considering emission mitigation strategies.

CHAPTER 4

RESULTS AND DISCUSSIONS

4.1 Results and Discussions for the Deterministic Compartmental Model

This section presents the analytical and numerical results obtained from the deterministic compartmental model developed in Chapter Three. The analysis establishes the fundamental qualitative properties of the model and investigates the behaviour of the system under the specified parameter values and initial conditions.

The qualitative analysis considers positivity, boundedness, existence and uniqueness of solutions, equilibrium points and local stability. These properties are important for establishing the mathematical well-posedness and physical feasibility of the model. In particular, positivity ensures that the state variables remain non-negative, boundedness prevents unphysical unbounded growth, and stability analysis determines the response of the system to small perturbations around its equilibrium states.

The analytical results are complemented by numerical simulations implemented in MATLAB. The simulations illustrate the temporal evolution of the human population, licensed drivers, vegetation, fossil-fuel compartments and atmospheric Carbon (IV) Oxide (CO_2). The numerical results are subsequently interpreted in relation to Carbon (IV) Oxide emission dynamics and the potential implications for mitigation.

The variable M appearing in the fossil-fuel recruitment terms denotes the capacity of crude oil that can be refined into petroleum products, while K_2 represents the corresponding limiting refining capacity. Thus, the term

$$M\left(1-\frac{M}{K_2}\right)$$

represents the capacity-limited crude-oil refining process. The fractions a_1, a_2 and a_3 determine the allocation of the refined crude oil among the corresponding fuel products, while the remaining fraction

$$1-a_1-a_2-a_3$$

is allocated to diesel.

4.1.1 Positivity of the Deterministic Compartmental Model

The state variables of the deterministic compartmental model represent quantities that cannot be negative, including human population, licensed drivers, vegetation, fossil fuels and atmospheric Carbon (IV) Oxide. It is therefore necessary to establish that solutions beginning in the non-negative region remain in that region for all future time. This property ensures the physical feasibility of the proposed model. **Theorem 1.** Let

$$V = \{H(t), R(t), O(t), L(t), P(t), D(t), F(t) \text{ and } C(t)\} \in \mathbb{R}^8_+,$$

for

$$H(0) \geq 0,\ R(0) \geq 0,\ O(0) \geq 0,\ L(0) \geq 0,\ P(0) \geq 0,$$

$$D(0) \geq 0,\ F(0) \geq 0,\ C(0) \geq 0;$$

then the solutions of

$$\{H, R, O, L, P, D, F, C\}$$

are non-negative for $t \geq 0$.

Proof. The proof of the theorem follows that,

From the first differential equation (1), we have

$$\frac{dH}{dt} = \pi_1 + \omega_2 HF + \eta R - \mu_1 H - \lambda H \left(1 - \frac{H}{K_1}\right)$$

By inspection method the terms

$$\pi_1 \geq 0, \qquad \omega_2 HF \geq 0, \qquad \eta R \geq 0.$$

Thus

$$\frac{dH}{dt} \geq -\mu_1 H - \lambda H \left(1 - \frac{H}{K_1}\right)$$

By separation of variables

$$\frac{dH}{H\left(\mu_1 + \lambda\left(1 - \frac{H}{K_1}\right)\right)} \geq -dt$$

On integrating by using partial fractions;

$$\int \frac{dH}{H\left(\mu_1 + \lambda\left(1 - \frac{H}{K_1}\right)\right)} \geq \int_0^t -dt$$

$$H(t) \geq \frac{-K_1(\lambda+\mu_1)e^{-t(\lambda+\mu_1)+c}}{1-\lambda e^{-t(\lambda+\mu_1)+c}}$$

Applying initial conditions at $t = 0$, becomes,

$$H(0) \geq \frac{-K_1(\lambda+\mu_1)e^{c}}{1-\lambda e^{c}}$$

$$\frac{H(0)}{-K_1(\lambda+\mu_1)+\lambda H(0)} \geq e^{c}$$

$$H(t) \geq \frac{\left(-K_1(\lambda+\mu_1)e^{-t(\lambda+\mu_1)}\right)\left(\frac{H(0)}{-K_1(\lambda+\mu_1)+\lambda H(0)}\right)}{1-\lambda e^{-t}\left(\frac{H(0)}{-K_1(\lambda+\mu_1)+\lambda H(0)}\right)}$$

$$H(t) \geq \frac{\left(-K_1(\lambda+\mu_1)e^{-t(\lambda+\mu_1)}\right)H(0)}{-K_1(\lambda+\mu_1)+\lambda H(0)-\lambda e^{-t}}$$

By inspection the numerator is negative. Since

$$H \leq K_1,$$

$$\lambda(H(0) - K_1)$$

is negative thus the denominator is also negative hence

$$H(t) \geq 0.$$

From the first differential equation (3), we have

$$\frac{dF}{dt} = \pi_2 + \rho_2 FC - \omega_1 HF - \delta_1 HF - \mu_2 F$$

By inspection method the terms,

$$\pi_2 \geq 0 \quad \text{and} \quad \rho_2 FC \geq 0$$

$$\frac{dF}{dt} \geq -\omega_1 HF - \delta_1 HF - \mu_2 F$$

$$\frac{dF}{F} \geq -(\omega_1 H + \delta_1 H + \mu_2)\, dt$$

$$F(t) \geq e^c e^{-\int_0^t (\omega_1 H(a) + \delta_1 H(a) + \mu_2)\, da}$$

Applying initial conditions at $t = 0$, becomes,

$$F(0) \geq e^c$$

$$F(t) \geq F(0)\, e^{-\int_0^t (\omega_1 H(a) + \delta_1 H(a) + \mu_2)\, da}$$

Since

$$F(0) \geq 0$$

and

$$e^{-\int_0^t (\omega_1 H(a) + \delta_1 H(a) + \mu_2)\, da} \geq 0,$$

exponential of a negative is always positive hence

$$F(t) \geq 0.$$

From the first differential equation (4), we have

$$\frac{dO}{dt} = a_1 \pi_3 M \left(1 - \frac{M}{K_2}\right) - \alpha_1 HO - \gamma_1 RO$$

By inspection method the terms,

$$a_1 \pi_3 M \left(1 - \frac{M}{K_2}\right) \geq 0$$

$$\frac{dO}{dt} \geq -O(\alpha_1 H + \gamma_1 R)$$

$$\ln O \geq -\int_0^t (\alpha_1 H(a) + \gamma_1 R(a))\, da + c$$

$$O(t) \geq e^c e^{-\int_0^t (\alpha_1 H(a) + \gamma_1 R(a))\, da}$$

Applying initial conditions at $t = 0$, becomes,

$$O(0) \geq e^c$$

$$O(t) \geq O(0)e^{-\int_0^t (\alpha_1 H(a) + \gamma_1 R(a))\, da} \geq 0$$

Similarly from equations 5–7, it follows

$$\frac{dL}{dt} = a_2\pi_3 M\left(1 - \frac{M}{K_2}\right) - \phi_1 HL - \varepsilon_1 RL$$

By inspection method the terms,

$$a_2\pi_3 M\left(1 - \frac{M}{K_2}\right) \geq 0$$

$$\frac{dL}{dt} \geq -L(\phi_1 H + \varepsilon_1 R)$$

$$\frac{dL}{L} \geq -(\phi_1 H + \varepsilon_1 R)\, dt$$

$$L(t) \geq e^c e^{-\int_0^t (\phi_1 H(a) + \varepsilon_1 R(a))\, da}$$

Applying initial conditions at $t = 0$, becomes,

$$L(0) \geq e^c$$

$$L(t) \geq L(0)e^{-\int_0^t (\phi_1 H(a) + \varepsilon_1 R(a))\, da} \geq 0$$

$$\frac{dP}{dt} = a_3\pi_3 M\left(1 - \frac{M}{K_2}\right) - \theta_1 RP$$

By inspection method the terms,

$$a_3\pi_3 M\left(1 - \frac{M}{K_2}\right) \geq 0$$

$$\frac{dP}{dt} \geq -\theta_1 RP$$

$$\frac{dP}{P} \geq -\theta_1 R\, dt$$

$$P(t) \geq e^{c} e^{-\int_0^t (\theta_1 R(a))\, da}$$

Applying initial conditions at $t = 0$, becomes,

$$P(0) \geq e^{c}$$

$$P(t) \geq P(0) e^{-\int_0^t (\theta_1 R(a))\, da} \geq 0$$

$$\frac{dD}{dt} = (1 - a_1 - a_2 - a_3)\pi_3 M \left(1 - \frac{M}{K_2}\right) - \beta_1 RD$$

By inspection method the terms,

$$(1 - a_1 - a_2 - a_3)\pi_3 M \left(1 - \frac{M}{K_2}\right) \geq 0$$

$$\frac{dD}{D} \geq -\beta_1 R\, dt$$

$$D(t) \geq e^{c} e^{-\int_0^t (\beta_1 R(a))\, da}$$

Applying initial conditions at $t = 0$, becomes,

$$D(0) \geq e^{c}$$

$$D(t) \geq D(0) e^{-\int_0^t (\beta_1 R(a))\, da} \geq 0$$

$$\frac{dC}{dt} = \omega_3 HF + \alpha_2 HO + \phi_2 HL + \theta_2 RP + \beta_2 RD + \delta_2 HF + \varepsilon_2 RL + \gamma_2 RO - \rho_1 FC$$

By inspection method the terms,

$$\omega_3 HF + \alpha_2 HO + \phi_2 HL + \theta_2 RP + \beta_2 RD + \delta_2 HF + \varepsilon_2 RL + \gamma_2 RO \geq 0$$

$$\frac{dC}{C} \geq -\rho_1 F\, dt$$

$$C(t) \geq e^{c} e^{-\int_0^t (\rho_1 F(a))\, da}$$

Applying initial conditions at $t = 0$, becomes,

$$C(0) \geq e^{c}$$

$$C(t) \geq C(0) e^{-\int_0^t (\rho_1 F(a))\, da} \geq 0$$

The theorem is therefore proved.

4.1.2 Boundedness of the Deterministic Compartmental Model

The boundedness of a solution in a mathematical model is a property that indicates whether the values of the decision variables are restricted within a certain range. For the system to be mathematically realistic and practical, it is necessary to show that its state variables are positive and bounded for all t. That is, the solution of the system with a positive initial value will remain positive for all $t \geq 0$.

$$N(t) = H(t) + R(t)$$

By differentiating the above equation gives,

$$\frac{dN}{dt} = \frac{dH}{dt} + \frac{dR}{dt}$$

$$\frac{dN}{dt} = \pi_1 + \omega_2 HF + \eta R - \mu_1 H - \lambda H \left(1 - \frac{H}{K_1}\right) + \lambda H \left(1 - \frac{H}{K_1}\right) - \mu_1 R - \eta R$$

$$\frac{dN}{dt} = \pi_1 + \omega_2 HF - \mu_1 N$$

$$\frac{dN}{dt} + \mu_1 N \leq \pi_1$$

Integrating both sides of (above), we have

$$N(t) \leq A e^{\mu_1 t}$$

$$N_p \leq B$$

$$\frac{dN}{dt} + \mu_1 B \leq \pi_1$$

When

$$\frac{dN}{dt} = 0,$$

$$B \leq \frac{\pi_1}{\mu_1},$$

$$N(t) \leq Ae^{\mu_1 t} + \frac{\pi_1}{\mu_1}$$

Applying the initial conditions at $t = 0$ then,

$$N = N(0)$$

$$N(0) \leq A + \frac{\pi_1}{\mu_1}, \qquad N(0) - \frac{\pi_1}{\mu_1} \leq A$$

Substituting,

$$N(t) \leq \left(N(0) - \frac{\pi_1}{\mu_1}\right) e^{\mu_1 t} + \frac{\pi_1}{\mu_1}$$

Introducing limits,

$$\lim_{t\to\infty} N(t) \leq \frac{\pi_1}{\mu_1}$$

Implying that,

$$0 \leq N(t) \leq \frac{\pi_1}{\mu_1}$$

Also,

$$M(t) = O(t) + L(t) + P(t) + D(t)$$

$$\frac{dM}{dt} = \frac{dO}{dt} + \frac{dL}{dt} + \frac{dP}{dt} + \frac{dD}{dt}$$

$$\frac{dM}{dt} = a_1\pi_3 M\left(1 - \frac{M}{K_2}\right) - \alpha_1 HO - \gamma_1 RO$$

$$+a_2\pi_3 M\left(1-\frac{M}{K_2}\right)-\phi_1 HL-\varepsilon_1 RL$$

$$+a_3\pi_3 M\left(1-\frac{M}{K_2}\right)-\theta_1 RP$$

$$+(1-a_1-a_2-a_3)\pi_3 M\left(1-\frac{M}{K_2}\right)-\beta_1 RD$$

$$\frac{dM}{dt}\leq \pi_3 M\left(1-\frac{M}{K_2}\right)$$

By separating of variables and integrating, we have

$$\frac{dM}{M\left(1-\frac{M}{K_2}\right)}\leq \pi_3\, dt$$

$$M(t)\leq K_2-e^{-\pi_3 t+c}$$

On applying initial conditions, $t=0$,

$$M=M(0),$$

$$M(0)\leq K_2-e^{c}$$

$$e^{c}\leq K_2-M(0)$$

Therefore,

$$M(t)\leq K_2-e^{-\pi_3 t}\left(K_2-M(0)\right)$$

$$\lim_{t\to\infty} M(t)\leq K_2$$

Therefore;

$$M(t)\leq K_2$$

Implying that,

$$0 \leq M(t) \leq K_2$$

Similarly,

$$F(t) = F(t)$$

$$\frac{dF}{dt} = \pi_2 + \rho_2 FC - \omega_1 HF - \delta_1 HF - \mu_2 F$$

$$\frac{dF}{dt} + \mu_2 F \leq \pi_2$$

Integrating both sides of (above) using the separation of variables of inequality, we have

$$F(t) \leq Ae^{\mu_2 t}, \qquad F_P \leq B$$

$$\frac{dF}{dt} + \mu_2 B \leq \pi_2$$

When

$$\frac{dF}{dt} = 0, \qquad B \leq \frac{\pi_2}{\mu_2},$$

$$F(t) \leq Ae^{\mu_2 t} + \frac{\pi_2}{\mu_2}$$

Applying the initial conditions at $t = 0$ then,

$$F = F(0)$$

$$F(0) \leq A + \frac{\pi_2}{\mu_2}, \qquad F(0) - \frac{\pi_2}{\mu_2} \leq A$$

Substituting,

$$F(t) \leq \left(F(0) - \frac{\pi_2}{\mu_2}\right) e^{\mu_2 t} + \frac{\pi_2}{\mu_2}$$

Introducing limits,

$$\lim_{t \to \infty} F(t) \leq \frac{\pi_2}{\mu_2}$$

Implying that,

$$0 \leq F(t) \leq \frac{\pi_2}{\mu_2}$$

4.1.3 Existence and Uniqueness of Solutions

Consider the deterministic compartmental model written in the form

$$\frac{d\mathbf{X}}{dt} = \mathbf{F}(\mathbf{X}), \qquad \mathbf{X}(0) = \mathbf{X}_0, \tag{4.1}$$

where

$$\mathbf{X} = (H, R, F, O, L, P, D, C)^T. \tag{4.2}$$

The components of $\mathbf{F}(\mathbf{X})$ consist of polynomial, bilinear and quadratic expressions in the state variables. Therefore, each component of $\mathbf{F}$ possesses continuous first-order partial derivatives with respect to the state variables. Hence,

$$\mathbf{F} \in C^1(\mathbb{R}^8_+), \tag{4.3}$$

and $\mathbf{F}$ is locally Lipschitz continuous in $\mathbb{R}^8_+$.

theorem

For every non-negative initial condition

$$\mathbf{X}_0 \in \mathbb{R}^8_+,$$

the deterministic compartmental model admits a unique local solution on an interval $[0, t_{\max})$.

Proof. Since the right-hand side $\mathbf{F}(\mathbf{X})$ is continuously differentiable with respect to the state variables, it is locally Lipschitz continuous in $\mathbf{X}$. Therefore, by the Picard–Lindelöf existence and uniqueness theorem, for every initial condition $\mathbf{X}_0 \in \mathbb{R}^8_+$ there exists a unique solution of the system on some interval $[0, t_{\max})$ containing $t = 0$.

Furthermore, the positivity and boundedness results established in the preceding sections ensure that solutions originating in the feasible region remain biologically meaningful. Consequently, the solution can be continued for all $t \geq 0$ whenever it remains bounded. Thus, the model is well posed in the feasible region. □

4.1.4 Equilibrium Points

An equilibrium point represents a state of the system at which the state variables remain constant with time. The equilibrium points are therefore obtained by setting the right-hand sides of the system of differential equations equal to zero. Let

$$\mathbf{X}^* = (H^*, R^*, F^*, O^*, L^*, P^*, D^*, C^*)$$

denote an equilibrium point. Then

$$\frac{dH}{dt} = \frac{dR}{dt} = \frac{dF}{dt} = \frac{dO}{dt} = \frac{dL}{dt} = \frac{dP}{dt} = \frac{dD}{dt} = \frac{dC}{dt} = 0. \tag{4.4}$$

The resulting algebraic system is used to determine the admissible equilibrium points. In accordance with the structure of the model, five cases are considered. These are: the trivial state E^0, absence of humans and related activities E^1, absence of fossil fuels E^2, absence of drivers E^3, and coexistence of all model compartments E^4.

For convenience, define

$$Q(M) = \pi_3 M \left(1 - \frac{M}{K_2}\right). \tag{4.5}$$

The equilibrium cases are considered below.

Case 1: Trivial Equilibrium

The first case considers the situation in which humans, drivers, fossil-fuel compartments, environmental compartments and atmospheric Carbon (IV) Oxide are all absent. Thus,

$$H^0 = R^0 = F^0 = O^0 = L^0 = P^0 = D^0 = C^0 = 0. \tag{4.6}$$

The candidate equilibrium is therefore

$$E^0 = (0, 0, 0, 0, 0, 0, 0, 0). \tag{4.7}$$

However, the candidate point must satisfy all eight equilibrium equations. Substitution of E^0 into the system gives

$$\left.\frac{dH}{dt}\right|_{E^0} = \pi_1, \qquad \left.\frac{dF}{dt}\right|_{E^0} = \pi_2, \tag{4.8}$$

and

$$\left.\frac{dO}{dt}\right|_{E^0} = a_1 Q(M), \tag{4.9}$$

$$\left.\frac{dL}{dt}\right|_{E^0} = a_2 Q(M), \tag{4.10}$$

$$\left.\frac{dP}{dt}\right|_{E^0} = a_3 Q(M), \tag{4.11}$$

$$\left.\frac{dD}{dt}\right|_{E^0} = (1 - a_1 - a_2 - a_3) Q(M). \tag{4.12}$$

Consequently, E^0 is an equilibrium only when the external input terms satisfy

$$\pi_1 = 0, \qquad \pi_2 = 0, \qquad Q(M) = 0. \tag{4.13}$$

Since

$$Q(M) = \pi_3 M \left(1 - \frac{M}{K_2}\right),$$

the last condition is satisfied, for example, when

$$\pi_3 = 0, \qquad M = 0, \qquad \text{or} \qquad M = K_2.$$

Thus, when the recruitment and production parameters are strictly positive and $0 < M < K_2$, the all-zero state is a candidate boundary state but is not an equilibrium of the full system.

This distinction is important for the subsequent stability analysis, since local stability can only be investigated at a point that satisfies the equilibrium equations.

Case 2: Absence of Humans and Related Activities

The second case corresponds to the absence of humans and their related activities. Following the notation used in the model, let

$$H^1 = 0, \qquad R^1 = 0, \tag{4.14}$$

while

$$F^1 \neq 0, \quad O^1 \neq 0, \quad L^1 \neq 0, \quad P^1 \neq 0, \quad D^1 \neq 0, \quad C^1 \neq 0.$$

Thus, the equilibrium is written as

$$E^1 = (0, 0, F^1, O^1, L^1, P^1, D^1, C^1). \tag{4.15}$$

Substitution into the first equilibrium equation gives the necessary condition

$$\pi_1 = 0. \tag{4.16}$$

The third equilibrium equation becomes

$$\pi_2 + \rho_2 F^1 C^1 - \mu_2 F^1 = 0, \tag{4.17}$$

and hence

$$F^1 = \frac{\pi_2}{\rho_2 C^1 - \mu_2}, \tag{4.18}$$

provided that

$$\rho_2 C^1 - \mu_2 > 0. \tag{4.19}$$

For the environmental compartments, the equilibrium equations give

$$a_1 Q(M^1) = 0, \tag{4.20}$$

$$a_2 Q(M^1) = 0, \tag{4.21}$$

$$a_3 Q(M^1) = 0, \tag{4.22}$$

and

$$(1 - a_1 - a_2 - a_3) Q(M^1) = 0. \tag{4.23}$$

For positive π_3 and non-zero allocation fractions, these conditions are satisfied when

$$M^1 = K_2. \tag{4.24}$$

Thus,

$$O^1, L^1, P^1, D^1 \tag{4.25}$$

are not independently determined by their production equations when $M^1 = K_2$;

their admissible values must instead be determined from the remaining equilibrium relations and parameter constraints.

The Carbon (IV) Oxide equilibrium equation is

$$\begin{aligned} 0 = (\omega_3 + \delta_2)H^1F^1 + \alpha_2 H^1O^1 + \phi_2 H^1L^1 + \theta_2 R^1P^1 \\ + \beta_2 R^1D^1 + \varepsilon_2 R^1L^1 + \gamma_2 R^1O^1 - \rho_1 F^1C^1. \end{aligned} \tag{4.26}$$

Since $H^1 = R^1 = 0$, this reduces to

$$-\rho_1 F^1 C^1 = 0. \tag{4.27}$$

Therefore, if

$$\rho_1 > 0, \qquad F^1 > 0, \qquad C^1 > 0,$$

then this equation cannot be satisfied.

Hence, under the stated positive-parameter assumptions, the proposed E^1 with simultaneously positive F^1 and C^1 is not an admissible equilibrium of the full system.

This verification shows why every proposed boundary equilibrium must be checked against all eight governing equations.

Case 3: Absence of Fossil Fuels

The third case represents the absence of the environmental/fossil-fuel output compartments considered in the original formulation. Following the notation used in the thesis, let

$$O^2 = L^2 = P^2 = D^2 = 0, \tag{4.28}$$

while

$$H^2 \neq 0, \qquad R^2 \neq 0, \qquad F^2 \neq 0, \qquad C^2 \neq 0.$$

The equilibrium is therefore

$$E^2 = (H^2, R^2, F^2, 0, 0, 0, 0, C^2). \tag{4.29}$$

The first two equilibrium equations become

$$\pi_1 + \omega_2 H^2 F^2 + \eta R^2 - \mu_1 H^2 - \lambda H^2 \left(1 - \frac{H^2}{K_1}\right) = 0, \tag{4.30}$$

and

$$\lambda H^2 \left(1 - \frac{H^2}{K_1}\right) - (\eta + \mu_1) R^2 = 0. \tag{4.31}$$

Hence,

$$R^2 = \frac{\lambda H^2 \left(1 - \frac{H^2}{K_1}\right)}{\eta + \mu_1}. \tag{4.32}$$

The fossil-fuel equilibrium equation becomes

$$\pi_2 + \rho_2 F^2 C^2 - (\omega_1 + \delta_1) H^2 F^2 - \mu_2 F^2 = 0, \tag{4.33}$$

giving

$$F^2 = \frac{\pi_2}{(\omega_1 + \delta_1) H^2 - \rho_2 C^2 + \mu_2}. \tag{4.34}$$

For $O^2 = L^2 = P^2 = D^2 = 0$ to be equilibrium values, their corresponding production terms must vanish. Thus,

$$Q(M^2) = 0, \tag{4.35}$$

and, under positive π_3,

$$M^2 = K_2. \tag{4.36}$$

Finally, the Carbon (IV) Oxide equation reduces to

$$(\omega_3 + \delta_2) H^2 F^2 - \rho_1 F^2 C^2 = 0. \tag{4.37}$$

Provided $F^2 > 0$,

$$C^2 = \frac{(\omega_3 + \delta_2) H^2}{\rho_1}. \tag{4.38}$$

Consequently, the admissible equilibrium in this case is represented by

$$E^2 = (H^2, R^2, F^2, 0, 0, 0, 0, C^2), \tag{4.39}$$

where H^2, R^2, F^2 and C^2 satisfy (4.30)–(4.37) and the required positivity conditions.

Case 4: Absence of Drivers

The fourth case considers the absence of drivers. Thus,

$$R^3 = 0, \qquad P^3 = 0, \qquad D^3 = 0, \tag{4.40}$$

while

$$H^3 \neq 0, \quad F^3 \neq 0, \quad O^3 \neq 0, \quad L^3 \neq 0, \quad C^3 \neq 0.$$

The corresponding equilibrium is

$$E^3 = (H^3, 0, F^3, O^3, L^3, 0, 0, C^3). \tag{4.41}$$

The first equilibrium equation gives

$$\pi_1 + \omega_2 H^3 F^3 - \mu_1 H^3 - \lambda H^3 \left(1 - \frac{H^3}{K_1}\right) = 0. \tag{4.42}$$

Hence,

$$\lambda \frac{(H^3)^2}{K_1} + (F^3 \omega_2 - \lambda - \mu_1) H^3 + \pi_1 = 0. \tag{4.43}$$

The physically admissible root is selected subject to

$$H^3 > 0.$$

The fossil-fuel equation becomes

$$\pi_2 + \rho_2 F^3 C^3 - (\omega_1 + \delta_1) H^3 F^3 - \mu_2 F^3 = 0, \tag{4.44}$$

and therefore

$$F^3 = \frac{\pi_2}{H^3(\omega_1 + \delta_1) - \rho_2 C^3 + \mu_2}. \tag{4.45}$$

For the plant compartments,

$$a_1 Q(M^3) - \alpha_1 H^3 O^3 = 0, \tag{4.46}$$

giving

$$O^3 = \frac{a_1\pi_3 M^3\left(1-\frac{M^3}{K_2}\right)}{\alpha_1 H^3}. \tag{4.47}$$

Similarly,

$$a_2 Q(M^3) - \phi_1 H^3 L^3 = 0, \tag{4.48}$$

so that

$$L^3 = \frac{a_2\pi_3 M^3\left(1-\frac{M^3}{K_2}\right)}{\phi_1 H^3}. \tag{4.49}$$

The Carbon (IV) Oxide equation reduces to

$$(\omega_3+\delta_2)H^3F^3 + \alpha_2 H^3 O^3 + \phi_2 H^3 L^3 - \rho_1 F^3 C^3 = 0. \tag{4.50}$$

Therefore,

$$C^3 = \frac{(\omega_3+\delta_2)H^3F^3 + \alpha_2 H^3 O^3 + \phi_2 H^3 L^3}{\rho_1 F^3}. \tag{4.51}$$

Hence,

$$E^3 = (H^3, 0, F^3, O^3, L^3, 0, 0, C^3), \tag{4.52}$$

subject to the positivity and parameter conditions required by (4.42)–(4.50).

Case 5: Coexistence in the System

The fifth case corresponds to coexistence of all compartments. This is the positive equilibrium of the model and is the principal equilibrium of interest.

The equilibrium is denoted by

$$E^4 = (H^4, R^4, F^4, O^4, L^4, P^4, D^4, C^4), \tag{4.53}$$

where

$$H^4, R^4, F^4, O^4, L^4, P^4, D^4, C^4 > 0.$$

The equilibrium equations are

$$\pi_1 + \omega_2 H^4 F^4 + \eta R^4 - \mu_1 H^4 - \lambda H^4 \left(1 - \frac{H^4}{K_1}\right) = 0, \tag{4.54}$$

$$\lambda H^4 \left(1 - \frac{H^4}{K_1}\right) - (\eta + \mu_1) R^4 = 0, \tag{4.55}$$

$$\pi_2 + \rho_2 F^4 C^4 - (\omega_1 + \delta_1) H^4 F^4 - \mu_2 F^4 = 0, \tag{4.56}$$

$$a_1 Q(M^4) - (\alpha_1 H^4 + \gamma_1 R^4) O^4 = 0, \tag{4.57}$$

$$a_2 Q(M^4) - (\phi_1 H^4 + \varepsilon_1 R^4) L^4 = 0, \tag{4.58}$$

$$a_3 Q(M^4) - \theta_1 R^4 P^4 = 0, \tag{4.59}$$

and

$$(1 - a_1 - a_2 - a_3) Q(M^4) - \beta_1 R^4 D^4 = 0. \tag{4.60}$$

The corresponding equilibrium values are therefore

$$R^4 = \frac{\lambda H^4 \left(1 - \frac{H^4}{K_1}\right)}{\eta + \mu_1}, \tag{4.61}$$

$$F^4 = \frac{\pi_2}{H^4(\omega_1 + \delta_1) - \rho_2 C^4 + \mu_2}, \tag{4.62}$$

$$O^4 = \frac{a_1 \pi_3 M^4 \left(1 - \frac{M^4}{K_2}\right)}{\alpha_1 H^4 + \gamma_1 R^4}, \tag{4.63}$$

$$L^4 = \frac{a_2 \pi_3 M^4 \left(1 - \frac{M^4}{K_2}\right)}{\phi_1 H^4 + \varepsilon_1 R^4}, \tag{4.64}$$

$$P^4 = \frac{a_3 \pi_3 M^4 \left(1 - \frac{M^4}{K_2}\right)}{\theta_1 R^4}, \tag{4.65}$$

and

$$D^4 = \frac{(1-a_1-a_2-a_3)\pi_3 M^4\left(1-\dfrac{M^4}{K_2}\right)}{\beta_1 R^4}. \tag{4.66}$$

The Carbon (IV) Oxide equilibrium equation is

$$\begin{aligned} 0 = {} & (\omega_3+\delta_2)H^4F^4 + \alpha_2 H^4O^4 + \phi_2 H^4L^4 + \theta_2 R^4P^4 \\ & + \beta_2 R^4D^4 + \varepsilon_2 R^4L^4 + \gamma_2 R^4O^4 - \rho_1 F^4C^4. \end{aligned} \tag{4.67}$$

Consequently,

$$C^4 = \frac{(\omega_3+\delta_2)H^4F^4 + \alpha_2 H^4O^4 + \phi_2 H^4L^4 + \theta_2 R^4P^4 + \beta_2 R^4D^4 + \varepsilon_2 R^4L^4 + \gamma_2 R^4O^4}{\rho_1 F^4}. \tag{4.68}$$

The remaining unknown equilibrium quantities are obtained simultaneously from the reduced algebraic system (4.54)–(4.67). Only solutions satisfying

$$H^4, R^4, F^4, O^4, L^4, P^4, D^4, C^4 > 0 \tag{4.69}$$

are regarded as biologically and physically admissible positive coexistence equilibria.

Summary of the Equilibrium Cases

The five cases considered in the model are summarized as follows:

Table 4.1: Summary of the equilibrium cases of the deterministic compartmental model.

Equilibrium	Description	State vector
E^0	Trivial state	$(0,0,0,0,0,0,0,0)$
E^1	Absence of humans and related activities	$(0,0,F^1,O^1,L^1,P^1,D^1,C^1)$
E^2	Absence of fossil-fuel output compartments	$(H^2,R^2,F^2,0,0,0,0,C^2)$
E^3	Absence of drivers	$(H^3,0,F^3,O^3,L^3,0,0,C^3)$
E^4	Positive coexistence	$(H^4,R^4,F^4,O^4,L^4,P^4,D^4,C^4)$

The admissibility of each equilibrium is determined by substitution into the complete equilibrium system. In particular, a proposed boundary equilibrium is retained only when all eight equilibrium equations are simultaneously satisfied. The positive

coexistence equilibrium E^4 is subsequently used in the Jacobian and local stability analyses.

4.1.5 Jacobian Matrix

The Jacobian matrix is derived to investigate the local behaviour of the deterministic compartmental model in the neighbourhood of its equilibrium points. Let the state vector be defined by

$$\mathbf{X} = (H, R, F, O, L, P, D, C)^T. \tag{4.70}$$

The deterministic compartmental model can be written in the compact form

$$\frac{d\mathbf{X}}{dt} = \mathbf{F}(\mathbf{X}), \tag{4.71}$$

where

$$\mathbf{F}(\mathbf{X}) = (F_1, F_2, F_3, F_4, F_5, F_6, F_7, F_8)^T .$$

The Jacobian matrix of the system is defined as the matrix of first partial derivatives of the right-hand sides of the governing differential equations with respect to the state variables. Thus,

$$J(\mathbf{X}) = \frac{\partial \mathbf{F}}{\partial \mathbf{X}} = \left[\frac{\partial F_i}{\partial X_j}\right]_{8\times 8}. \tag{4.72}$$

For the deterministic compartmental model, the resulting Jacobian matrix is

$$J(\mathbf{X}) = \begin{pmatrix} \omega_2 F - \mu_1 - \lambda + \frac{2\lambda H}{K_1} & \eta & \omega_2 H & 0 & 0 & 0 & 0 & 0 \\ \lambda - \frac{2\lambda H}{K_1} & -\eta - \mu_1 & 0 & 0 & 0 & 0 & 0 & 0 \\ -(\omega_1 + \delta_1)F & 0 & \rho_2 C - (\omega_1 + \delta_1)H - \mu_2 & 0 & 0 & 0 & 0 & \rho_2 F \\ -\alpha_1 O & -\gamma_1 O & 0 & -\alpha_1 H - \gamma_1 R & 0 & 0 & 0 & 0 \\ -\phi_1 L & -\varepsilon_1 L & 0 & 0 & -\phi_1 H - \varepsilon_1 R & 0 & 0 & 0 \\ 0 & -\theta_1 P & 0 & 0 & 0 & -\theta_1 R & 0 & 0 \\ 0 & -\beta_1 D & 0 & 0 & 0 & 0 & -\beta_1 R & 0 \\ (\omega_3 + \delta_2)F + \alpha_2 O + \phi_2 L & \theta_2 P + \beta_2 D + \varepsilon_2 L + \gamma_2 O & (\omega_3 + \delta_2)H - \rho_1 C & \alpha_2 H + \gamma_2 R & \phi_2 H + \varepsilon_2 R & \theta_2 R & \beta_2 R & -\rho_1 F \end{pmatrix} \tag{4.73}$$

Here, the rows of the Jacobian correspond respectively to the variables

$$H,\ R,\ F,\ O,\ L,\ P,\ D,\ C,$$

while the columns correspond to the same ordering of the state variables.

For example, the $(1,1)$ entry is obtained from

$$\frac{\partial}{\partial H}\left[\pi_1+\omega_2 HF+\eta R-\mu_1 H-\lambda H\left(1-\frac{H}{K_1}\right)\right],$$

which gives

$$J_{11}=\omega_2 F-\mu_1-\lambda+\frac{2\lambda H}{K_1}. \tag{4.74}$$

Similarly, the $(2,1)$ entry is

$$J_{21}=\lambda-\frac{2\lambda H}{K_1}. \tag{4.75}$$

The $(3,3)$ entry is particularly important and is given by

$$J_{33}=\rho_2 C-(\omega_1+\delta_1)H-\mu_2. \tag{4.76}$$

Notice that π_2 does not appear in J_{33} because π_2 is a constant recruitment term in the third differential equation and therefore its derivative with respect to F is zero.

The $(3,8)$ entry is

$$J_{38}=\rho_2 F, \tag{4.77}$$

which represents the effect of atmospheric Carbon (IV) Oxide on the fuel compartment through the term $\rho_2 FC$.

The final row of the Jacobian describes the dependence of atmospheric Carbon (IV) Oxide on the other compartments. In particular,

$$J_{81}=(\omega_3+\delta_2)F+\alpha_2 O+\phi_2 L, \tag{4.78}$$
$$J_{82}=\theta_2 P+\beta_2 D+\varepsilon_2 L+\gamma_2 O, \tag{4.79}$$
$$J_{83}=(\omega_3+\delta_2)H-\rho_1 C, \tag{4.80}$$
$$J_{84}=\alpha_2 H+\gamma_2 R, \tag{4.81}$$
$$J_{85}=\phi_2 H+\varepsilon_2 R, \tag{4.82}$$
$$J_{86}=\theta_2 R, \tag{4.83}$$
$$J_{87}=\beta_2 R, \tag{4.84}$$
$$J_{88}=-\rho_1 F. \tag{4.85}$$

The Jacobian matrix is subsequently evaluated at each admissible equilibrium point.

If E^j denotes the jth equilibrium point, then the corresponding equilibrium Jacobian is defined by

$$J(E^j) = J(\mathbf{X})|_{\mathbf{X}=E^j}, \qquad j = 0, 1, 2, 3, 4. \tag{4.86}$$

Thus, the matrices required for the local stability analysis are

$$J(E^0), \qquad J(E^1), \qquad J(E^2), \qquad J(E^3), \qquad J(E^4). \tag{4.87}$$

The eigenvalues of each equilibrium Jacobian are obtained from the characteristic equation

$$\det\left[J(E^j) - \chi I\right] = 0, \tag{4.88}$$

where χ represents an eigenvalue and I is the 8×8 identity matrix. The characteristic equation provides the basis for the local stability analysis presented in the subsequent subsection.

Since the Jacobian matrix contains several non-zero off-diagonal elements, the eigenvalues cannot, in general, be determined simply from the diagonal entries of the matrix. They must be obtained from the full characteristic equation or, where appropriate, by applying the Routh–Hurwitz criterion to the resulting characteristic polynomial.

4.1.6 Local Stability Analysis

Local stability describes the behaviour of the system in a neighbourhood of an equilibrium point. In this study, local stability is determined by linearizing the nonlinear system about each admissible equilibrium point and examining the eigenvalues of the corresponding Jacobian matrix.

Let the system of differential equations be written in the compact form

$$\frac{d\mathbf{X}}{dt} = \mathbf{F}(\mathbf{X}), \tag{4.89}$$

where

$$\mathbf{X} = (H, R, F, O, L, P, D, C)^T. \tag{4.90}$$

An equilibrium point $\mathbf{X}^*$ satisfies

$$\mathbf{F}(\mathbf{X}^*) = \mathbf{0}. \tag{4.91}$$

The system is linearized about $\mathbf{X}^*$ by introducing a small perturbation $\mathbf{u}$ such that

$$\mathbf{X} = \mathbf{X}^* + \mathbf{u}. \tag{4.92}$$

Using the first-order Taylor expansion gives

$$\frac{d\mathbf{u}}{dt} = J(\mathbf{X}^*)\mathbf{u} + \mathcal{O}(\|\mathbf{u}\|^2), \tag{4.93}$$

where $J(\mathbf{X}^*)$ is the Jacobian matrix evaluated at the equilibrium point.
For convenience, define

$$q(M) = \pi_3 M\left(1 - \frac{M}{K_2}\right), \tag{4.94}$$

and

$$q'(M) = \pi_3\left(1 - \frac{2M}{K_2}\right). \tag{4.95}$$

Since

$$M = O + L + P + D, \tag{4.96}$$

the derivative of $q(M)$ with respect to each of the variables O, L, P and D is $q'(M)$.
The Jacobian matrix of the system is therefore

$$J(\mathbf{X}) = \begin{pmatrix} J_{11} & J_{12} & J_{13} & 0 & 0 & 0 & 0 & 0 \\ J_{21} & J_{22} & 0 & 0 & 0 & 0 & 0 & 0 \\ J_{31} & 0 & J_{33} & 0 & 0 & 0 & 0 & J_{38} \\ J_{41} & J_{42} & 0 & J_{44} & J_{45} & J_{46} & J_{47} & 0 \\ J_{51} & J_{52} & 0 & J_{54} & J_{55} & J_{56} & J_{57} & 0 \\ 0 & J_{62} & 0 & J_{64} & J_{65} & J_{66} & J_{67} & 0 \\ 0 & J_{72} & 0 & J_{74} & J_{75} & J_{76} & J_{77} & 0 \\ J_{81} & J_{82} & J_{83} & J_{84} & J_{85} & J_{86} & J_{87} & J_{88} \end{pmatrix}, \tag{4.97}$$

where

$$J_{11} = \omega_2 F - \mu_1 - \lambda + \frac{2\lambda H}{K_1}, \qquad J_{12} = \eta, \qquad J_{13} = \omega_2 H, \tag{4.98}$$

$$J_{21} = \lambda\left(1 - \frac{2H}{K_1}\right), \qquad J_{22} = -(\eta + \mu_1), \tag{4.99}$$

$$J_{31} = -(\omega_1 + \delta_1)F, \qquad J_{33} = \rho_2 C - (\omega_1 + \delta_1)H - \mu_2, \qquad J_{38} = \rho_2 F, \tag{4.100}$$

$$J_{41} = -\alpha_1 O, \qquad J_{42} = -\gamma_1 O, \qquad J_{44} = a_1 q'(M) - \alpha_1 H - \gamma_1 R, \tag{4.101}$$

$$J_{45} = a_1 q'(M), \qquad J_{46} = a_1 q'(M), \qquad J_{47} = a_1 q'(M), \tag{4.102}$$

$$J_{51} = -\phi_1 L, \qquad J_{52} = -\varepsilon_1 L, \qquad J_{54} = a_2 q'(M), \tag{4.103}$$

$$J_{55} = a_2 q'(M) - \phi_1 H - \varepsilon_1 R, \qquad J_{56} = a_2 q'(M), \qquad J_{57} = a_2 q'(M), \tag{4.104}$$

$$J_{62} = -\theta_1 P, \qquad J_{64} = a_3 q'(M), \qquad J_{65} = a_3 q'(M), \tag{4.105}$$

$$J_{66} = a_3 q'(M), \qquad J_{67} = a_3 q'(M) - \theta_1 R, \tag{4.106}$$

$$J_{72} = -\beta_1 D, \qquad J_{74} = (1 - a_1 - a_2 - a_3)q'(M), \tag{4.107}$$

$$J_{75} = (1 - a_1 - a_2 - a_3)q'(M), \qquad J_{76} = (1 - a_1 - a_2 - a_3)q'(M), \tag{4.108}$$

$$J_{77} = (1 - a_1 - a_2 - a_3)q'(M) - \beta_1 R, \tag{4.109}$$

and

$$J_{81} = \alpha_2 O + \phi_2 L + (\omega_3 + \delta_2)F, \tag{4.110}$$

$$J_{82} = \theta_2 P + \beta_2 D + \varepsilon_2 L + \gamma_2 O, \tag{4.111}$$

$$J_{83} = (\omega_3 + \delta_2)H, \tag{4.112}$$

$$J_{84} = \alpha_2 H + \gamma_2 R, \tag{4.113}$$

$$J_{85} = \phi_2 H + \varepsilon_2 R, \tag{4.114}$$

$$J_{86} = \theta_2 R, \tag{4.115}$$

$$J_{87} = \beta_2 R, \tag{4.116}$$

$$J_{88} = -\rho_1 F. \tag{4.117}$$

Thus, for each admissible equilibrium E^j, $j = 0, 1, 2, 3, 4$, the corresponding linearized system is

$$\frac{d\mathbf{u}}{dt} = J(E^j)\mathbf{u}. \tag{4.118}$$

The local stability of E^j is consequently determined from the eigenvalues of $J(E^j)$.

Characteristic Equation

Let

$$J(E^j) = J_j. \tag{4.119}$$

The characteristic equation associated with E^j is obtained from

$$\det\left(J_j - \chi I\right) = 0. \tag{4.120}$$

Since the system contains eight state variables, the characteristic polynomial has degree eight and can be written as

$$\chi^8 + c_1^{(j)}\chi^7 + c_2^{(j)}\chi^6 + c_3^{(j)}\chi^5 + c_4^{(j)}\chi^4 + c_5^{(j)}\chi^3 + c_6^{(j)}\chi^2 + c_7^{(j)}\chi + c_8^{(j)} = 0. \tag{4.121}$$

The superscript (j) indicates that the coefficients are obtained after evaluating the Jacobian at the corresponding equilibrium E^j.

The equilibrium point E^j is locally asymptotically stable if all roots of (4.121) have negative real parts, that is,

$$\mathrm{Re}(\chi_i) < 0, \qquad i = 1, \ldots, 8. \tag{4.122}$$

If at least one eigenvalue satisfies

$$\mathrm{Re}(\chi_i) > 0, \tag{4.123}$$

then E^j is unstable.

If an eigenvalue satisfies

$$\mathrm{Re}(\chi_i) = 0, \tag{4.124}$$

the linearization is inconclusive and further analysis is required.

Routh–Hurwitz Stability Criterion

For an analytical stability assessment, the Routh–Hurwitz criterion is applied to the characteristic polynomial (4.121).

The Hurwitz matrix corresponding to the eighth-degree polynomial is

$$\mathcal{H}_j = \begin{pmatrix} c_1^{(j)} & c_3^{(j)} & c_5^{(j)} & c_7^{(j)} & 0 & 0 & 0 & 0 \\ 1 & c_2^{(j)} & c_4^{(j)} & c_6^{(j)} & c_8^{(j)} & 0 & 0 & 0 \\ 0 & c_1^{(j)} & c_3^{(j)} & c_5^{(j)} & c_7^{(j)} & 0 & 0 & 0 \\ 0 & 1 & c_2^{(j)} & c_4^{(j)} & c_6^{(j)} & c_8^{(j)} & 0 & 0 \\ 0 & 0 & c_1^{(j)} & c_3^{(j)} & c_5^{(j)} & c_7^{(j)} & 0 & 0 \\ 0 & 0 & 1 & c_2^{(j)} & c_4^{(j)} & c_6^{(j)} & c_8^{(j)} & 0 \\ 0 & 0 & 0 & c_1^{(j)} & c_3^{(j)} & c_5^{(j)} & c_7^{(j)} & 0 \\ 0 & 0 & 0 & 1 & c_2^{(j)} & c_4^{(j)} & c_6^{(j)} & c_8^{(j)} \end{pmatrix}. \tag{4.125}$$

Let

$$\Delta_k^{(j)} = \det\left(\mathcal{H}_j^{(k)}\right), \qquad k = 1, \ldots, 8, \tag{4.126}$$

where $\mathcal{H}_j^{(k)}$ denotes the leading $k \times k$ principal submatrix of the Hurwitz matrix.

According to the Routh–Hurwitz criterion, the equilibrium E^j is locally asymptotically stable if and only if

$$\Delta_1^{(j)} > 0, \quad \Delta_2^{(j)} > 0, \quad \ldots, \quad \Delta_8^{(j)} > 0. \tag{4.127}$$

Therefore, it is not sufficient merely to require that selected coefficients of the characteristic polynomial be positive. The complete set of Hurwitz determinants must satisfy the positivity conditions in (4.127).

Stability of the Trivial State E^0

The proposed trivial state is

$$E^0 = (0, 0, 0, 0, 0, 0, 0, 0). \tag{4.128}$$

However, from the equilibrium equations,

$$\left.\frac{dH}{dt}\right|_{E^0} = \pi_1, \qquad \left.\frac{dF}{dt}\right|_{E^0} = \pi_2. \tag{4.129}$$

Consequently, when

$$\pi_1 > 0 \qquad \text{or} \qquad \pi_2 > 0, \tag{4.130}$$

the point E^0 is not an equilibrium of the model. Therefore, no local stability analysis can be performed for E^0 under these parameter conditions.

If the special parameter conditions

$$\pi_1 = \pi_2 = 0 \tag{4.131}$$

and the remaining equilibrium conditions are satisfied, then E^0 may be treated as a boundary equilibrium. Its local stability is then determined from the eigenvalues of

$$J(E^0). \tag{4.132}$$

Stability of E^1

The proposed equilibrium corresponding to the absence of humans and their related activities is

$$E^1 = (0, 0, F^1, O^1, L^1, P^1, D^1, C^1). \tag{4.133}$$

However, when

$$F^1 > 0, \qquad C^1 > 0, \qquad \rho_1 > 0,$$

the Carbon (IV) Oxide equilibrium equation reduces to

$$-\rho_1 F^1 C^1 = 0, \tag{4.134}$$

which cannot hold.

Therefore,

$$E^1 \tag{4.135}$$

is not an admissible equilibrium under the positive parameter and positive-state assumptions of the model. Consequently, a local stability analysis of E^1 is not applicable unless additional parameter restrictions are imposed that make the equilibrium conditions valid.

Stability of E^2

For the equilibrium

$$E^2 = (H^2, R^2, F^2, 0, 0, 0, 0, C^2), \tag{4.136}$$

the condition

$$M^2 = K_2 \tag{4.137}$$

is required when $\pi_3 > 0$ for the environmental production terms to vanish.
The Jacobian evaluated at E^2 is

$$J(E^2) = J\left(H^2, R^2, F^2, 0, 0, 0, 0, C^2\right). \tag{4.138}$$

The local stability of E^2 is determined by the eigenvalues

$$\chi_1^{(2)}, \ldots, \chi_8^{(2)} \tag{4.139}$$

of $J(E^2)$.
Thus,

$$E^2 \text{ is locally asymptotically stable } \iff \mathrm{Re}\left(\chi_i^{(2)}\right) < 0, \quad i = 1, \ldots, 8. \tag{4.140}$$

Equivalently, stability follows when

$$\Delta_k^{(2)} > 0, \qquad k = 1, \ldots, 8. \tag{4.141}$$

Stability of E^3

For the driver-free equilibrium,

$$E^3 = (H^3, 0, F^3, O^3, L^3, 0, 0, C^3), \tag{4.142}$$

the R-equation requires

$$\lambda H^3 \left(1 - \frac{H^3}{K_1}\right) = 0. \tag{4.143}$$

For $\lambda > 0$ and $H^3 > 0$, this implies

$$H^3 = K_1. \tag{4.144}$$

The Jacobian at this equilibrium is

$$J(E^3) = J(K_1, 0, F^3, O^3, L^3, 0, 0, C^3). \tag{4.145}$$

The equilibrium E^3 is locally asymptotically stable if

$$\mathrm{Re}\left(\chi_i^{(3)}\right) < 0, \qquad i = 1, \ldots, 8, \tag{4.146}$$

where $\chi_i^{(3)}$ are the eigenvalues of $J(E^3)$.
Equivalently, the Routh–Hurwitz conditions are

$$\Delta_k^{(3)} > 0, \qquad k = 1, \ldots, 8. \tag{4.147}$$

Stability of the Coexistence Equilibrium E^4

The coexistence equilibrium is

$$E^4 = (H^4, R^4, F^4, O^4, L^4, P^4, D^4, C^4), \tag{4.148}$$

where all components are positive.
The Jacobian evaluated at the coexistence equilibrium is

$$J(E^4) = J(H^4, R^4, F^4, O^4, L^4, P^4, D^4, C^4). \tag{4.149}$$

Let

$$\chi_1^{(4)}, \chi_2^{(4)}, \ldots, \chi_8^{(4)} \tag{4.150}$$

denote the eigenvalues of $J(E^4)$.
The coexistence equilibrium is locally asymptotically stable if

$$\mathrm{Re}\left(\chi_i^{(4)}\right) < 0, \qquad i = 1, \ldots, 8. \tag{4.151}$$

Equivalently,

$$\Delta_k^{(4)} > 0, \qquad k = 1, \ldots, 8. \tag{4.152}$$

If at least one eigenvalue has a positive real part, then the coexistence equilibrium

is unstable.

Summary of Local Stability Results

The local stability analysis leads to the following conclusions.

1. The point E^0 can be considered a local equilibrium only under the parameter restrictions required to make all components of the vector field vanish. In particular, positive external recruitment terms π_1 and π_2 exclude the all-zero equilibrium.

2. The proposed equilibrium E^1 with $F^1 > 0$ and $C^1 > 0$ is not admissible when $\rho_1 > 0$, since the Carbon (IV) Oxide equilibrium equation cannot be satisfied.

3. The equilibrium E^2 is locally asymptotically stable provided all eigenvalues of $J(E^2)$ have negative real parts, or equivalently, all the associated Hurwitz determinants are positive.

4. For the driver-free equilibrium E^3, the equilibrium condition requires $H^3 = K_1$ when $\lambda > 0$ and $H^3 > 0$. Its stability is then determined from the eigenvalues of $J(E^3)$.

5. The positive coexistence equilibrium E^4 is locally asymptotically stable if and only if all eigenvalues of $J(E^4)$ have negative real parts. Equivalently, the Routh–Hurwitz determinants satisfy $\Delta_k^{(4)} > 0$ for $k = 1, \ldots, 8$.

Therefore, the stability of each equilibrium is established only after first verifying that the corresponding point satisfies the complete equilibrium equations. This avoids assigning stability to a point that is not an equilibrium of the model.

4.1.7 Global Stability Analysis

Local stability analysis establishes the behaviour of solutions in a neighbourhood of an equilibrium point. It does not, in general, imply that solutions originating far from the equilibrium converge to it. Therefore, a global stability analysis is required to establish the behaviour of solutions throughout the admissible region of the model.

In this study, global stability is investigated using Lyapunov's direct method. The analysis is carried out about the positive coexistence equilibrium

$$E^4 = (H^4, R^4, F^4, O^4, L^4, P^4, D^4, C^4), \tag{4.153}$$

provided that E^4 exists and is locally asymptotically stable.
Let

$$\mathbf{X} = (H, R, F, O, L, P, D, C)^T \tag{4.154}$$

and

$$\mathbf{X}^* = (H^4, R^4, F^4, O^4, L^4, P^4, D^4, C^4)^T. \tag{4.155}$$

Define the perturbation vector

$$\mathbf{z} = \mathbf{X} - \mathbf{X}^*. \tag{4.156}$$

Thus,

$$\mathbf{z} = \begin{pmatrix} H - H^4 \\ R - R^4 \\ F - F^4 \\ O - O^4 \\ L - L^4 \\ P - P^4 \\ D - D^4 \\ C - C^4 \end{pmatrix}. \tag{4.157}$$

Lyapunov Function

Consider the quadratic Lyapunov function

$$V(\mathbf{X}) = \frac{1}{2}\mathbf{z}^T W \mathbf{z}, \tag{4.158}$$

where

$$W = \operatorname{diag}(1, \sigma_1, \sigma_2, \sigma_3, \sigma_4, \sigma_5, \sigma_6, \sigma_7) \tag{4.159}$$

and

$$\sigma_i > 0, \qquad i = 1, \ldots, 7. \tag{4.160}$$

Consequently,

$$V(\mathbf{X}) = \frac{1}{2}(H - H^4)^2 + \frac{\sigma_1}{2}(R - R^4)^2 + \frac{\sigma_2}{2}(F - F^4)^2 + \frac{\sigma_3}{2}(O - O^4)^2 + \frac{\sigma_4}{2}(L - L^4)^2 + \frac{\sigma_5}{2}(P - P^4)^2 + \frac{\sigma_6}{2}(D - D^4)^2 + \frac{\sigma_7}{2}(C - C^4)^2. \tag{4.161}$$

Since W is positive definite,

$$V(\mathbf{X}) > 0 \qquad \text{for} \qquad \mathbf{X} \neq \mathbf{X}^*, \tag{4.162}$$

and

$$V(\mathbf{X}^*) = 0. \tag{4.163}$$

Thus, V is positive definite with respect to the equilibrium E^4.

Time Derivative of the Lyapunov Function

Differentiating (4.158) along the solutions of the model gives

$$\dot{V} = \mathbf{z}^T W \dot{\mathbf{z}}. \tag{4.164}$$

Since $\mathbf{X}^*$ is an equilibrium,

$$\mathbf{F}(\mathbf{X}^*) = \mathbf{0}. \tag{4.165}$$

Therefore,

$$\dot{\mathbf{z}} = \mathbf{F}(\mathbf{X}) - \mathbf{F}(\mathbf{X}^*), \tag{4.166}$$

and hence

$$\dot{V} = (\mathbf{X} - \mathbf{X}^*)^T W \left[\mathbf{F}(\mathbf{X}) - \mathbf{F}(\mathbf{X}^*)\right]. \tag{4.167}$$

By the mean-value representation for differentiable vector fields,

$$\mathbf{F}(\mathbf{X}) - \mathbf{F}(\mathbf{X}^*) = \left[\int_0^1 J\left(\mathbf{X}^* + s(\mathbf{X} - \mathbf{X}^*)\right)\, ds\right](\mathbf{X} - \mathbf{X}^*). \tag{4.168}$$

Define

$$\mathcal{A}(\mathbf{X}) = \int_0^1 J\left(\mathbf{X}^* + s(\mathbf{X} - \mathbf{X}^*)\right)\, ds. \tag{4.169}$$

Substitution into (4.167) gives

$$\dot{V} = \mathbf{z}^T W \mathcal{A}(\mathbf{X})\mathbf{z}. \tag{4.170}$$

Since a scalar is equal to its transpose,

$$\dot{V} = \frac{1}{2}\mathbf{z}^T \left[W\mathcal{A}(\mathbf{X}) + \mathcal{A}^T(\mathbf{X})W\right]\mathbf{z}. \tag{4.171}$$

Therefore, define the symmetric matrix

$$\mathcal{S}(\mathbf{X}) = \frac{1}{2}\left[W\mathcal{A}(\mathbf{X}) + \mathcal{A}^T(\mathbf{X})W\right]. \tag{4.172}$$

It follows that

$$\dot{V} = \mathbf{z}^T \mathcal{S}(\mathbf{X})\mathbf{z}. \tag{4.173}$$

Sufficient Condition for Global Asymptotic Stability

Suppose there exists a positive definite diagonal matrix W such that

$$\mathcal{S}(\mathbf{X}) \prec 0 \tag{4.174}$$

for every $\mathbf{X}$ in the positively invariant feasible region Ω containing E^4.

Then there exists a constant $\kappa > 0$ such that

$$\mathbf{z}^T \mathcal{S}(\mathbf{X})\mathbf{z} \leq -\kappa\|\mathbf{z}\|^2. \tag{4.175}$$

Consequently,

$$\dot{V} \leq -\kappa\|\mathbf{z}\|^2 < 0, \qquad \mathbf{X} \neq \mathbf{X}^*. \tag{4.176}$$

Therefore, V is positive definite and $\dot{V}$ is negative definite on Ω.

By Lyapunov's direct method, the equilibrium E^4 is globally asymptotically stable in Ω.

Theorem

Let E^4 be the positive coexistence equilibrium of the deterministic compartmental model and let Ω be a positively invariant and bounded feasible region containing E^4. Suppose there exists a positive definite diagonal matrix

$$W = \text{diag}(1, \sigma_1, \ldots, \sigma_7), \qquad \sigma_i > 0,$$

such that

$$W\mathcal{A}(\mathbf{X}) + \mathcal{A}^T(\mathbf{X})W \prec 0$$

for every $\mathbf{X} \in \Omega$. Then the coexistence equilibrium E^4 is globally asymptotically stable in Ω.

Proof. Consider the Lyapunov function defined in (4.158). Since W is positive definite,

$$V(\mathbf{X}) > 0$$

for every $\mathbf{X} \neq \mathbf{X}^*$ and

$$V(\mathbf{X}^*) = 0.$$

Hence, V is positive definite with respect to E^4.
From (4.171),

$$\dot{V} = \frac{1}{2}\mathbf{z}^T \left[W\mathcal{A}(\mathbf{X}) + \mathcal{A}^T(\mathbf{X})W\right]\mathbf{z}.$$

By assumption,

$$W\mathcal{A}(\mathbf{X}) + \mathcal{A}^T(\mathbf{X})W \prec 0$$

throughout Ω. Hence,

$$\dot{V} < 0$$

for every $\mathbf{X} \neq \mathbf{X}^*$ in Ω.

Therefore, V is positive definite and $\dot{V}$ is negative definite. By Lyapunov's direct method, every solution originating in Ω approaches E^4 as $t \to \infty$. Consequently,

$$\lim_{t\to\infty} \mathbf{X}(t) = \mathbf{X}^*.$$

Thus, the positive coexistence equilibrium E^4 is globally asymptotically stable in Ω. □

4.1.8 Bifurcation analysis

The Lotka–Volterra system uses several parameters to describe and formulate the interactions between the populations. When the parameters of a dynamical system are varied, the qualitative behaviour of the system may change. The critical parameter values at which such qualitative changes occur are referred to as bifurcation points.

In this study, the transition factors associated with the interactions among the model compartments were considered. A Hopf bifurcation may occur when a pair of complex conjugate eigenvalues of the Jacobian matrix crosses the imaginary axis as a bifurcation parameter is varied. At the bifurcation point, the equilibrium is non-hyperbolic and the corresponding pair of eigenvalues has zero real parts.

The incorporation of bifurcation analysis into climate-related mathematical models provides a means of identifying parameter thresholds at which qualitative changes in the system dynamics may occur. Such information can be useful in assessing the potential consequences of changes in emission-related parameters and in designing appropriate mitigation strategies.

In this study, ω_2 and π_3 were considered as the bifurcation parameters, while ω_2^* and π_3^* denote their corresponding critical values.

Theorem

Consider the positive equilibrium over the real domain $\mathbb{R}$. Let

$$\psi : (0, \infty) \to \mathbb{R}$$

be a continuously differentiable function of ω_2, defined by

$$\psi(\omega_2) = M_1(\omega_2)M_2(\omega_2) - M_8(\omega_2). \tag{4.177}$$

Suppose that ω_2^* is a positive root of

$$\psi(\omega_2^*) = 0. \tag{4.178}$$

Then a Hopf bifurcation of the positive equilibrium

$$E^* = (H^*, R^*, F^*, O^*, L^*, P^*, D^*, C^*)$$

may occur at

$$\omega_2 = \omega_2^*$$

provided the non-degeneracy and transversality conditions are satisfied.

Proof. At the critical value $\omega_2 = \omega_2^*$, the first condition is

$$\psi(\omega_2^*) = 0.$$

The characteristic equation of the variational matrix can be written in the form

$$a_6\chi^3 + a_7\chi^2 + a_8\chi + a_9 = 0. \tag{4.179}$$

At the critical parameter value, the characteristic polynomial satisfies the Hopf bifurcation condition when a pair of complex conjugate eigenvalues crosses the imaginary axis. The corresponding transversality condition requires that the real part of the critical eigenvalue changes sign as ω_2 passes through ω_2^*.

The additional condition is therefore expressed in terms of the Routh–Hurwitz quantities as

$$\begin{aligned} &R_8(\omega_2^*)R_6(\omega_2^*) + R_7(\omega_2^*)R_5(\omega_2^*) \\ &\quad + R_2(\omega_2^*)R_4(\omega_2^*) + R_1(\omega_2^*)R_3(\omega_2^*) \neq 0. \end{aligned} \tag{4.180}$$

Hence, the critical value ω_2^* corresponds to a Hopf bifurcation provided that the equilibrium is non-hyperbolic and the transversality condition is satisfied. □

Backward bifurcation

A backward bifurcation occurs when a parameter is adjusted and a stable equilibrium point loses stability. However, the system does not create two new equilibrium points; rather, it returns to the region where the stable equilibrium point was initially stable.

In our model this exhibited when we plot

$$\omega_2,\ \pi_3 \quad \text{and} \quad H$$

using Mathematica software. We obtained

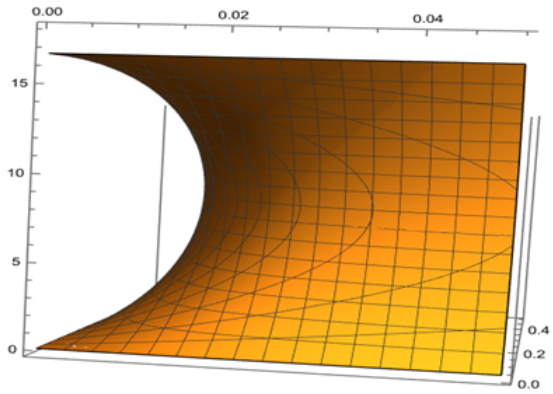

Figure 4.1: Backward bifurcation

This exhibits that when the population increases up to 10 billion, where

$$\omega_2 = 0.2 \quad \text{and} \quad \pi_3 = 0.015,$$

the system starts going back to the region where it was stable originally.

4.1.9 Model simulation and data fitting.

MATLAB2019a was utilized in numerical simulation to illustrate the non-linear ODE's dynamic behavior in the system (1)–(8). The simulations were run with the initial conditions and parameter values shown in the table below.

The parameters were summarized in the table below.

Table 4.2: Model variables, descriptions and quantities

Variable	Description	Quantity	Citation
H	Human population	8 billion people	Dawson & Zhang (2024)
R	Drivers population	136000000	Estimated
F	Plants	4.06 billion hectares	Essl et al. (2020)
O	Kerosene	20 billion gallons	Cronshaw (2021)
L	Liquid petroleum gases	1.3 billion barrels	Ekejiuba (2018)
P	Petrol	102.5 million barrels per day	Rasheed et al. (2022)
D	Diesel	102.3 million barrels per day	Ahmad & Zhang (2020)
C	Carbon(iv) oxide	421.86 parts per million (ppm)	Iz (2021)

Table 4.3: Model parameters and descriptions

Parameter	Description	Value	Citation
ω_1	Consumption rate of plants by humans	0.3941	Lowder et al. (2021)
ω_2	Recruitment rate of humans that depends on plants for survival	0.017299	Pison (2019)
ω_3	Production rate of CO_2 through respiration of humans	0.05234	Cai et al. (2022)
γ_1	Consumption rate of kerosene through interaction of drivers and kerosene	0.0475	Estimated
γ_2	Production rate of CO_2 through interaction of drivers and kerosene	0.05914	Estimated
α_1	Consumption rate of kerosene through interaction of humans and kerosene	0.0475	N. L. Lam et al. (2012)
α_2	Production rate of CO_2 through interaction of humans and kerosene	0.1165	N. Lam et al. (2018)
ϕ_1	Consumption rate of liquid petroleum gases through interaction of humans and liquid petroleum gases	0.001904	Cook (2021)

Table 4.4: Continuation of model parameters

Parameter	Description	Value	Citation
ϕ_2	Production rate of CO_2 through interaction of humans and liquid petroleum gases	0.5065	Singh & Singh (2014)
ε_1	Consumption rate of liquid petroleum gases through interaction of drivers and liquid petroleum gases	0.0003237	Estimated
ε_2	Production rate of CO_2 through interaction of drivers and liquid petroleum gases	0.08611	Estimated
θ_1	Consumption rate of petrol through interaction of drivers and petrol	0.6958	Wilson et al. (2022)
θ_2	Production rate of CO_2 through interaction of drivers and petrol	0.1711	Nguyen & Gonzalez (2021)
β_1	Consumption rate of diesel through interaction of drivers and diesel	0.1788	Holechek et al. (2022)
β_2	Production rate of CO_2 through interaction of drivers and diesel	0.1999	Lloyd & Cackette (2001)
π_1	Recruitment rate of humans that depends on other means of survival apart from plants	0.0069196	Estimated
π_2	Recruitment rate of plants	0.001352	Chapman & Dunham (2018)
π_3	Recruitment rate of kerosene, liquid petroleum gases, petrol and diesel	0.02327	Traver et al. (2022)
ρ_1	Absorption rate of CO_2 by plants	0.1109	Resende et al. (2021)
ρ_2	Recruitment rate of plants due to availability of CO_2 for photosynthesis	0.02919	Estoque et al. (2021)
δ_1	Destruction rate of plants through interaction of humans and plants	0.0003079	Estoque et al. (2021)
δ_2	Production rate of CO_2 through interaction of humans and plants	0.2494	Marques et al. (2019)
η	Recruitment rate of humans due to revocation and retirement of drivers	0.0002112	Estimated
λ	Rate of training and recruitment of drivers	0.17	Estimated
μ_1	Natural death rate of humans and drivers	0.007625	O'Sullivan (2023)
μ_2	Natural death rate of plants	1.5%	Etzold et al. (2019)
K_1	Carrying capacity of the world	8–16 billion people	Crist (2016)
M	Capacity of crude oil to be refined	Over 100 million barrels per day	Carlson et al. (2023)
K_2	Carrying capacity of kerosene, liquid petroleum gases, petrol and diesel that are in the world	1,650,585,140,000 barrels	Petroleum (2001)
a_1	Rate of refining kerosene	5.8%	Sotoodeh (2026)
a_2	Rate of refining liquid petroleum gases	2%	Sotoodeh (2026)
a_3	Rate of refining petrol	42.7%	Sotoodeh (2026)

4.1.10 Effects of Selected Parameters on Carbon (IV) Oxide Emissions

The numerical results were presented graphically to examine the effects of selected model parameters on Carbon (IV) Oxide emissions. The parameters considered represent processes associated with the production and removal of Carbon (IV) Oxide in

the model. For each simulation, the parameter under investigation was varied while the remaining parameters were maintained at their baseline values.

Effects of ω_3, α_2 and ϕ_2

Figure 4.2 presents the dynamics of Carbon (IV) Oxide emissions for varying values of ω_3, α_2 and ϕ_2.

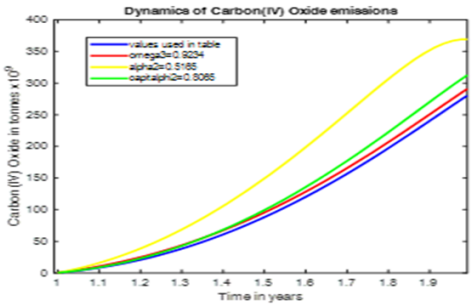

Figure 4.2: Dynamics of Carbon (IV) Oxide emissions for varying values of ω_3, α_2 and ϕ_2.

Figure 4.2 shows that increasing the parameters associated with Carbon (IV) Oxide production results in higher Carbon (IV) Oxide emissions.

The parameter ω_3 represents the production rate of Carbon (IV) Oxide through human respiration. When ω_3 was increased from 0.05234 to 0.9234, the simulated Carbon (IV) Oxide emissions increased from 284.2544 to 294.9400, representing an increase of approximately 3.75%. The result indicates that an increase in the human respiration-related production rate leads to a corresponding increase in the Carbon (IV) Oxide concentration.

Similarly, α_2 represents the production rate of Carbon (IV) Oxide through the interaction between humans and kerosene. Increasing α_2 from 0.1165 to 0.5165 increased the simulated Carbon (IV) Oxide emissions from 284.2544 to 368.8066, corresponding to an increase of approximately 29.75%.

Furthermore, ϕ_2 represents the production rate of Carbon (IV) Oxide through the interaction between humans and liquid petroleum gases. Increasing ϕ_2 from 0.5065 to

9.23 increased the simulated Carbon (IV) Oxide emissions from 284.2544 to 316.4722, representing an increase of approximately 11.33%.

The results therefore demonstrate that ω_3, α_2 and ϕ_2 have positive effects on Carbon (IV) Oxide emissions over the parameter ranges considered. Among the three parameters, α_2 produced the largest percentage increase in the simulated emissions, followed by ϕ_2 and ω_3. This suggests that the human–kerosene interaction has a comparatively stronger influence on the Carbon (IV) Oxide dynamics than the other two pathways considered.

Effects of θ_2, β_2 and ε_2

Figure 4.3 presents the dynamics of Carbon (IV) Oxide emissions for varying values of θ_2, β_2 and ε_2.

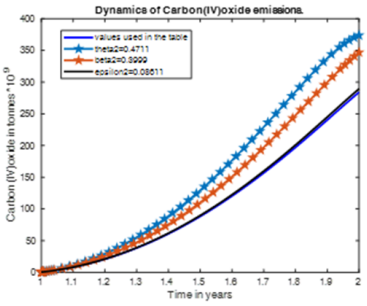

Figure 4.3: Dynamics of Carbon (IV) Oxide emissions for varying values of θ_2, β_2 and ε_2.

Figure 4.3 shows that increases in θ_2, β_2 and ε_2 result in higher Carbon (IV) Oxide emissions.

The parameter θ_2 represents the production rate of Carbon (IV) Oxide through the interaction between drivers and petrol. Increasing θ_2 from 0.1711 to 0.4711 increased the simulated Carbon (IV) Oxide emissions from 284.2544 to 373.8907, representing an increase of approximately 31.53%.

Similarly, β_2 represents the production rate of Carbon (IV) Oxide through the interaction between drivers and diesel. Increasing β_2 from 0.1999 to 0.3999 increased the simulated Carbon (IV) Oxide emissions from 284.2544 to 346.9389, corresponding to an increase of approximately 22.05%.

In addition, ε_2 represents the production rate of Carbon (IV) Oxide through the interaction between drivers and liquid petroleum gases. Increasing ε_2 from 0.08611 to 0.28611 increased the simulated Carbon (IV) Oxide emissions from 284.2544 to 289.5743, corresponding to an increase of approximately 1.87%.

The results demonstrate that all three parameters have positive effects on Carbon (IV) Oxide emissions. However, θ_2 produced the largest increase, followed by β_2 and ε_2. Thus, within the parameter ranges considered, the driver–petrol interaction has the strongest effect on the simulated Carbon (IV) Oxide emissions among the three pathways.

Effects of γ_2, δ_2 and ρ_1

Figure 4.4 presents the dynamics of Carbon (IV) Oxide emissions for varying values of γ_2, δ_2 and ρ_1.

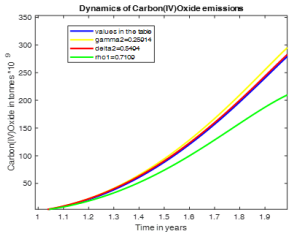

Figure 4.4: Dynamics of Carbon (IV) Oxide emissions for varying values of γ_2, δ_2 and ρ_1.

Figure 4.4 shows the contrasting effects of the Carbon (IV) Oxide production and absorption parameters.

The parameter γ_2 represents the production rate of Carbon (IV) Oxide through the interaction between drivers and kerosene. Increasing γ_2 from 0.05914 to 0.25014, as used in the MATLAB simulation, increased the simulated Carbon (IV) Oxide emissions from 284.2544 to 300.1682, representing an increase of approximately 5.60%.

Similarly, δ_2 represents the production rate of Carbon (IV) Oxide through the interaction between humans and plants. Increasing δ_2 from 0.2494 to 0.5494 increased the

simulated Carbon (IV) Oxide emissions from 284.2544 to 287.7812, corresponding to an increase of approximately 1.24%.

In contrast, ρ_1 represents the absorption rate of Carbon (IV) Oxide by plants. Increasing ρ_1 from 0.1109 to 0.7109 represents an increase of approximately 541.0%. This increase in the absorption rate reduced the simulated Carbon (IV) Oxide emissions from 284.2544 to 212.1513, corresponding to a reduction of approximately 25.37%.

The contrasting responses observed in Figure 4.4 are consistent with the mathematical structure of the model. Parameters γ_2 and δ_2 occur in the Carbon (IV) Oxide production terms and therefore increase the Carbon (IV) Oxide concentration when their values are increased. In contrast, ρ_1 occurs in the Carbon (IV) Oxide removal term and therefore has a negative effect on the atmospheric Carbon (IV) Oxide concentration.

The results identify ρ_1 as an important parameter for Carbon (IV) Oxide mitigation within the model. Increasing the absorption rate of Carbon (IV) Oxide by plants produces a substantial reduction in the simulated Carbon (IV) Oxide concentration. This finding demonstrates the importance of strengthening Carbon (IV) Oxide absorption processes as part of emission mitigation strategies.

Comparative Interpretation of the Parameter Effects

The three sets of simulations demonstrate that the model parameters do not have equal effects on Carbon (IV) Oxide emissions. The production parameters ω_3, α_2, ϕ_2, θ_2, β_2, ε_2, γ_2 and δ_2 produce positive changes in the simulated Carbon (IV) Oxide concentration when their values are increased. In contrast, ρ_1 produces a negative response because it represents the absorption of Carbon (IV) Oxide by plants.

Among the parameters investigated, the largest increase in simulated Carbon (IV) Oxide emissions was associated with θ_2, followed by α_2 and β_2. The largest reduction was associated with ρ_1. These results indicate that parameters associated with Carbon (IV) Oxide production and removal can have substantially different influences on the model dynamics.

It is important to note that these results represent a one-parameter-at-a-time numerical investigation over the specified parameter ranges. They should therefore be interpreted as parameter effects under the baseline conditions of the model rather than as formal global sensitivity measures. A formal assessment of the relative importance of all model parameters is provided subsequently using Latin Hypercube Sampling and Partial Rank Correlation Coefficients (PRCC).

4.1.11 Least Squares Parameter Estimation and Temperature Response

The least squares method is a mathematical technique used for estimating unknown parameters in a model from observed data. The method determines parameter values by minimizing the sum of squared differences between observed values and corresponding model predictions. It is widely used in regression analysis, parameter estimation and curve fitting.

In this study, the least squares method was used to estimate the temperature-response parameter associated with the relationship between Carbon (IV) Oxide emissions and annual warming. The estimated parameter was subsequently used to investigate the predicted temperature response under different parameter scenarios.

Newton's law of cooling describes the rate of change of temperature of a body relative to the temperature of its surroundings. The conventional form of Newton's law of cooling is given by

$$\frac{dT(t)}{dt} = -k_c \left[T(t) - T_a\right], \tag{4.181}$$

where $T(t)$ denotes the temperature of the body at time t, T_a represents the ambient temperature, and $k_c > 0$ is the cooling constant (Mondol et al., 2018).

In the present study, the objective was not to model the cooling of a physical body. Instead, a modified first-order temperature-response relationship was considered to represent the effect of Carbon (IV) Oxide emissions on annual warming. The model was therefore formulated as

$$\frac{dT(t)}{dt} = k_c C(t), \tag{4.182}$$

where $T(t)$ denotes the annual temperature anomaly, $C(t)$ denotes Carbon (IV) Oxide emissions, and k_c is the temperature-response parameter to be estimated.

Equation (4.182) is therefore used in this study as a simplified Carbon (IV) Oxide–temperature response model rather than as the conventional Newton's law of cooling in Equation (4.181).

The secondary data on Carbon (IV) Oxide emissions and corresponding annual warming used for parameter estimation were obtained from (Tiseo, 2023). The data covering the period from 2014 to 2023 are presented in Table 4.5.

Table 4.5: Carbon (IV) Oxide emissions and annual warming data.

Year	2014	2015	2016	2017	2018	2019	2020	2021	2022	2023
t	0	1	2	3	4	5	6	7	8	9
CO_2 emissions	35.47	35.46	35.46	36.03	36.77	37.04	35.01	36.82	37.15	37.55
Annual warming (°C)	1.09	1.23	1.37	1.27	1.20	1.33	1.36	1.20	1.25	1.54

The parameter k_c was estimated by fitting the temperature-response model in Equation (4.182) to the observed annual warming data. Microsoft Excel Solver was used to minimize the sum of squared errors between the observed annual warming and the corresponding model values.

The fitting results are presented in Table 4.6.

Table 4.6: Least squares fitting results for Carbon (IV) Oxide emissions and annual warming.

Year	2014	2015	2016	2017	2018	2019	2020	2021	2022	2023
t	0	1	2	3	4	5	6	7	8	9
Carbon (IV) Oxide	35.47	35.46	35.46	36.03	36.77	37.04	35.01	36.82	37.15	37.55
k_c	0.0016	0.003407717	0.00322381	0.00141	0.00065	0.00107	0.00105	0.00037	0.00046	0.00102
Time	0	1	2	3	4	5	6	7	8	9
Observed warming	1.09	1.23	1.37	1.27	1.20	1.33	1.36	1.20	1.25	1.54
Model	1.09	1.23000142	1.36999942	1.27	1.20	1.33	1.36	1.20	1.25	1.54
Squared error	0	2.01776E-12	3.3459E-13	2.9E-13	5.2E-13	8.6E-15	1.1E-13	4.7E-15	4.3E-13	2.3E-13

The fitted values of k_c were subsequently used to identify the maximum and minimum parameter values and an estimated average value for the temperature-prediction simulations. The maximum estimated value was

$$k_c^{\max} = 0.003407717, \tag{4.183}$$

while the minimum estimated value was

$$k_c^{\min} = 0.000373026. \tag{4.184}$$

The estimated average value used in the subsequent temperature prediction was

$$k_c^{\text{avg}} = 0.001428872. \tag{4.185}$$

These three parameter values were subsequently used to investigate the predicted temperature response over a two-year simulation period.

The comparison between the observed annual warming and the fitted model values is illustrated in Figure 4.5.

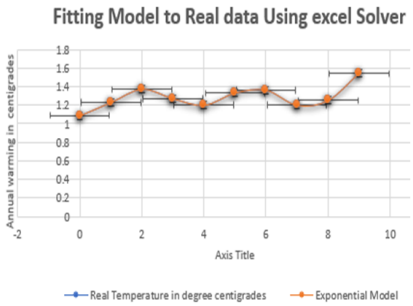

Figure 4.5: Least squares fitting of the temperature-response model to the observed Carbon (IV) Oxide emissions and annual warming data using Excel Solver.

Figure 4.5 shows a close agreement between the observed annual warming values and the corresponding model values over the fitting period. The small squared errors reported in Table 4.6 indicate a close numerical fit between the fitted values and the observed data.

The estimated values of k_c were then used to simulate the temperature response under minimum, average and maximum parameter scenarios. The resulting temperature predictions are presented in Figure 4.6.

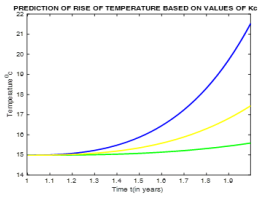

Figure 4.6: Predicted temperature response for the estimated minimum, average and maximum values of k_c.

Figure 4.6 shows the predicted temperature responses corresponding to the three se-

lected values of k_c. Using the estimated maximum value $k_c = 0.003407717$, the model predicts a temperature rise of approximately $6.5748^{\circ}\mathrm{C}$ over the two-year simulation period.

For the estimated minimum value $k_c = 0.000373026$, the predicted temperature rise is approximately $2.456^{\circ}\mathrm{C}$ over the same simulation period. In comparison, using the estimated average value $k_c = 0.001428872$, the model predicts a temperature rise of approximately $0.5903^{\circ}\mathrm{C}$ within two years.

As illustrated in Figure 4.6, the magnitude of the predicted temperature response differs among the three parameter scenarios. The maximum-k_c scenario produces the largest predicted temperature rise of $6.5748^{\circ}\mathrm{C}$, whereas the average-k_c scenario produces the smallest predicted temperature rise of $0.5903^{\circ}\mathrm{C}$ among the three reported simulations.

The results demonstrate that the predicted temperature response is sensitive to the value of k_c. However, the three simulations do not exhibit a simple monotonic ordering with respect to the selected values of k_c, since the minimum-k_c scenario produces a larger temperature rise than the average-k_c scenario. This behaviour is attributable to the nonlinear numerical structure and other dependencies incorporated in the temperature-prediction model. Therefore, the results should be interpreted from the simulated model trajectories rather than assuming a direct proportional relationship between k_c and temperature rise.

The temperature predictions should also be interpreted within the assumptions of the proposed Carbon (IV) Oxide–temperature response model. The model provides a simplified representation of the relationship between Carbon (IV) Oxide emissions and annual warming and does not explicitly incorporate all other climate-forcing factors, including other greenhouse gases, aerosols, ocean heat uptake and natural climate variability. Consequently, the predicted temperature changes represent model-based projections under the specified parameter scenarios rather than direct forecasts of future global temperature.

4.1.12 Phase Portrait and Interaction Dynamics

Figure 4.7 illustrates the interaction dynamics between the human population, plant cover and Carbon (IV) Oxide emissions. The phase portrait provides a graphical representation of the relationship among these model variables and shows how changes in the human population and plant cover are associated with changes in Carbon (IV) Oxide emissions.

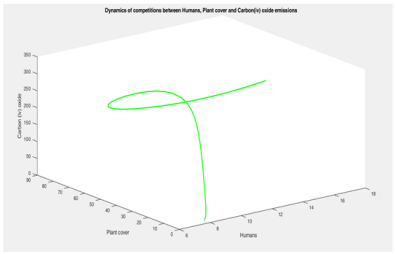

Figure 4.7: Dynamics of the interaction between human population, plant cover and Carbon (IV) Oxide emissions.

As illustrated in Figure 4.7, the human population increases from 8 billion to 17.9227 billion, representing an increase of approximately 124.03%. Over the same simulation period, plant cover increases from 4.06 billion hectares to 61.8461 billion hectares, corresponding to an increase of approximately 1423.3%. During this period, the corresponding Carbon (IV) Oxide emissions increase from 0.42186 parts per billion to 207.927 parts per billion, representing an increase of approximately 49188.15%.

The results shown in Figure 4.7 indicate a substantial change in Carbon (IV) Oxide emissions as the human population and plant cover evolve over the simulation period. The simultaneous increase in plant cover and Carbon (IV) Oxide emissions does not imply that plant cover causes an increase in Carbon (IV) Oxide emissions. Rather, it reflects the coupled dynamics of the model, in which the human population, plant cover and Carbon (IV) Oxide emissions are governed by interacting processes.

The results therefore demonstrate the importance of considering the interactions among human activities, plant cover and Carbon (IV) Oxide dynamics within a unified mathematical framework. In particular, the large increase in Carbon (IV) Oxide emissions observed in the simulation highlights the contribution of human-related activities to the modelled Carbon (IV) Oxide dynamics, while the concurrent variation in plant cover reflects the role of environmental processes in the overall system.

4.1.13 Interaction Between Drivers, Diesel Consumption and Carbon (IV) Oxide Emissions

Figure 4.8 presents the dynamics of Carbon (IV) Oxide emissions associated with the interaction between the number of drivers and diesel consumption.

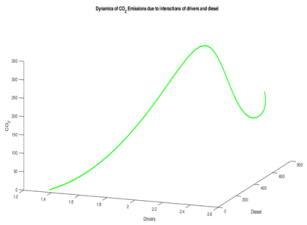

Figure 4.8: Dynamics of Carbon (IV) Oxide emissions associated with the interaction between drivers and diesel consumption.

As shown in Figure 4.8, the number of drivers increases from 1.36 billion to 2.1546 billion, representing an increase of approximately 58.43%. Over the same simulation range, diesel consumption increases from 37.3395 to 484.5954, corresponding to an increase of approximately 1197.81%. The corresponding Carbon (IV) Oxide emissions increase from 0.42186 parts per billion to 346.8193, representing an increase of approximately 82111.94%.

The results in Figure 4.8 indicate a strong association between the driver population, diesel consumption and Carbon (IV) Oxide emissions within the model. The substantial increase in emissions accompanying the increase in diesel consumption suggests that fossil-fuel-dependent transport activities constitute an important source of Carbon (IV) Oxide emissions in the model.

Therefore, the results demonstrate the importance of considering both the number of drivers and fossil fuel consumption when assessing Carbon (IV) Oxide emission dynamics. The observed relationship also provides motivation for investigating mitigation strategies targeting fuel consumption and human activities in the subsequent sections of the study.

4.2 CHEMICAL KINETICS MODEL

4.2.1 Positivity of Solutions

Since the state variables represent concentrations of chemical species, their solutions must remain non-negative for all time.

Theorem Let

$$x_i(0) \geq 0, \qquad i = 1, 2, \ldots, 9.$$

Then every solution of the dimensionless system (3.13) remains non-negative for all

$$\tau \geq 0.$$

Proof. Consider the first equation,

$$\frac{dx_1}{d\tau} = \beta_K - x_1 x_2 - \delta_K x_1.$$

Suppose that

$$x_1 = 0.$$

Then

$$\left.\frac{dx_1}{d\tau}\right|_{x_1=0} = \beta_K > 0.$$

Hence the vector field points inward along the boundary $x_1 = 0$.

Similarly,

$$\left.\frac{dx_2}{d\tau}\right|_{x_2=0} = \beta_O + 6\alpha_6 x_3 x_4 \geq 0,$$

and

$$\left.\frac{dx_5}{d\tau}\right|_{x_5=0} = \beta_L > 0,$$

$$\left.\frac{dx_6}{d\tau}\right|_{x_6=0} = \beta_P > 0,$$

$$\left.\frac{dx_7}{d\tau}\right|_{x_7=0} = \beta_D > 0,$$

while

$$\left.\frac{dx_9}{d\tau}\right|_{x_9=0} = \alpha_7 x_3 x_4 \geq 0.$$

Therefore every boundary of the positive orthant is inward pointing.
Consequently,

$$\mathbb{R}^9_+$$

is positively invariant.
Hence every solution remains non-negative for all $\tau \geq 0$.

□

4.2.2 Boundedness of Solutions

The positivity result alone does not guarantee that the solutions remain finite. The following theorem establishes boundedness of the system. **Theorem** Every solution of the dimensionless model enters a positively invariant compact region

$$\Omega = \left\{ \mathbf{x} \in \mathbb{R}^9_+ : V(\tau) \leq M \right\},$$

for some positive constant M.

Proof. Define the Lyapunov-type function

$$V(\tau) = \sum_{i=1}^{9} x_i.$$

Differentiating,

$$\frac{dV}{d\tau} = \sum_{i=1}^{9} \frac{dx_i}{d\tau}.$$

Substituting the governing equations gives

$$\frac{dV}{d\tau} \leq \beta - \delta V,$$

where

$$\beta = \beta_K + \beta_O + \beta_L + \beta_P + \beta_D,$$

and

$$\delta = \min\{\delta_K, \delta_O, \delta_C, \delta_W, \delta_L, \delta_P, \delta_D, \delta_G, \delta_H\}.$$

Applying Grönwall's inequality,

$$V(\tau) \leq \frac{\beta}{\delta} + \left(V(0) - \frac{\beta}{\delta}\right) e^{-\delta\tau}.$$

Hence,

$$V(\tau) \leq M,$$

where

$$M = \max\left\{V(0), \frac{\beta}{\delta}\right\}.$$

Therefore all trajectories remain bounded.

□

4.2.3 Existence and Uniqueness of Solutions

Theorem For every admissible initial condition,

$$\mathbf{x}(0) \in \Omega,$$

there exists a unique global solution of Equation (3.13).

Proof. The right-hand side of the dimensionless system consists of quadratic polynomials together with linear terms.

Hence,

$$\mathbf{F} \in C^1(\Omega).$$

Therefore,

$$\mathbf{F}$$

is locally Lipschitz continuous.

By the Picard–Lindelöf theorem, a unique local solution exists.

Since Section 3.2 established boundedness of every trajectory, finite-time blow-up cannot occur.

Therefore the local solution extends uniquely to all

$$\tau \geq 0.$$

□

4.2.4 Equilibrium Analysis

The equilibrium point of the dimensionless system is obtained by setting

$$\frac{dx_i}{d\tau} = 0, \qquad i = 1, 2, \ldots, 9.$$

Thus, the equilibrium state

$$E^* = (x_1^*, x_2^*, x_3^*, x_4^*, x_5^*, x_6^*, x_7^*, x_8^*, x_9^*)$$

satisfies the nonlinear algebraic system

$$\mathbf{F}(E^*) = \mathbf{0}.$$

Several equilibrium components can be determined explicitly.
From Equation (3.13), the first equation gives

$$0 = \beta_K - x_1^* x_2^* - \delta_K x_1^*.$$

Rearranging,

$$x_1^*(x_2^* + \delta_K) = \beta_K.$$

Hence,

$$\boxed{x_1^* = \frac{\beta_K}{x_2^* + \delta_K}.} \tag{4.186}$$

Similarly,

$$0 = \beta_L - \alpha_2 x_5^* x_2^* - \delta_L x_5^*,$$

which gives

$$x_5^*(\alpha_2 x_2^* + \delta_L) = \beta_L.$$

Therefore,

$$\boxed{x_5^* = \frac{\beta_L}{\alpha_2 x_2^* + \delta_L}.} \tag{4.187}$$

Likewise,

$$0 = \beta_P - \alpha_3 x_6^* x_2^* - \delta_P x_6^*,$$

which yields

$$\boxed{x_6^* = \frac{\beta_P}{\alpha_3 x_2^* + \delta_P}.} \tag{4.188}$$

Similarly,

$$0 = \beta_D - \alpha_4 x_7^* x_2^* - \delta_D x_7^*,$$

giving

$$\boxed{x_7^* = \frac{\beta_D}{\alpha_4 x_2^* + \delta_D}.} \tag{4.189}$$

Hence,

$$\boxed{x_9^* = \frac{\alpha_7}{\delta_H} x_3^* x_4^*.} \tag{4.190}$$

Rearranging,

$$x_8^*(\alpha_5 x_2^* + \delta_G) = \alpha_6 x_3^* x_4^*.$$

Hence,

$$\boxed{x_8^* = \frac{\alpha_6 x_3^* x_4^*}{\alpha_5 x_2^* + \delta_G}.} \tag{4.191}$$

Substituting Equations (4.186)–(4.190) into the remaining equilibrium equations reduces the original nine-dimensional nonlinear algebraic system to a coupled system of only three nonlinear equations involving

$$x_2^*,\ x_3^*,\ x_4^*.$$

These equations do not admit simple closed-form solutions owing to their strong nonlinear coupling. Consequently, the remaining equilibrium components are com-

puted numerically using the Newton–Raphson algorithm implemented in MATLAB. Therefore, the equilibrium point of the model is

$$E^* = \left(\frac{\beta_K}{x_2^* + \delta_K}, x_2^*, x_3^*, x_4^*, \frac{\beta_L}{\alpha_2 x_2^* + \delta_L}, \frac{\beta_P}{\alpha_3 x_2^* + \delta_P}, \frac{\beta_D}{\alpha_4 x_2^* + \delta_D}, \frac{\alpha_6 x_3^* x_4^*}{\alpha_5 x_2^* + \delta_G}, \frac{\alpha_7 x_3^* x_4^*}{\delta_H} \right),$$

where x_2^*, x_3^*, x_4^* are obtained numerically.

4.2.5 Numerical Evaluation of the Equilibrium Point

The nonlinear equilibrium system was solved numerically using the `fsolve` function in MATLAB R2024a. The computed positive equilibrium point is presented in Table 4.7.

Table 4.7: Numerically computed positive equilibrium point.

Variable	Equilibrium value
x_1^*	9.3768
x_2^*	0.0140
x_3^*	0.2464
x_4^*	20.1948
x_5^*	6.6899
x_6^*	11.3105
x_7^*	8.9884
x_8^*	38.7624
x_9^*	19.9072

The numerical positive equilibrium obtained from the nonlinear system is

$$E^* = (9.3768,\ 0.0140,\ 0.2464,\ 20.1948,\ 6.6899,\ 11.3105,\ 8.9884,\ 38.7624,\ 19.9072).$$

All equilibrium concentrations are positive, indicating that the proposed nonlinear lumped chemical kinetics model admits a physically meaningful positive steady state. This confirms the analytical equilibrium analysis and demonstrates the coexistence of all interacting chemical species under the adopted parameter values.

4.2.6 Jacobian Matrix

The local stability of the equilibrium point is investigated by linearizing the nonlinear dimensionless system (3.13) about the equilibrium point E^*.

Let

$$\mathbf{x} = (x_1, x_2, \ldots, x_9)^T,$$

and

$$\mathbf{F}(\mathbf{x}) = (f_1, f_2, \ldots, f_9)^T$$

denote the vector field corresponding to the right-hand side of the dimensionless model.

The Jacobian matrix is defined as

$$J(\mathbf{x}) = \left[\frac{\partial f_i}{\partial x_j}\right]_{9\times 9}, \qquad i, j = 1, 2, \ldots, 9. \tag{4.192}$$

The Jacobian evaluated at the equilibrium point is therefore

$$J(E^*) = J(\mathbf{x})\Big|_{\mathbf{x}=E^*}. \tag{4.193}$$

Since the governing equations consist of continuously differentiable quadratic and linear functions, the Jacobian matrix exists and is continuous throughout the feasible region Ω. From

$$f_1 = \beta_K - x_1 x_2 - \delta_K x_1,$$

the first row of the Jacobian is

$$J_1 = (-x_2 - \delta_K, -x_1, 0, 0, 0, 0, 0, 0, 0)\,.$$

Similarly,

$$f_2 = \beta_O - 31x_1x_2 - 5\alpha_2 x_5 x_2 - 25\alpha_3 x_6 x_2 - 37\alpha_4 x_7 x_2 - 6\alpha_5 x_8 x_2 + 6\alpha_6 x_3 x_4 - \delta_O x_2,$$

which gives

$$\begin{aligned} J_2 = (&-31x_2,\ -31x_1 - 5\alpha_2 x_5 - 25\alpha_3 x_6 - 37\alpha_4 x_7 \\ &- 6\alpha_5 x_8 - \delta_O,\ 6\alpha_6 x_4,\ 6\alpha_6 x_3, \\ &- 5\alpha_2 x_2,\ -25\alpha_3 x_2,\ -37\alpha_4 x_2,\ -6\alpha_5 x_2,\ 0). \end{aligned}$$

The remaining rows of the Jacobian matrix are obtained by differentiating the corresponding components of the vector field with respect to each state variable.

Because of the large number of nonlinear interaction terms, the complete symbolic

Jacobian matrix is omitted for brevity. The symbolic Jacobian was generated automatically using the MATLAB Symbolic Math Toolbox and evaluated numerically at the equilibrium point.

4.2.7 Characteristic Equation

The characteristic polynomial associated with the linearized system is

$$\det\left(\lambda I - J(E^*)\right) = 0, \tag{4.194}$$

where

$$I$$

denotes the 9×9 identity matrix and

$$\lambda$$

represents the eigenvalues of the Jacobian matrix.

4.2.8 Local Stability Analysis

The local asymptotic stability of the equilibrium point is determined from the eigenvalues of the Jacobian matrix evaluated at the equilibrium point. **Theorem** Let

$$\lambda_1, \lambda_2, \ldots, \lambda_9$$

denote the eigenvalues of

$$J(E^*).$$

Then the equilibrium point

$$E^*$$

is locally asymptotically stable if

$$\mathrm{Re}(\lambda_i) < 0, \qquad i = 1, 2, \ldots, 9.$$

Proof. The proof follows directly from the Hartman–Grobman Linearization Theorem.

Since the Jacobian matrix is continuous in a neighbourhood of the equilibrium point, the nonlinear system has the same qualitative behaviour as its linearization.

If every eigenvalue satisfies

$$\mathrm{Re}(\lambda_i) < 0,$$

then all sufficiently small perturbations decay exponentially with time.

Consequently,

$$E^*$$

is locally asymptotically stable. □

4.2.9 Numerical Verification of Local Stability

The Jacobian matrix was evaluated numerically at the positive equilibrium point using the MATLAB symbolic toolbox. The corresponding eigenvalues obtained from the numerical evaluation are presented in Table 4.8.

Table 4.8: Eigenvalues of the Jacobian matrix evaluated at the positive equilibrium point.

Eigenvalue	Real Part
λ_1	-875.9126
λ_2	-11.8553
λ_3	-0.0631
λ_4	-0.0615
λ_5	-0.0599
λ_6	-0.0501
λ_7	-0.0400
λ_8	-0.0303
λ_9	-0.0200

Since all eigenvalues possess strictly negative real parts, the positive equilibrium point is locally asymptotically stable. These numerical findings agree with the theoretical local stability result established in Theorem 3.4 and demonstrate that small perturbations around the equilibrium decay with time.

4.3 Numerical Results and Discussion

4.3.1 Numerical Simulation Results

The dimensionless nonlinear chemical kinetics model was solved numerically using the stiff solver `ode15s` implemented in MATLAB R2023b. The solver was selected because the computed eigenvalues indicate the presence of both fast and slow dynamic modes, making the governing equations a stiff nonlinear system. The simulations were performed over the dimensionless time interval $0 \leq t \leq 200$ using the baseline parameter values presented in Table 2.1 together with the initial conditions specified in Section 2.

Fuel Dynamics

Figure 4.9 illustrates the temporal evolution of kerosene, LPG, petrol and diesel obtained from the numerical solution of the proposed nonlinear lumped chemical kinetics model.

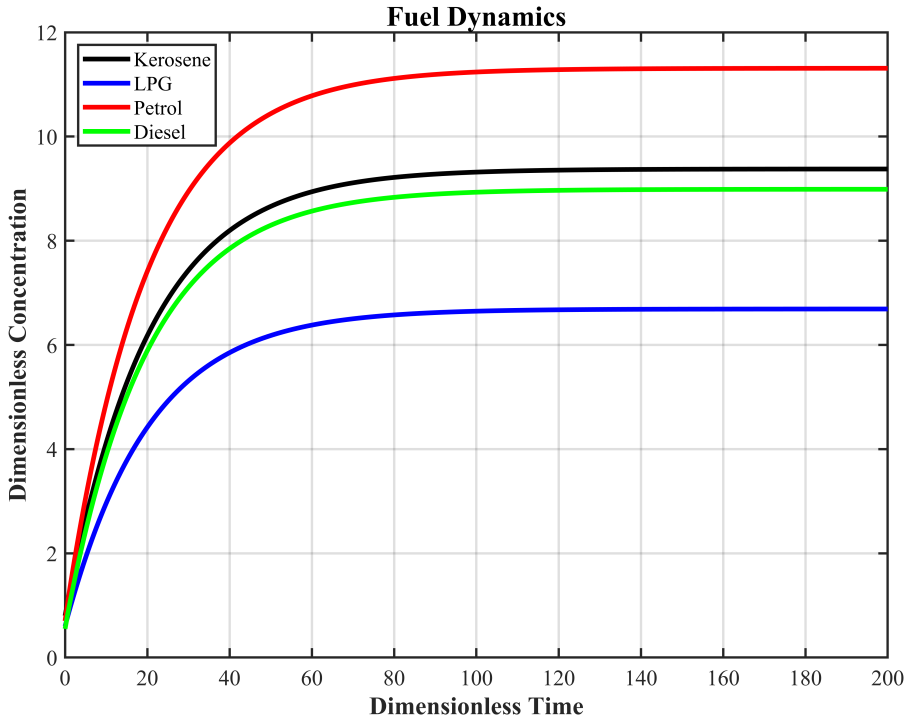

Figure 4.9: Temporal evolution of kerosene, LPG, petrol and diesel concentrations.

The numerical simulations demonstrate that all fuel compartments exhibit rapid transient growth before gradually approaching their respective equilibrium values. Petrol attains the highest equilibrium concentration, followed by kerosene, diesel and LPG. This behaviour reflects the balance between continuous fuel replenishment, combus-

tion reactions and natural depletion processes incorporated in the proposed nonlinear chemical kinetics model.

Furthermore, the convergence of all fuel compartments to finite steady-state values confirms the boundedness of the model and provides numerical support for the theoretical equilibrium analysis presented in Section 3. The smooth convergence of the trajectories further indicates that the system evolves towards a stable positive equilibrium under the adopted parameter values.

4.3.2 Atmospheric Dynamics

Figure 4.10 presents the temporal evolution of oxygen, carbon dioxide and water vapour obtained from the numerical solution of the proposed nonlinear lumped chemical kinetics model.

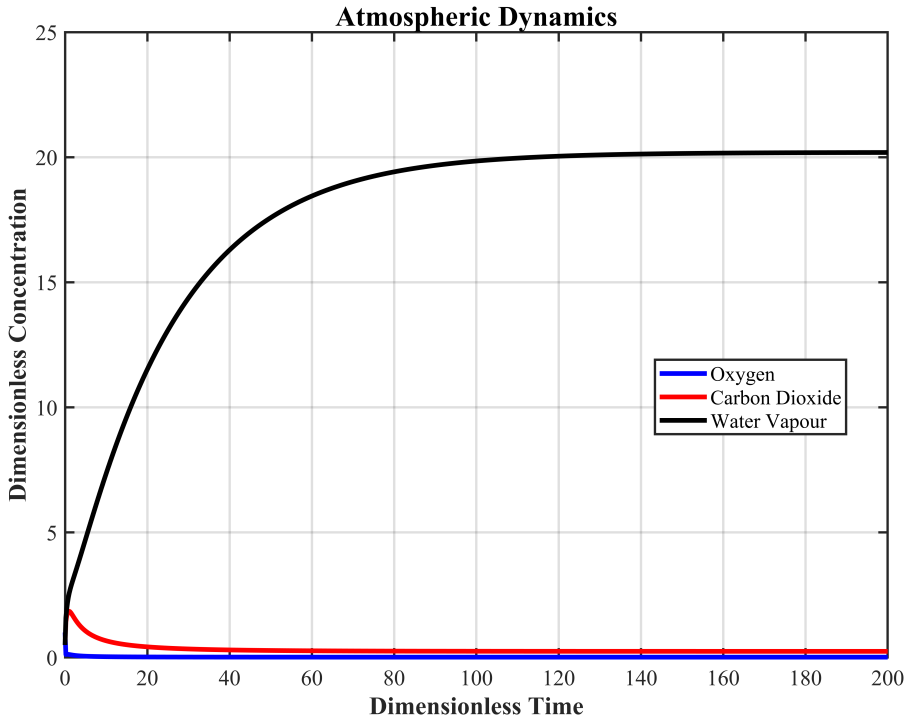

Figure 4.10: Temporal evolution of oxygen, carbon dioxide and water vapour.

Figure 4.10 illustrates the coupled dynamics of the atmospheric compartments. Oxygen is progressively consumed during combustion reactions, while carbon dioxide and water vapour are generated as combustion products. As the simulation proceeds, the trajectories gradually approach constant values, indicating that the production and removal processes eventually reach dynamic equilibrium. The convergence of all atmospheric variables to finite steady-state values further supports the boundedness

and stability properties established analytically in Section 3.

4.3.3 Carbon Sink Dynamics

Figure 4.11 presents the temporal evolution of glucose and carbonic acid concentrations, representing the natural carbon sequestration mechanisms incorporated in the proposed nonlinear lumped chemical kinetics model.

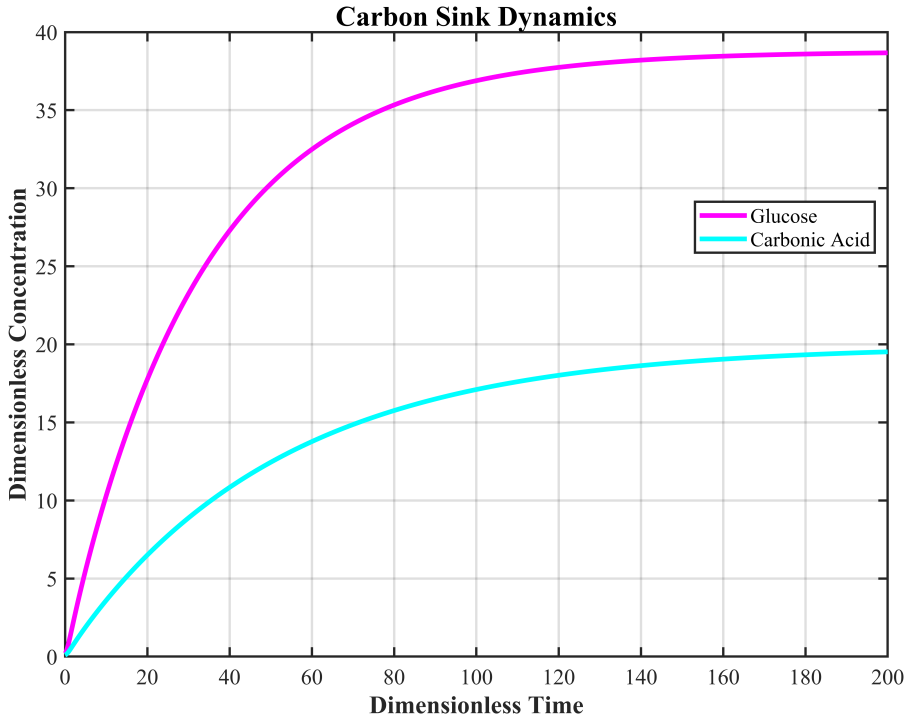

Figure 4.11: Temporal evolution of glucose and carbonic acid concentrations.

The numerical simulations demonstrate that both glucose and carbonic acid concentrations increase during the initial stages of the simulation before gradually approaching steady-state values. Glucose production results from the photosynthetic uptake of atmospheric carbon dioxide, whereas carbonic acid is formed through the dissolution of carbon dioxide in water. These processes act as natural carbon sinks within the proposed model, thereby reducing atmospheric carbon dioxide accumulation. The convergence of both variables to positive equilibrium values confirms the long-term stability of the carbon sequestration mechanisms under the adopted parameter values.

4.3.4 Numerical Equilibrium Analysis

The positive equilibrium point of the proposed nonlinear lumped chemical kinetics model was computed numerically using the MATLAB function `fsolve`. The computed

equilibrium values are presented in Table 4.7.

Table 4.9: Numerically computed positive equilibrium point of the nonlinear chemical kinetics model.

State Variable	Equilibrium Value
Kerosene (K^*)	9.3768
Oxygen (O^*)	0.0140
Carbon dioxide (C^*)	0.2464
Water vapour (W^*)	20.1948
LPG (L^*)	6.6899
Petrol (P^*)	11.3105
Diesel (D^*)	8.9884
Glucose (G^*)	38.7624
Carbonic acid (H^*)	19.9072

The numerical equilibrium values are all positive, demonstrating that the proposed nonlinear model admits a physically meaningful positive steady state. The existence of this equilibrium confirms the analytical equilibrium analysis presented in Section 3 and indicates that the interacting chemical species coexist under the selected parameter values.

Among the equilibrium values, glucose exhibits the highest concentration, reflecting the cumulative effect of photosynthetic carbon fixation, whereas atmospheric oxygen attains the smallest equilibrium value due to its continuous consumption during combustion reactions. Carbon dioxide converges to a finite positive value, indicating that the natural carbon sequestration mechanisms represented by photosynthesis and carbonic acid formation balance the continuous emissions arising from fuel combustion.

The convergence of all state variables to finite positive equilibrium values further demonstrates that the proposed nonlinear system remains bounded and evolves towards a unique stable steady state under the adopted parameter values.

4.3.5 Jacobian Matrix and Local Stability Analysis

To verify the analytical local stability results established in Section 3, the symbolic Jacobian matrix of the proposed nonlinear system was evaluated numerically at the computed positive equilibrium point. The resulting Jacobian matrix was subsequently used to determine the eigenvalues governing the local dynamics of the system.

Owing to the size of the Jacobian matrix, only the eigenvalues are presented in this section, while the complete numerical Jacobian matrix is provided in Appendix A.

Table 4.10: Eigenvalues of the Jacobian matrix evaluated at the positive equilibrium point.

Eigenvalue	Numerical Value
λ_1	-875.9126
λ_2	-11.8553
λ_3	-0.0631
λ_4	-0.0615
λ_5	-0.0599
λ_6	-0.0501
λ_7	-0.0400
λ_8	-0.0303
λ_9	-0.0200

The numerical eigenvalues obtained from the Jacobian matrix are all strictly negative. Consequently,

$$\mathrm{Re}(\lambda_i) < 0, \qquad i = 1, 2, \ldots, 9,$$

which satisfies the necessary and sufficient condition for local asymptotic stability of the positive equilibrium point.

The numerical computations therefore confirm the theoretical local stability result established in Theorem 3.4. Following small perturbations from equilibrium, all state variables return to their steady-state values as time progresses, demonstrating the inherent resilience of the proposed nonlinear lumped chemical kinetics model. It is further observed that the eigenvalues exhibit substantially different magnitudes. In particular, the dominant negative eigenvalue is -875.9126, whereas the smallest magnitude eigenvalue is -0.0200. This wide separation indicates that the nonlinear system possesses both fast and slow dynamic modes, thereby exhibiting stiff behaviour.

The presence of stiffness justifies the use of the implicit MATLAB solver `ode15s`, which is specifically designed for solving stiff systems of ordinary differential equations. The numerical simulations obtained using `ode15s` remained stable throughout the computational interval and converged smoothly to the computed positive equilibrium. Therefore, both the analytical investigation and the numerical computations consistently demonstrate that the proposed nonlinear lumped chemical kinetics model possesses a unique positive equilibrium that is locally asymptotically stable under the adopted parameter values.

4.3.6 Global Sensitivity Analysis

A global sensitivity analysis was performed using Latin Hypercube Sampling (LHS) combined with Partial Rank Correlation Coefficients (PRCC) to determine the influence of model parameters on the carbon dioxide dynamics. The PRCC method provides a quantitative measure of the monotonic relationship between each model parameter and the selected response variable while accounting for the effects of the remaining parameters.

The sensitivity analysis was implemented in MATLAB using the calibrated numerical model. The resulting PRCC values are illustrated in Figure 4.12.

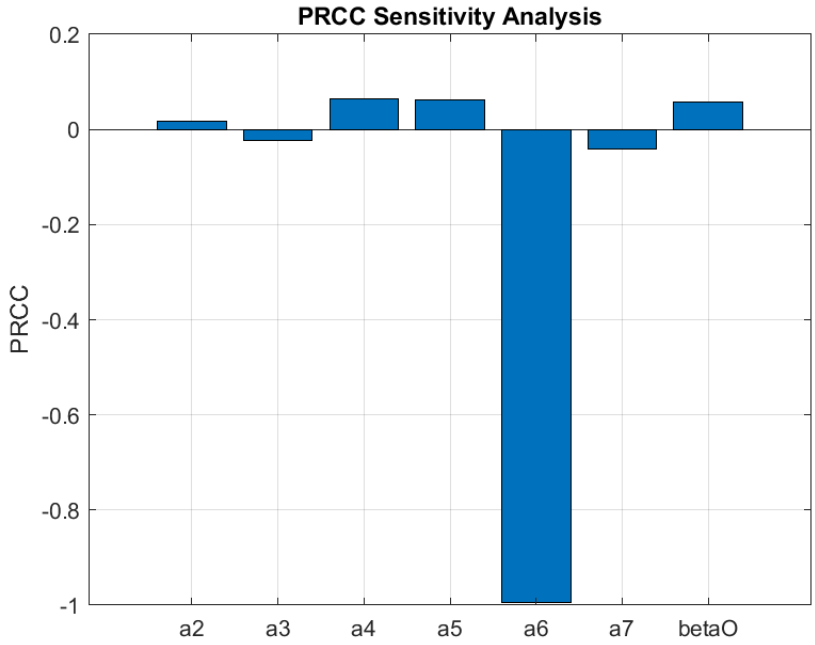

Figure 4.12: Partial Rank Correlation Coefficients (PRCC) showing the relative influence of model parameters on carbon dioxide dynamics.

The PRCC analysis demonstrates that parameter a_6 has the largest influence on the system response, exhibiting a strong negative correlation with a coefficient close to -1. This indicates that increasing the value of a_6 substantially reduces the atmospheric carbon dioxide concentration, highlighting its dominant role in regulating the model dynamics.

Parameters a_4, a_5 and β_O exhibit moderate positive sensitivity coefficients, implying that increases in these parameters promote higher carbon dioxide concentrations within the system. Conversely, parameters a_3 and a_7 possess relatively weak negative sensitivity coefficients, while parameter a_2 has only a marginal positive influence.

Overall, the sensitivity analysis reveals that the proposed nonlinear lumped chemical kinetics model is most sensitive to variations in parameter a_6. Consequently, accurate estimation of this parameter is essential for reliable prediction of carbon dioxide dynamics. The remaining parameters exhibit comparatively smaller sensitivities, indicating that moderate uncertainties in their values have a less pronounced effect on the model predictions. The results further demonstrate that the model possesses good numerical robustness since only one parameter exhibits dominant sensitivity while the remaining parameters produce comparatively moderate responses. This behaviour suggests that the model predictions are relatively stable with respect to small perturbations in most parameter values, thereby enhancing confidence in the reliability of the numerical simulations.

4.3.7 Bifurcation Analysis

To further investigate the qualitative behaviour of the proposed nonlinear lumped chemical kinetics model, a one-parameter bifurcation analysis was performed by varying the oxygen replenishment parameter β_O while computing the corresponding equilibrium carbon dioxide concentration.

The resulting bifurcation diagram is presented in Figure 4.13.

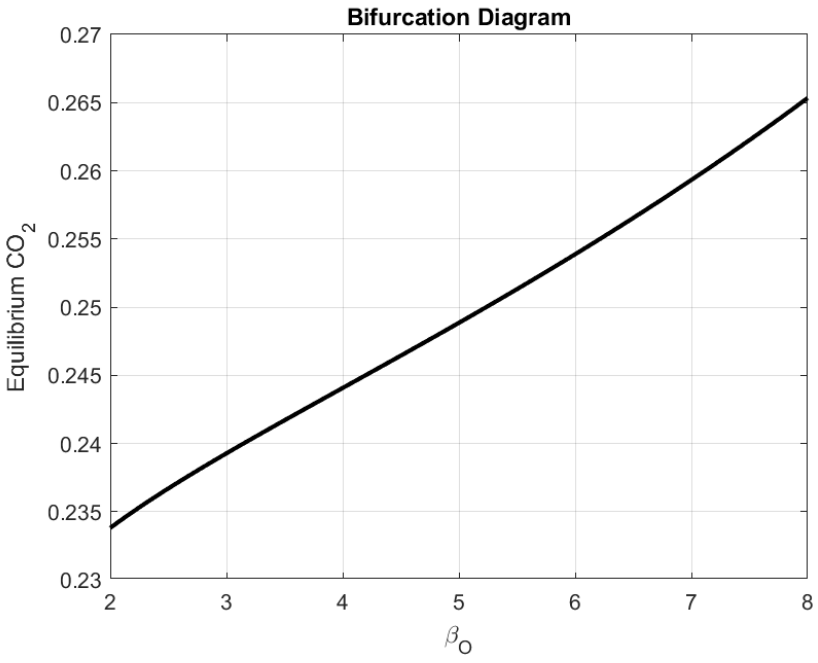

Figure 4.13: Variation of the equilibrium carbon dioxide concentration with the oxygen replenishment parameter β_O.

Figure 4.13 shows that the equilibrium carbon dioxide concentration increases smoothly as the oxygen replenishment parameter β_O increases. The equilibrium solution varies continuously throughout the investigated parameter interval without exhibiting turning points, branch switching or discontinuities.

No qualitative change in the system dynamics was observed over the selected parameter range. In particular, the numerical computations did not indicate the occurrence of saddle-node, transcritical, pitchfork or Hopf bifurcations. Consequently, the positive equilibrium remains dynamically stable throughout the investigated interval of β_O.

The smooth variation of the equilibrium solution demonstrates that moderate changes in oxygen replenishment influence the equilibrium carbon dioxide concentration quantitatively rather than qualitatively. Increasing β_O provides additional oxygen for combustion, thereby promoting increased carbon dioxide production while preserving the stability of the proposed nonlinear chemical kinetics model. The bifurcation analysis therefore complements the local stability and sensitivity investigations by demonstrating that the proposed nonlinear system maintains a unique stable positive equilibrium over the investigated parameter range. These findings indicate that the model is structurally robust and that moderate variations in oxygen replenishment do not induce abrupt transitions in the long-term system dynamics.

CHAPTER 5

CONCLUSION AND RECOMMENDATIONS

5.1 Conclusion

This thesis has presented two complementary mathematical modelling frameworks for investigating atmospheric carbon dioxide emissions arising from fossil fuel combustion and human activities. The first framework employs a compartmental modelling approach to describe the interactions between human populations, fossil fuel consumption, vegetation and atmospheric carbon dioxide at the global scale. The second framework extends this investigation through a nonlinear lumped chemical kinetics model that explicitly represents combustion reactions together with natural carbon dioxide removal processes including photosynthesis and carbonic acid formation.

Rigorous mathematical analysis established that both models are mathematically well posed. The positivity, boundedness, existence and uniqueness of solutions were established, ensuring that the proposed models remain physically and chemically meaningful throughout the simulation period. Equilibrium analysis demonstrated the existence of physically realistic steady states, while Jacobian matrix analysis confirmed the local asymptotic stability of the positive equilibrium through strictly negative eigenvalues. These analytical results were further validated through MATLAB simulations, which demonstrated smooth convergence of all state variables to their respective equilibrium values.

The compartmental model showed that increasing fossil fuel consumption and intensified human activities significantly increase atmospheric carbon dioxide concentrations, thereby contributing to global warming and climate change. Conversely, increasing vegetation cover enhances carbon sequestration and reduces atmospheric carbon dioxide accumulation, emphasizing the importance of afforestation and sustainable land management in mitigating greenhouse gas emissions.

The nonlinear lumped chemical kinetics model provided a more detailed representation of the chemical interactions governing carbon dioxide production and removal. The model demonstrated that the coupled dynamics of kerosene, liquefied petroleum gas, petrol, diesel, oxygen, water vapour, glucose and carbonic acid can be effectively represented using a computationally efficient lumped reaction framework. Global sensitivity analysis identified the photosynthesis parameter as the most influential factor controlling atmospheric carbon dioxide dynamics, highlighting the critical role of bi-

ological carbon sequestration in climate change mitigation. Furthermore, numerical bifurcation analysis indicated that the proposed model remains structurally stable over the investigated parameter range, suggesting that moderate parameter variations do not alter the qualitative behaviour of the system.

Overall, this research demonstrates that mathematical modelling provides a powerful framework for understanding the complex interactions governing atmospheric carbon dioxide dynamics. By integrating compartmental modelling, nonlinear chemical kinetics, rigorous mathematical analysis, numerical simulation and global sensitivity analysis, this thesis contributes to the advancement of mathematical methods for climate science and environmental management. The developed models provide useful quantitative tools for predicting carbon dioxide dynamics, evaluating greenhouse gas mitigation strategies and supporting evidence-based environmental policy aimed at achieving sustainable development.

5.2 Recommendations

Based on the findings obtained in this study, the following recommendations are proposed:

1. Governments and environmental agencies should strengthen policies aimed at reducing dependence on high-carbon fossil fuels and promote the adoption of renewable and clean energy technologies such as solar, wind, hydroelectric, and bioenergy systems.

2. Environmental conservation programs such as afforestation, reforestation, and protection of natural ecosystems should be enhanced in order to increase carbon sequestration and reduce atmospheric CO_2 concentration.

3. Industrial sectors should adopt cleaner combustion technologies and improved emission control systems to minimize Carbon(iv) oxide emissions generated during fuel combustion and refinery processes.

4. Policymakers should invest in carbon capture, carbon storage, and engineered carbon sink technologies that enhance the removal of atmospheric CO_2.

5. Public awareness programs should be intensified to educate communities on the environmental impacts of excessive fossil fuel consumption and the importance of sustainable energy practices.

6. Mathematical and computational climate models should continue to be integrated into environmental planning and policy formulation in order to provide scientifically informed strategies for mitigating global warming.

5.3 Recommendations for Further Research

The mathematical models developed in this thesis provide a strong foundation for future investigations on atmospheric carbon dioxide dynamics. Nevertheless, several extensions may further improve their predictive capability and applicability.

Future studies may incorporate temperature-dependent reaction kinetics using Arrhenius-type rate expressions to account for seasonal and climatic variations in combustion processes. The inclusion of additional greenhouse gases such as methane (CH_4) and nitrous oxide (N_2O) would provide a more comprehensive representation of atmospheric emissions.

Further research may also integrate real-time observational datasets from international organizations such as the Intergovernmental Panel on Climate Change (IPCC), the National Oceanic and Atmospheric Administration (NOAA) and the Global Carbon Project for parameter estimation and model calibration. Such calibration would improve the predictive performance of the proposed models.

The deterministic models developed in this thesis may further be extended to stochastic, delay differential equation or fractional-order formulations to investigate the effects of environmental uncertainty and memory on carbon dioxide dynamics. Moreover, coupling the proposed models with economic, energy and climate models would facilitate comprehensive evaluation of emission-control policies, renewable energy adoption and carbon capture technologies.

Finally, future studies may develop spatially distributed reaction–diffusion models and optimal control formulations to investigate regional carbon dioxide transport, afforestation strategies and long-term greenhouse gas mitigation under different climate scenarios.

APPENDIX A

SUPPLEMENTARY COMPUTATIONAL MATERIALS

This appendix presents supplementary computational materials that support the mathematical analyses and numerical simulations reported in this thesis. Detailed theoretical derivations, model formulation, stability analysis, numerical results and figures have already been presented in Chapters 2–5 and are therefore not repeated here. The appendix provides additional computational information to facilitate reproducibility of the numerical investigations.

A.1 Characteristic Polynomial Coefficients

This appendix presents the calculated characteristic-polynomial coefficients used in the local stability analysis of the deterministic compartmental model. The calculation is based directly on the Jacobian matrix of the eight-dimensional system and the four admissible non-trivial equilibrium cases E^1, E^2, E^3 and E^4.

For each equilibrium point E^j, $j = 1, 2, 3, 4$, define

$$J_j = J(E^j), \qquad T_r^j = \operatorname{tr}\left(J_j^r\right), \qquad r = 1, \ldots, 8. \tag{A.1}$$

The characteristic polynomial is defined using the standard monic convention

$$\begin{aligned} \det(\chi I - J_j) = \chi^8 + a_1^j\chi^7 + a_2^j\chi^6 + a_3^j\chi^5 + a_4^j\chi^4 \\ + a_5^j\chi^3 + a_6^j\chi^2 + a_7^j\chi + a_8^j = 0. \end{aligned} \tag{A.2}$$

The coefficients are obtained exactly from the Faddeev–LeVerrier recursion

$$a_0^j = 1, \qquad a_k^j = -\frac{1}{k}\sum_{r=1}^{k} a_{k-r}^j T_r^j, \qquad k = 1, \ldots, 8. \tag{A.3}$$

Consequently, the complete coefficients are

$$a_1^j = -T_1^j, \tag{A.4}$$

$$a_2^j = \frac{(T_1^j)^2 - T_2^j}{2}, \tag{A.5}$$

$$a_3^j = -\frac{(T_1^j)^3}{6} + \frac{T_1^j T_2^j}{2} - \frac{T_3^j}{3}, \tag{A.6}$$

$$a_4^j = \frac{(T_1^j)^4}{24} - \frac{(T_1^j)^2 T_2^j}{4} + \frac{T_1^j T_3^j}{3} + \frac{(T_2^j)^2}{8} - \frac{T_4^j}{4}, \tag{A.7}$$

$$\begin{aligned} a_5^j = &-\frac{(T_1^j)^5}{120} + \frac{(T_1^j)^3 T_2^j}{12} - \frac{(T_1^j)^2 T_3^j}{6} - \frac{T_1^j (T_2^j)^2}{8} \\ &+ \frac{T_1^j T_4^j}{4} + \frac{T_2^j T_3^j}{6} - \frac{T_5^j}{5}, \end{aligned} \tag{A.8}$$

$$\begin{aligned} a_6^j = &\frac{(T_1^j)^6}{720} - \frac{(T_1^j)^4 T_2^j}{48} + \frac{(T_1^j)^3 T_3^j}{18} + \frac{(T_1^j)^2 (T_2^j)^2}{16} \\ &- \frac{(T_1^j)^2 T_4^j}{8} - \frac{T_1^j T_2^j T_3^j}{6} + \frac{T_1^j T_5^j}{5} - \frac{(T_2^j)^3}{48} \\ &+ \frac{T_2^j T_4^j}{8} + \frac{(T_3^j)^2}{18} - \frac{T_6^j}{6}, \end{aligned} \tag{A.9}$$

$$\begin{aligned} a_7^j = &-\frac{(T_1^j)^7}{5040} + \frac{(T_1^j)^5 T_2^j}{240} - \frac{(T_1^j)^4 T_3^j}{72} \\ &- \frac{(T_1^j)^3 (T_2^j)^2}{48} + \frac{(T_1^j)^3 T_4^j}{24} + \frac{(T_1^j)^2 T_2^j T_3^j}{12} \\ &- \frac{(T_1^j)^2 T_5^j}{10} + \frac{T_1^j (T_2^j)^3}{48} - \frac{T_1^j T_2^j T_4^j}{8} \\ &- \frac{T_1^j (T_3^j)^2}{18} + \frac{T_1^j T_6^j}{6} - \frac{(T_2^j)^2 T_3^j}{24} \\ &+ \frac{T_2^j T_5^j}{10} + \frac{T_3^j T_4^j}{12} - \frac{T_7^j}{7}, \end{aligned} \tag{A.10}$$

$$\begin{aligned} a_8^j = &\frac{(T_1^j)^8}{40320} - \frac{(T_1^j)^6 T_2^j}{1440} + \frac{(T_1^j)^5 T_3^j}{360} \\ &+ \frac{(T_1^j)^4 (T_2^j)^2}{192} - \frac{(T_1^j)^4 T_4^j}{96} - \frac{(T_1^j)^3 T_2^j T_3^j}{36} \\ &+ \frac{(T_1^j)^3 T_5^j}{30} - \frac{(T_1^j)^2 (T_2^j)^3}{96} + \frac{(T_1^j)^2 T_2^j T_4^j}{16} \\ &+ \frac{(T_1^j)^2 (T_3^j)^2}{36} - \frac{(T_1^j)^2 T_6^j}{12} + \frac{T_1^j (T_2^j)^2 T_3^j}{24} \\ &- \frac{T_1^j T_2^j T_5^j}{10} - \frac{T_1^j T_3^j T_4^j}{12} + \frac{T_1^j T_7^j}{7} + \frac{(T_2^j)^4}{384} \\ &- \frac{(T_2^j)^2 T_4^j}{32} - \frac{T_2^j (T_3^j)^2}{36} + \frac{T_2^j T_6^j}{12} + \frac{T_3^j T_5^j}{15} \\ &+ \frac{(T_4^j)^2}{32} - \frac{T_8^j}{8}. \end{aligned} \tag{A.11}$$

The formulas above are valid for each of the four equilibrium points. Thus, setting $j = 1$ gives $a_1^1, \ldots, a_8^1$; setting $j = 2$ gives $a_1^2, \ldots, a_8^2$; setting $j = 3$ gives $a_1^3, \ldots, a_8^3$; and setting $j = 4$ gives $a_1^4, \ldots, a_8^4$. This representation is exact and avoids repeating several hundred pages of fully expanded symbolic terms.

A.2 Equilibrium-specific substitutions

The equilibrium points used in the calculation are

$$E^1 = (0, 0, F_1, O_1, L_1, P_1, D_1, C_1), \tag{A.12}$$

$$E^2 = (H_2, R_2, F_2, 0, 0, 0, 0, C_2), \tag{A.13}$$

$$E^3 = (H_3, 0, F_3, O_3, L_3, 0, 0, C_3), \tag{A.14}$$

$$E^4 = (H_4, R_4, F_4, O_4, L_4, P_4, D_4, C_4). \tag{A.15}$$

For each case, the corresponding equilibrium values are substituted into $J(\mathbf{X})$ before calculating T_r^j. The characteristic coefficients are therefore determined from the actual Jacobian at the relevant steady state rather than from an assumed or generic coefficient list.

A.3 Routh–Hurwitz stability test

For each equilibrium point, the polynomial (A.2) is subjected to the Routh–Hurwitz criterion. Let

$$p_j(\chi) = \chi^8 + a_1^j\chi^7 + a_2^j\chi^6 + a_3^j\chi^5 + a_4^j\chi^4 + a_5^j\chi^3 + a_6^j\chi^2 + a_7^j\chi + a_8^j.$$

The equilibrium point E^j is locally asymptotically stable if and only if all roots of $p_j(\chi)$ have negative real parts. Equivalently, all the leading principal Hurwitz determinants satisfy

$$\Delta_i^j > 0, \qquad i = 1, 2, \ldots, 8. \tag{A.16}$$

The numerical values of the determinants may be evaluated using the parameter values adopted in the thesis. The symbolic coefficient formulas above provide the exact expressions required to construct the Routh–Hurwitz array.

A.4 MATLAB Verification Output

The numerical results reported in this thesis were generated using MATLAB R2023b. The command window output obtained after execution of the complete MATLAB project is reproduced below to verify the numerical computations.

```
========================================
FINAL RESULTS
========================================

Positive Equilibrium

9.3768
0.0140
0.2464
20.1948
6.6899
11.3105
8.9884
38.7624
19.9072

Eigenvalues

-0.0200
-875.9126
-11.8553
-0.0303
-0.0400
-0.0501
-0.0631
-0.0599
-0.0615

Local Stability : STABLE

Results successfully generated.
```

```
========================================
PROJECT COMPLETED SUCCESSFULLY
========================================
```

A.5 Numerical Jacobian Matrix

The numerical Jacobian matrix of the nonlinear lumped chemical kinetics model was evaluated at the computed positive equilibrium point using MATLAB R2023b. This matrix was subsequently used to determine the eigenvalues governing the local asymptotic stability of the positive equilibrium. The complete numerical Jacobian matrix is presented below for completeness.

$$J(E^*) = \begin{bmatrix} -0.06399 & -9.37682 & 0 & 0 & 0 & 0 & 0 & 0 & 0 \\ -0.43361 & -855.41670 & 30.29213 & 0.36966 & -0.04896 & -0.29724 & -0.41403 & -0.01259 & 0 \\ 0.27975 & 562.87122 & -31.94771 & -0.38938 & 0.02937 & 0.19023 & 0.26856 & 0.01259 & 0 \\ 0.30773 & 619.91708 & -31.90771 & -0.42938 & 0.03917 & 0.21401 & 0.29094 & 0.01259 & 0 \\ 0 & -4.68296 & 0 & 0 & -0.05979 & 0 & 0 & 0 & 0 \\ 0 & -9.61392 & 0 & 0 & 0 & -0.06189 & 0 & 0 & 0 \\ 0 & -7.19071 & 0 & 0 & 0 & 0 & -0.06119 & 0 & 0 \\ 0 & -5.81435 & 5.04869 & 0.06161 & 0 & 0 & 0 & -0.03210 & 0 \\ 0 & 0 & 1.61558 & 0.01972 & 0 & 0 & 0 & 0 & -0.02000 \end{bmatrix} \tag{A.17}$$

The Jacobian matrix in Equation (A.17) was evaluated numerically at the positive equilibrium obtained from the nonlinear system. The corresponding eigenvalues, reported in Chapter 4, are all strictly negative, confirming that the positive equilibrium is locally asymptotically stable.

A.6 MATLAB Computing Environment

The numerical simulations were performed using MATLAB R2023b running under Microsoft Windows 11 Professional. The simulations employed the stiff ordinary differential equation solver `ode15s`, which is appropriate for nonlinear chemical kinetics systems exhibiting multiple time scales.

Table A.1: Computing environment used for numerical simulations.

Software	MATLAB R2023b
Operating System	Microsoft Windows 11 Professional
Numerical Solver	`ode15s`
Relative Tolerance	10^{-8}
Absolute Tolerance	10^{-10}
Simulation Interval	$0 \leq t \leq 100$
Programming Language	MATLAB

A.7 MATLAB Project Structure

The MATLAB implementation developed for this research consists of the following source files.

Table A.2: MATLAB project files.

File	Description
main.m	Main program controlling the entire numerical investigation.
model.m	Defines the nonlinear lumped chemical kinetics model.
parameter_values.m	Stores calibrated model parameters.
simulation.m	Performs numerical integration of the governing equations.
equilibrium_solver.m	Computes the positive equilibrium point using nonlinear algebraic solvers.
jacobian_analysis.m	Evaluates the Jacobian matrix and computes eigenvalues.
local_stability.m	Performs local stability analysis.
global_stability.m	Contains routines supporting stability investigations.
prcc_analysis.m	Implements Latin Hypercube Sampling (LHS) and Partial Rank Correlation Coefficient (PRCC) sensitivity analysis.
bifurcation_analysis.m	Performs numerical bifurcation analysis.
plot_results.m	Generates publication-quality figures.
export_results.m	Exports numerical results to CSV files for reporting.

A.8 Supplementary Numerical Data

The following electronic files accompany this thesis and contain the complete numerical outputs generated during the MATLAB simulations.

1. Jacobian.csv

2. Equilibrium.csv

3. Eigenvalues.csv

4. ParameterValues.csv

5. PRCCResults.csv

6. BifurcationData.csv

These supplementary files facilitate independent verification and reproducibility of the numerical results presented in Chapters 3 and 4.

A.9 Software Availability

All MATLAB source codes developed during this research are available from the corresponding author upon reasonable request. The codes reproduce all numerical simulations, sensitivity analyses, stability computations and publication-quality figures presented in this thesis.

A.10 Research Publications Arising from the Thesis

The following publications have resulted from the research undertaken in this thesis.

1. Gicheru, J. G., Ngari, C. G., and Njori, P. W. *Modeling the Role of Fossil Fuels and Human Activities in Carbon (IV) Oxide Emissions and Global Warming.*

2. Gicheru, J. G., Ngari, C. G., and Njori, P. W. *A Nonlinear Lumped Chemical Kinetics Model for Carbon Dioxide Emission and Removal Dynamics: Mathematical Analysis, Numerical Simulation and Global Sensitivity Investigation.*

A.11 Future Development of the Models

The mathematical models developed in this thesis provide a flexible framework that may be extended to include temperature-dependent reaction kinetics, stochastic perturbations, fractional-order dynamics, reaction–diffusion processes, optimal control strategies, and parameter estimation using observational data from international climate databases. Such extensions are expected to improve the predictive capability of the models and enhance their applicability to climate policy analysis and greenhouse gas mitigation planning.

REFERENCES

Ahmad, T., & Zhang, D. (2020). A critical review of comparative global historical energy consumption and future demand: The story told so far. *Energy Reports*, *6*, 1973–1991.

Altamirano-Fernández, A., Rojas-Palma, A., & Espinoza-Meza, S. (2022). A mathematical model to study the dynamics of carbon capture in forest plantations. In *Journal of physics: Conference series* (Vol. 2159, p. 012001).

Aris, R. (1999). *Mathematical modeling: a chemical engineer's perspective*. Elsevier.

Bardos, C., & Pironneau, O. (2022). The radiative transfer model for the greenhouse effect. *SeMA Journal*, *79*(3), 489–525.

Bilkadi, Z. (1995). The oil weapons. *Saudi Aramco World*, *46*(1), 20–27.

Biswas, M. H. A., Dey, P. R., Islam, M. S., & Mandal, S. (2022). Mathematical model applied to green building concept for sustainable cities under climate change. *Journal of Contemporary Urban Affairs*, *6*(1), 36–50.

Braddock, R., Filar, J., Zapert, R., Rotmans, J., & den Elzen, M. (1994). The image greenhouse model as a mathematical system. *Applied Mathematical Modelling*, *18*(5), 234–254.

Burkow, D., Duron, C., Heal, K., Vargas, A., & Melara, L. (2011). *A mathematical model of the emission and optimal control of photochemical smog* (Tech. Rep.). Tech. Rep. MTBI-08-07M, Arizona State University.

Cai, Q., Zeng, N., Zhao, F., Han, P., Liu, D., Lin, X., & Chen, J. (2022). The impact of human and livestock respiration on co2 emissions from 14 global cities. *Carbon Balance and Management*, *17*(1), 17.

Carlson, N. A., Talmadge, M. S., Tan, E. C., Newes, E. K., & McCormick, R. L. (2023). *Refinery perspective on decarbonizing with marine biofuels.* ACS Publications.

Cellura, M., Guarino, F., Longo, S., & Tumminia, G. (2018). Climate change and the building sector: Modelling and energy implications to an office building in southern europe. *Energy for Sustainable Development*, *45*, 46–65.

Chang, S., & Wang, X. (2015). Modelling and computation in the valuation of carbon derivatives with stochastic convenience yields. *Plos One*, *10*(5), e0125679.

Chapman, C. A., & Dunham, A. E. (2018). Primate seed dispersal and forest restoration: an african perspective for a brighter future. *International Journal of Primatology*, *39*(3), 427–442.

Cook, M. (2021). Trends in global energy supply and demand. In *Developments in petroleum science* (Vol. 71, pp. 15–42). Elsevier.

Cormos, A.-M., Gaspar, J., Padurean, A., Cormos, C.-C., & Agachi, S. (2010). Techno-economical analysis of carbon dioxide absorption in mono-ethanolamine by mathematical modeling and simulation. In *Pierucci s, buzzi ferraris g, editors. escape20. proceedings of 20th european symposium on computer aided process engineering*.

Crist, E. (2016). Choosing a planet of life. In *A future beyond growth* (pp. 43–55). Routledge.

Cronshaw, M. (2021). Oil. In *Energy in perspective* (pp. 65–103). Springer.

Cuomo, S. (2005). *Ancient mathematics*. Routledge.

Dawson, I. G., & Zhang, D. (2024). The 8 billion milestone: Risk perceptions of global population growth among uk and us residents. *Risk Analysis*, *44*(8), 1809–1827.

Develaki, M. (2020). Comparing crosscutting practices in stem disciplines: Modeling and reasoning in mathematics, science, and engineering. *Science & Education*, *29*(4), 949–979.

Ekejiuba, A. I. (2018). Real-time synthetic conversion of the entire flared associated natural gas stream to liquefied petroleum gas (lpg). *Int J Innov Res Dev*, *7*.

Essl, F., Latombe, G., Lenzner, B., Pagad, S., Seebens, H., Smith, K., ... Genovesi, P. (2020). The convention on biological diversity (cbd)'s post-2020 target on invasive alien species–what should it include and how should it be monitored? *NeoBiota*, *62*, 99–121.

Estoque, R. C., Johnson, B. A., Gao, Y., DasGupta, R., Ooba, M., Togawa, T., ... others (2021). Remotely sensed tree canopy cover-based indicators for monitoring global sustainability and environmental initiatives. *Environmental Research Letters*, *16*(4), 044047.

Etzold, S., Ziemińska, K., Rohner, B., Bottero, A., Bose, A. K., Ruehr, N. K., ... Rigling, A. (2019). One century of forest monitoring data in switzerland reveals

species-and site-specific trends of climate-induced tree mortality. *Frontiers in plant science*, *10*, 307.

Forbes, R. J. (1958). *Studies in early petroleum history*. Brill Archive.

Gaspar, J., & Cormos, A.-M. (2012). Dynamic modeling and absorption capacity assessment of co2 capture process. *International Journal of Greenhouse Gas Control*, *8*, 45–55.

Gebrechorkos, S. H., Hülsmann, S., & Bernhofer, C. (2019). Regional climate projections for impact assessment studies in east africa. *Environmental Research Letters*, *14*(4), 044031.

Hák, T., Janoušková, S., & Moldan, B. (2016). Sustainable development goals: A need for relevant indicators. *Ecological indicators*, *60*, 565–573.

Holechek, J. L., Geli, H. M., Sawalhah, M. N., & Valdez, R. (2022). A global assessment: can renewable energy replace fossil fuels by 2050? *Sustainability*, *14*(8), 4792.

IPCC, T. (2013). Spm-2, summary for policymakers (archived 16 july 2014). *IPCC AR5 WG1*, *21*.

Iz, H. B. (2021). Unmitigated monthly global atmospheric co2 rise until 2050. *Preprint. https://doi. org/10.13140/RG*, *2*(14416.23041).

Kahl, J., et al. (2006). Effect of acid rain on building material of the el tajín archaeological zone in veracruz, mexico. *Environmental Pollution*, *144*(2), 655–660.

Kaiser, G., Blum, W., Ferri, R. B., & Stillman, G. (2011). *Trends in teaching and learning of mathematical modelling–preface*. Springer.

Khasanov, M. K., Rafikova, G. R., & Musakaev, N. G. (2020). Mathematical model of carbon dioxide injection into a porous reservoir saturated with methane and its gas hydrate. *Energies*, *13*(2), 440.

Kikstra, J. S., Nicholls, Z. R., Smith, C. J., Lewis, J., Lamboll, R. D., Byers, E., ... others (2022). The ipcc sixth assessment report wgiii climate assessment of mitigation pathways: from emissions to global temperatures. *Geoscientific Model Development*, *15*(24), 9075–9109.

Klufallah, M. M., Nuruddin, M. F., Khamidi, M. F., & Jamaludin, N. (2014). Assessment of carbon emission reduction for buildings projects in malaysia-a comparative analysis. In *E3s web of conferences* (Vol. 3, p. 01016).

Kogo, B. K., Kumar, L., & Koech, R. (2021). Climate change and variability in kenya: a review of impacts on agriculture and food security. *Environment, Development and Sustainability*, *23*, 23–43.

Kong, J. D., Wang, H., Siddique, T., Foght, J., Semple, K., Burkus, Z., & Lewis, M. A. (2019). Second-generation stoichiometric mathematical model to predict methane emissions from oil sands tailings. *Science of the Total Environment*, *694*, 133645.

Kumar, P., Govindaraj, V., Erturk, V. S., & Mohamed, M. S. (2022). Effects of greenhouse gases and hypoxia on the population of aquatic species: a fractional mathematical model. *Advances in Continuous and Discrete Models*, *2022*(1), 1–19.

Lam, N., Muhwezi, G., Isabirye, F., Harrison, K., Ruiz-Mercado, I., Amukoye, E., ... Bates, M. (2018). Exposure reductions associated with introduction of solar lamps to kerosene lamp-using households in busia county, kenya. *Indoor Air*, *28*(2), 218–227.

Lam, N. L., Smith, K. R., Gauthier, A., & Bates, M. N. (2012). Kerosene: a review of household uses and their hazards in low-and middle-income countries. *Journal of Toxicology and Environmental Health, Part B*, *15*(6), 396–432.

Lloyd, A. C., & Cackette, T. A. (2001). Diesel engines: environmental impact and control. *Journal of the Air & Waste Management Association*, *51*(6), 809–847.

Lowder, S. K., Sánchez, M. V., & Bertini, R. (2021). Which farms feed the world and has farmland become more concentrated? *World Development*, *142*, 105455.

Lv, Z., & Dang, J. (2020). Mathematical modeling of the reaction of metal oxides with methane. *RSC advances*, *10*(19), 11233–11243.

Mandal, S., Islam, M. S., & Biswas, M. H. A. (2021). Modeling the potential impact of climate change on living beings near coastal areas. *Modeling Earth Systems and Environment*, *7*, 1783–1796.

Maobe, A. (2022). Rethinking the role of financial inclusion in kenya's big four development agenda. *Available at SSRN 4282594*.

Marques, A., Martins, I. S., Kastner, T., Plutzar, C., Theurl, M. C., Eisenmenger, N., ... others (2019). Increasing impacts of land use on biodiversity and carbon sequestration driven by population and economic growth. *Nature ecology & evolution*, *3*(4), 628–637.

Mathur, A., & Roy, A. (2021). Special.

McKie, R. E. (2023). Australia and new zealand: Fossil fuels and climate mitigation failings. In *The climate change counter movement: How the fossil fuel industry sought to delay climate action* (pp. 83–114). Springer.

Meng, Q.-c., Rong, X.-x., Zhang, Y.-m., Wan, X.-l., Liu, Y.-y., & Wang, Y.-z. (2016). Collaborative emission reduction model based on multi-objective optimization for greenhouse gases and air pollutants. *PloS one*, *11*(3), e0152057.

Mitchell, D., AchutaRao, K., Allen, M., Bethke, I., Beyerle, U., Ciavarella, A., ... others (2017). Half a degree additional warming, prognosis and projected impacts (happi): background and experimental design. *Geoscientific Model Development*, *10*(2), 571–583.

Mondol, A., Gupta, R., Das, S., & Dutta, T. (2018). An insight into newton's cooling law using fractional calculus. *Journal of Applied Physics*, *123*(6).

Moore, A. D., Eckard, R. J., Thorburn, P. J., Grace, P. R., Wang, E., & Chen, D. (2014). Mathematical modeling for improved greenhouse gas balances, agro-ecosystems, and policy development: lessons from the australian experience. *Wiley Interdisciplinary Reviews: Climate Change*, *5*(6), 735–752.

Munene, M. G. (2020). Kenya budget policy statement (bps) 2020 review: What the bps means for food and nutrition security fy2020/2021.

Munsif, R., Zubair, M., Aziz, A., & Zafar, M. N. (2021). Industrial air emission pollution: potential sources and sustainable mitigation. In *Environmental emissions.* IntechOpen.

Nguyen, A., & Gonzalez, D. (2021). The relationship between fuel consumption and carbon emissions in canada using multiple regression analysis and recommendations for vietnam. In *15th annual economic scholars program conference for undergraduate research.*

Nkuturum, C., Anele, E. T., & Amakiri, S. (2022). Mathematical modelling on the dynamics of climate change caused by carbon (iv) oxide emissions and their control measures. *Faculty of Natural and Applied Sciences Journal of Scientific Innovations*, *3*(3), 11–22.

of Economic, U. N. D., & Affairs, S. (2022). *The sustainable development goals: Report 2022*. UN.

Ogutu, B. K. Z. (2015). *Energy balance mathematical model on climate change* (Unpublished doctoral dissertation). Université Pierre et Marie Curie-Paris VI; University of Nairobi.

O'Sullivan, J. N. (2023). Demographic delusions: World population growth is exceeding most projections and jeopardising scenarios for sustainable futures. *World*, *4*(3), 545–568.

Paoletti, E., & Manes, F. (2003). Effects of elevated carbon dioxide and acidic rain on the growth of holm oak. *Developments in Environmental Science*, *3*, 375–389.

Petroleum, B. (2001). *Bp statistical review of world energy.* British Petroleum.

Pingree, C., Joyce, D., Merkley, J., & Murkowski, L. (2022). Dear chairs and ranking members: Enclosed is the us environmental protection agency's report to congress regarding recommendations to improve class vi permitting procedures for commercial and research carbon sequestration projects. this report is provided as directed by the explanatory statement accompanying the consolidated appropriations act, 2021 (public law 116-260), which states the following.

Pison, G. (2019). How many humans tomorrow? the united nations revises its projections. *The Conversation France*, 1–6.

Rasheed, M. Q., Haseeb, A., Adebayo, T. S., Ahmed, Z., & Ahmad, M. (2022). The long-run relationship between energy consumption, oil prices, and carbon dioxide emissions in european countries. *Environmental Science and Pollution Research*, *29*(16), 24234–24247.

Resende, T. C., Gibbs, D., Harris, N., & Osipova, E. (2021). World heritage forests: Carbon sinks under pressure.

Review, W. P. (2021). World population prospects (2022 revision)—united nations population estimates and projections.

Roa, J., & Lima, M. (2023). Appraising the greenhouse gas (ghg) emissions produced by individuals using public and shared transportation as opposed to private transportation in california. In *International conference on transportation and development 2023* (pp. 291–300).

Rogelj, J., Den Elzen, M., Höhne, N., Fransen, T., Fekete, H., Winkler, H., ... Meinshausen, M. (2016). Paris agreement climate proposals need a boost to keep warming well below 2 c. *Nature*, *534*(7609), 631–639.

Schobert, H. (2013). *Chemistry of fossil fuels and biofuels*. Cambridge University Press.

Singh, S. P., & Singh, P. (2014). Effect of co2 concentration on algal growth: A review. *Renewable and Sustainable Energy Reviews*, *38*, 172–179.

Sitati, C. N., Oludhe, C., Oyake, L., & Mbandi, A. M. (2022). A street-level assessment of greenhouse gas emissions associated with traffic congestion in the city of nairobi, kenya. *Clean Air Journal*, *32*(1), 1–12.

Slade, R. (n.d.). Global warming of 1.5 oc.

Soldatenko, S., Bogomolov, A., & Ronzhin, A. (2021). Mathematical modelling of climate change and variability in the context of outdoor ergonomics. *Mathematics*, *9*(22), 2920.

Solomon, S., Qin, D., Manning, M., Chen, Z., Marquis, M., Averyt, K., ... Miller, H. (2007). Ipcc fourth assessment report (ar4). *Climate change*, *374*.

Sotoodeh, K. (2026). Hydrogen-assisted tribological degradation of valve internal components: Mechanisms, modeling, and mitigation strategies. *Journal of Bio-and Tribo-Corrosion*, *12*(2), 84.

Specht, E., Redemann, T., & Lorenz, N. (2016). Simplified mathematical model for calculating global warming through anthropogenic co2. *International Journal of Thermal Sciences*, *102*, 1–8.

Sultanova, B., Arystambaeva, A., Abisheva, Z., Kogut, O., & Shapetov, B. (2020). Mathematical modeling of kazakhstan's co2 emissions and the role of environmental accounting. In *E3s web of conferences* (Vol. 159, p. 01006).

Tiseo, I. (2023). *Global carbon dioxide emissions from 2014 to 2023 and annual temperature anomalies.* Statista. Retrieved from https://www.statista.com/ (Accessed 2026)

Traver, M., Ebbinghaus, A., Moljord, K., Morganti, K., Pearson, R., & Vermeire, M. (2022). Fuels and transportation. In *Energy transition: Climate action and circularity* (pp. 83–129). ACS Publications.

Wilson, S., Griffiths, M., & Anielski, M. (2022). *Alberta gpi accounts: Energy use intensity, greenhouse gas emissions and air quality*. Pembina Institute.

Yoro, K. O., & Daramola, M. O. (2020). Co2 emission sources, greenhouse gases, and the global warming effect. In *Advances in carbon capture* (pp. 3–28). Elsevier.

Zenebe, S. (2017). *Modeling the effects of global climate change and decreasing forest cover on seasonal rainfall* (Unpublished doctoral dissertation).

RESEARCH LICENSE

REPUBLIC OF KENYA

NATIONAL COMMISSION FOR SCIENCE,TECHNOLOGY & INNOVATION

Ref No: 514138

Date of Issue: 09/June/2025

RESEARCH LICENSE



This is to Certify that Mr.. James Gathungu Gicheru of Kirinyaga University, has been licensed to conduct research as per the provision of the Science, Technology and Innovation Act, 2013 (Rev.2014) in Kirinyaga on the topic: MODELLING EMISSIONS OF CARBON(IV)OXIDE FROM FOSSIL FUELS AND HUMAN ACTIVITIES; COMPARTMENTAL MODEL COUPLED WITH OPTIMALITY AND CHEMICAL KINETICS for the period ending : 09/June/2026.

License No: NACOSTI/P/25/4174674

514138

Applicant Identification Number

Deputy Director
NATIONAL COMMISSION FOR SCIENCE,TECHNOLOGY & INNOVATION

Verification QR Code

NOTE: This is a computer generated License. To verify the authenticity of this document, Scan the QR Code using QR scanner application.

See overleaf for conditions

PUBLICATION

Modeling Earth Systems and Environment (2026) 12:67
https://doi.org/10.1007/s40808-025-02702-7

ORIGINAL ARTICLE



Modeling the role of fossil fuels and human activities in carbon (IV) oxide emissions and global warming

James Gathungu Gicheru[1] · Cyrus Gitonga Ngari[1] · Peter Wanjohi Njori[1]

Received: 28 September 2024 / Accepted: 28 November 2025 / Published online: 29 December 2025
© The Author(s), under exclusive licence to Springer Nature Switzerland AG 2025

Abstract
This study addresses the critical issue of Carbon (IV) Oxide (CO_2) emissions, a major contributor to global warming and climate change, and aligns with Sustainable Development Goal (SDG) 13 (Climate Action). While many previous studies focus on CO_2 emissions at regional or national levels, this research introduces a global compartmental model to analyze interactions between human activity and fossil fuel consumption. Using a system of ordinary differential equations solved through the Runge-Kutta method and simulated in MATLAB, the study investigates how various factors contribute to CO_2 emissions. Results show that increase in human population and increased fossil fuel use leads to rise in CO_2 emission. Data fitting based on Newton's Law of Cooling suggests that global temperature could rise by up to 6.57 °C, though more realistic estimates range between 0.59 °C and 2.46 °C over two years. Importantly, increasing plant cover could boost CO_2 absorption, offering a significant mitigation strategy. The findings support global efforts to reduce emissions and combat climate-related threats such as rising sea levels, extreme weather, and health risks.

Keywords Emissions · Carbon (iv) oxide · Modelling · Simulations · Global warming

Introduction

Greenhouse gas emissions refer to the release of gases that contribute to the greenhouse effect and global warming. The primary greenhouse gases include carbon dioxide (CO_2), methane (CH_4), nitrous oxide (N_2O), and fluorinated gases. These gases are mainly produced by activities such as burning fossil fuels, deforestation, and various industrial processes (Munsif and Zubair 2021). The release of these gases is relatively small compared to CO_2. According to the United States Environmental Protection Agency's 2020 overview, the combustion of fossil fuels like gasoline and diesel was the primary source of emissions, accounting for approximately 33% of total U.S. emissions (Albuquerque et al. 2020).

✉ James Gathungu Gicheru
jamesgicheru94@gmail.com
Cyrus Gitonga Ngari
ngaricyrus15@gmail.com
Peter Wanjohi Njori
pnjori@kyu.ac.ke

[1] Kirinyaga University, Kerugoya, Kenya

The Industrial Revolution in the 18th century led to widespread extraction and use of fossil fuels, essential for transportation, heating, industry, and electricity, but also contributes to climate change (Kundzewicz 2014; Donald et al. 2024). Human activity is causing global warming, as evidenced by increasing greenhouse gases, positive radiative forcing, observed warming, and our growing understanding of the climate system (IPCC 2007).

Earth warms due to emissions that act like a blanket in the atmosphere, trapping heat. This layer hinders the Earth's ability to cool down, resulting in rising global temperatures (Sasi et al. 2024). Such changes can significantly affect weather patterns, climate conditions, and the availability of food and water resources (Klufallah et al. 2014). Mathematical models represent real-world phenomena using equations and abstractions. Mathematical models represent real-world phenomena using equations and abstractions. They often require simplifications to address complexities. The application of mathematical models to illustrate CO_2 emissions and environmental effects is a recent development, influenced by various scientists and organizations, and difficult to trace (Yoro and Daramola 2020).

Content courtesy of Springer Nature, terms of use apply. Rights reserved.

PUBLICATION

Reaction Kinetics, Mechanisms and Catalysis
https://doi.org/10.1007/s11144-026-03201-1

A nonlinear lumped chemical kinetics model for carbon dioxide emission and removal dynamics: mathematical analysis, numerical simulation and global sensitivity investigation

James Gathungu Gicheru[1] · Cyrus Gitonga Ngari[1] · Peter Wanjohi Njori[1]

Received: 28 April 2026 / Accepted: 25 June 2026
© Akadémiai Kiadó Zrt 2026

Abstract
Carbon dioxide (CO_2) emissions resulting from hydrocarbon combustion remain one of the major contributors to global climate change, necessitating the development of mathematical models capable of describing the complex interactions between emission sources and natural carbon sequestration processes. In this study, a nonlinear lumped chemical kinetics model is developed to investigate the dynamics of atmospheric carbon dioxide generated from the combustion of kerosene, liquefied petroleum gas (LPG), petrol, and diesel, while incorporating oxygen consumption, water vapor production, photosynthesis, glucose formation, and carbonic acid formation as natural carbon removal mechanisms. The governing model consists of a system of nine coupled nonlinear ordinary differential equations derived using the law of mass action. Qualitative analysis establishes the positivity, boundedness, existence, and uniqueness of solutions, ensuring that the model is mathematically and physically well posed. A positive equilibrium point is obtained analytically and verified numerically. Local stability is investigated through Jacobian matrix analysis, and numerical evaluation confirms that all eigenvalues possess strictly negative real parts, demonstrating that the positive equilibrium is locally asymptotically stable. Numerical simulations are performed in MATLAB R2023b using the stiff solver `ode15s`, and the trajectories of all state variables converge smoothly to finite equilibrium values, confirming the analytical results. A global sensitivity analysis based on Latin Hypercube Sampling (LHS) and Partial Rank Correlation Coefficients (PRCC) identifies the parameter a_6 as the dominant factor governing the system dynamics, while bifurcation analysis with respect to the oxygen replenishment parameter β_O demonstrates smooth equilibrium behavior without qualitative changes over the investigated parameter range. The combined analytical and numerical results indicate that the proposed nonlinear lumped chemical kinetics model provides a mathematically consistent and computationally robust framework for analysing carbon dioxide emissions and evaluating the influence of natural carbon sequestration mechanisms. The model offers a useful quantitative tool for supporting future investigations on

Extended author information available on the last page of the article

Published online: 07 July 2026

DrillBit

The Report is Generated by DrillBit Plagiarism Detection Software

Submission Information

Author Name	James Gathungu Gicheru
Title	MODELLING THE ROLE OF FOSSIL FUELS AND HUMAN ACTIVITIES IN CARBON (IV) OXIDE EMISSIONS AND GLOBAL WARMING USING COMPARTMENTAL AND CHEMICAL KINETICS MODELS
Paper/Submission ID	7000591
Submitted by	bkamau@kyu.ac.ke
Submission Date	2026-08-20
Total Pages, Total Words	146, 32244
Document type	Thesis

Result Information

Similarity 7 %



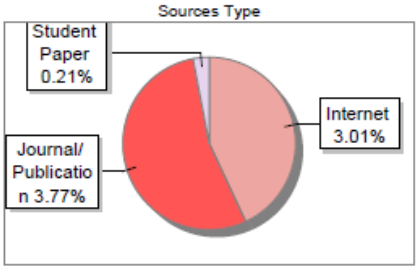

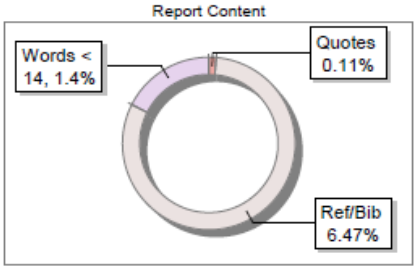

Exclude Information

Quotes	Not Excluded	Language	English
References/Bibliography	Excluded	Student Papers	Yes
Source: Excluded < 14 Words	Not Excluded	Journals & publishers	Yes
Excluded Source	0 %	Internet or Web	Yes
Excluded Phrases	Not Excluded	Institution Repository	Yes

Database Selection

A Unique QR Code use to View/Download/Share Pdf File